A STABLE ISOTOPE STUDY OF VEIN-HOSTED GOLD MINERALIZATION IN THE LIVENGOOD DEPOSIT, CENTRAL ALASKA

by

DANA LEIGH SUSINA

(Under the Direction of Douglas Crowe)

ABSTRACT

The Livengood deposit is an Intrusion Related Gold System (IRGS) in Central Alaska with abundant vein-hosted Au mineralization. There are multiple sets of veins, and although petrography suggests that each vein was deposited from a single mineralizing hydrothermal fluid, disequilibrium between coexisting sulfides indicates a change in temperature and/or $\delta^{34}S_{H2S}$ during emplacement. Stable isotope analyses of these mineralized vein sets show no difference in the isotopic ratios of arsenopyrite, stibnite, or quartz. Calculated fluid compositions of mineralized veins are $\delta^{34}S_{H2S}$=-2.7‰ to -1.6‰ and $\delta^{18}O_{H2O}$=8.1‰ to 11.7‰, which indicate a magmatic source. At Livengood, biotite, albite, and sericite alteration facies are associated with mineralization. Calculated temperatures from biotite-quartz and sericite-quartz pairs are, 490° C and 284° C, respectively, and are consistent with crosscutting relationships. Calculated fluid compositions of these alteration facies are 10.1‰ to 13.8‰, which indicate a magmatic source. Mineralization and alteration calculated fluid compositions are consistent with other IRGS's.

INDEX WORDS: Livengood, Money Knob, Central Alaska, Vein-hosted gold, Intrusion related gold, Intrusion Related Gold System, IRGS, Stable isotopes, Sulfur isotopes, Oxygen isotopes

A STABLE ISOTOPE STUDY OF VEIN-HOSTED GOLD MINERALIZATION IN THE LIVENGOOD DEPOSIT, CENTRAL ALASKA

by

DANA LEIGH SUSINA

BS, University of Georgia, 2010

A Thesis Submitted to the Graduate Faculty of The University of Georgia in Partial Fulfillment of the Requirements for the Degree

MASTER OF SCIENCE

ATHENS, GEORGIA

2013

A STABLE ISOTOPE STUDY OF VEIN-HOSTED GOLD MINERALIZATION IN THE LIVENGOOD DEPOSIT, CENTRAL ALASKA

by

DANA LEIGH SUSINA

Major Professor:	Douglas Crowe
Committee:	Samuel Swanson Paul Schroeder

Electronic Version Approved:

Maureen Grasso
Dean of the Graduate School
The University of Georgia
May 2013

ACKNOWLEDGEMENTS

First, I would like to acknowledge the faculty, staff, and students of the Geology Department at UGA. The incredible amount of assistance and encouragement I have received during my six-year-stay has been invaluable. I would like to recognize the following people in particular: Dr. Sam Swanson for sparking my interest in research as an undergraduate, and serving on the committee for this project; Dr. Paul Schroeder for his guidance as a member of my committee; Julia Cox and Chris Fleisher for their support and patience in their respective scientific laboratories. Second, this project would not have been possible without the guidance and financial assistance of International Tower Hill Mines and Northern Associates. In particular, I would like to thank Chris Puchner for sharing his immense knowledge of the deposit and allowing me to complete this study. Last, I owe a great deal of gratitude to my advisor, Dr. Doug Crowe. He has been an exceptional mentor on this project and in life, and I hope to make him proud.

TABLE OF CONTENTS

Page

APPENDICES

LIST OF TABLES

Page

LIST OF FIGURES

CHAPTER 1

INTRODUCTION

Tintina Gold Province

The Tintina gold province (Figure 1) is a belt of significant gold mineralization covering much of Central Alaska and the Yukon Territory, Canada. It is an east-west trending, 200-km-wide, 1,200-km-long arc that is roughly bounded to the north and south by the regional scale Kaltag-Tintina and Denali faults, respectively (Goldfarb et al., 2000; Smith et al., 2000).

The Tintina gold province encompasses numerous mining districts producing a variety of commodities from a suite of different types of mineral deposits. Some of the largest gold deposits, their location, endowment, grade, and production to date are summarized in table 1.

Table 1: Major gold deposits of the Tintina Gold Province. Updated by the USGS from Hart et al., 2002.

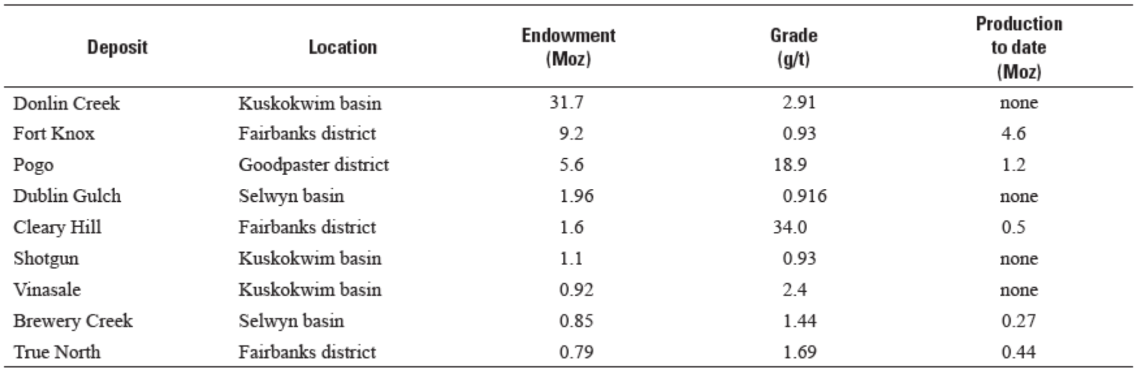

Deposit	Location	Endowment (Moz)	Grade (g/t)	Production to date (Moz)
Donlin Creek	Kuskokwim basin	31.7	2.91	none
Fort Knox	Fairbanks district	9.2	0.93	4.6
Pogo	Goodpaster district	5.6	18.9	1.2
Dublin Gulch	Selwyn basin	1.96	0.916	none
Cleary Hill	Fairbanks district	1.6	34.0	0.5
Shotgun	Kuskokwim basin	1.1	0.93	none
Vinasale	Kuskokwim basin	0.92	2.4	none
Brewery Creek	Selwyn basin	0.85	1.44	0.27
True North	Fairbanks district	0.79	1.69	0.44

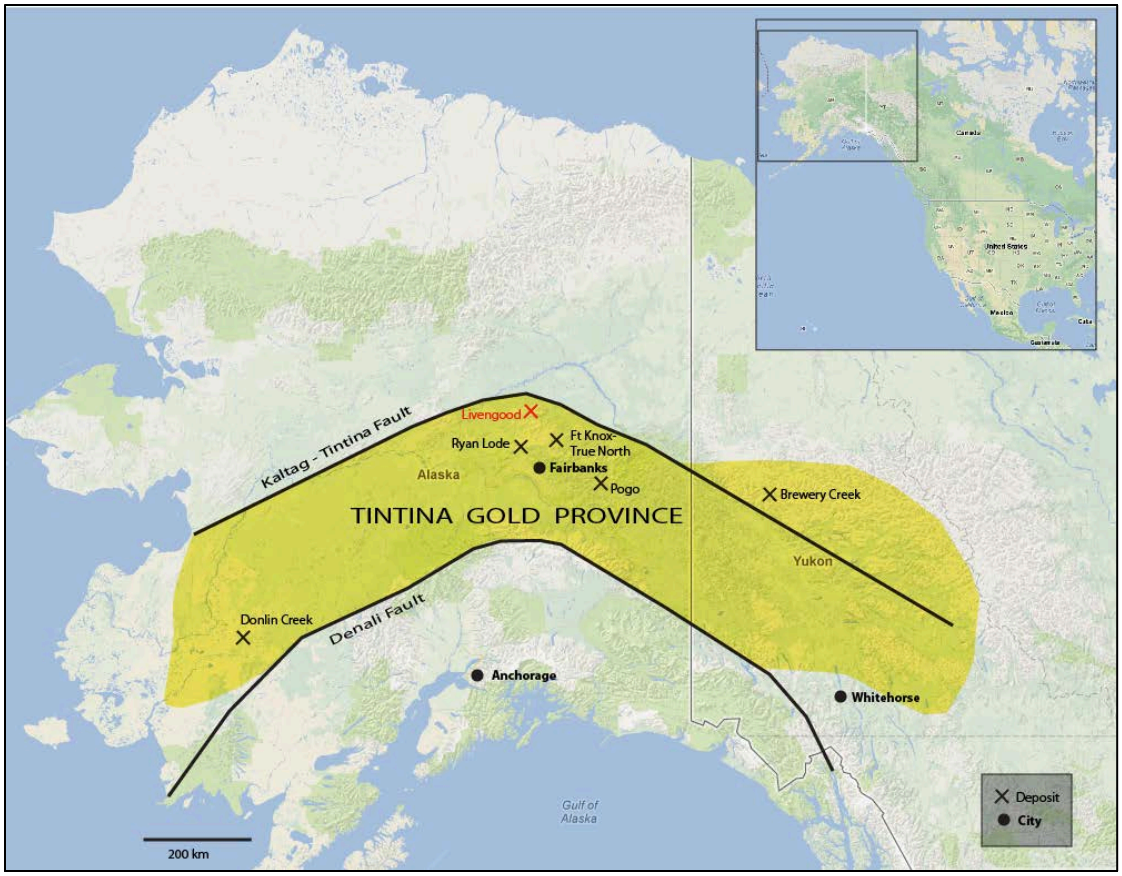

Figure 1: Map of the Tintina gold province. Major faults, cities and deposits are shown.

Tolovana-Livengood Mining District

The Tintina gold province encompasses numerous areas of concentrated mining activity, or mining districts. The mining district (Figure 2) surrounding the Livengood town site is known by two names - the Livengood mining district, for obvious reasons, as well as the Tolovana mining district because the area encompasses the headwater region of the Tolovana River. The district is historically known for placer gold mining, but more recently is recognized for it’s lode gold potential as well. Exploration in the district began in the early 20th century and has been fairly steady to present.

The stratigraphy of the area is variable, but is ubiquitously intruded by mid-Cretaceous (89-94 Ma), back-arc plutons associated with subduction of the Farallon plate (Plafker and Berg, 1994). These intrusions are shown to be associated with many of the Tolovana-Livengood lode gold deposits (Hart et al., 2002).

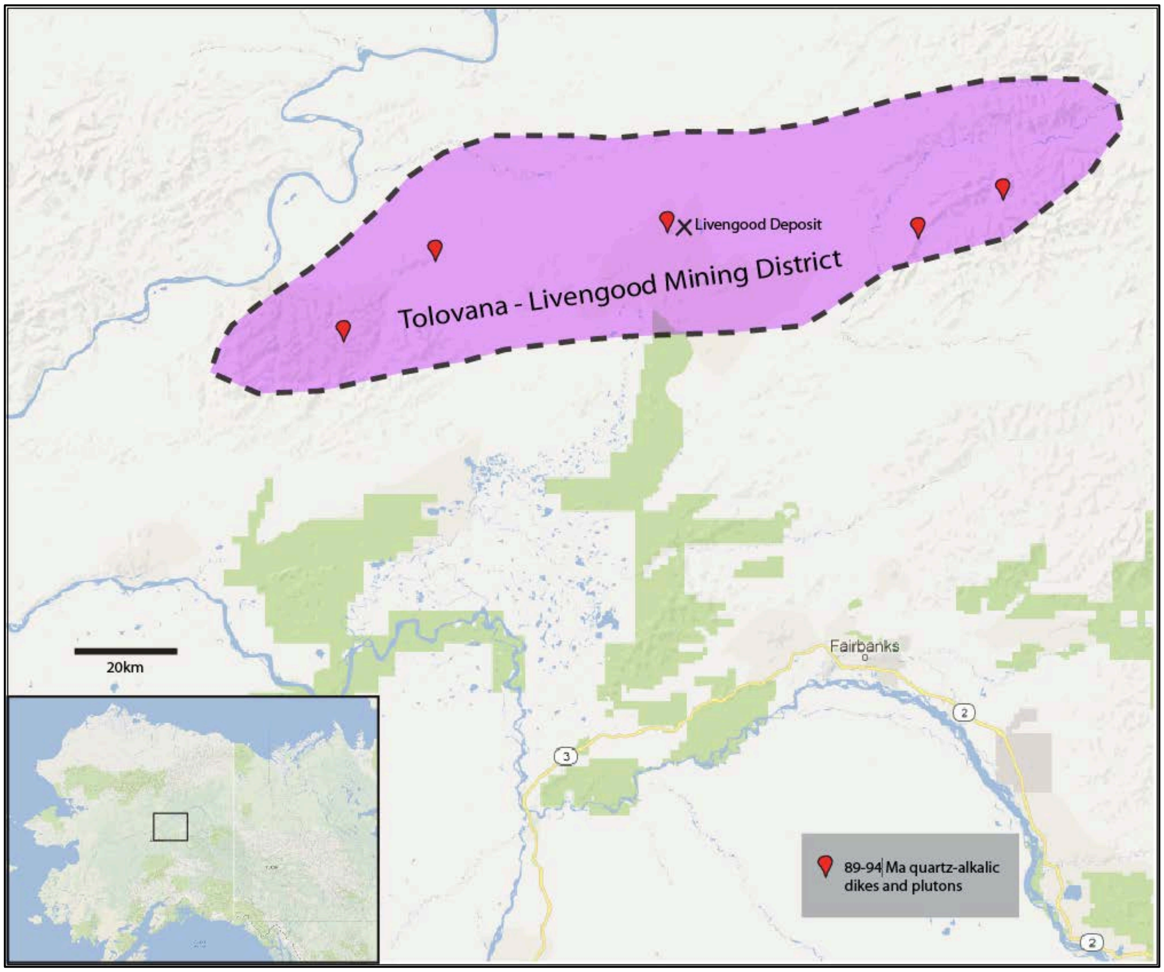

Figure 2: Map of the Tolovana-Livengood mining district. Approximate location of Cretaceous, back-arc plutons are shown. Modified from Newberry field trip guide and Hart et al., 2002.

Livengood Exploration History

Increased placer gold exploration in the Tolovana-Livengood district eventually led prospectors to the creeks around what would become the town of Livengood. Brooks (1915) reported the first discovery of gold in Livengood Creek by Jay Livengood and N. R. Hudson on July 24, 1914. Subsequently, prospectors flocked to the area, the town of Livengood was established, and mining of the rich placer deposits began. The Livengood placer deposits have proven to be among the richest in Alaska, producing over 500,000 ounces of gold over the last century (Klipfel et al., 2009).

Prospectors of the Livengood Creek placer deposits generally considered the ridgeline to the south, containing Money Knob, to be the probable lode gold source. In the 1950's, several exploratory trenches were dug into the ridgeline, but there is no evidence of any subsequent production. As placer mining in the area began to slow in the 1960's, government agencies were the first to conduct surveys of the area. The area was included in a heavy minerals assessment program conducted by the USGS in 1968, in which it was suggested that an "economically significant metal deposit" might exist in the area (Foster, 1968). Since this investigation, several others by the USGS and the Alaska State Division of Geological and Geophysical Survey have been conducted. These include Chapman et al. (1971), Chapman and Weber (1972), Cobb (1972), Albanese (1983), Robinson (1983), Waythomas et al. (1984), Arbogast et al. (1991), Athey and Craw (2004), and Athey and Craw (2004). In 1976, private entities began exploration for the lode source of gold around Money Knob. This activity is summarized in table 2.

Table 2: Summary of corporate exploration in the Livengood area. Modified from Brechtel et al. (2011).

Company	Year	Major Activities	Results	Comment
Homestake	1976	Geochemistry and 7 boreholes	Significant soil anomaly, low grade gold in drill holes and auger samples	Management decided on other priorities
Occidental Petroleum	1981	6 boreholes	Low-grade gold encountered in several holes	Other priorities
Alaska Placer Development	1981-84	Extensive soil and rock sampling, mapping, magnetic surveys, EM surveys, trenching and auger drilling	Defined soil and rock anomalies mostly on flanks of Money Knob	Changed focus to placer deposits
Amax	1990	3 RC holes, surface geochemistry, and auger drilling	Good geological mapping, lots of rock sampling, moderate gold grade in drill holes	Other priorities
Cambior	1999	Geochemistry	First to identify the areal extent of gold in soils around Money Knob	Corporate restructuring, no follow up
AGA	2003-05	Geochemistry, trenching, geophysics, 4 core and 8 RC drill holes	Established geochemical anomaly, numerous gold-bearing drill intersections	
ITH	2006-07	Surface geochemical sampling, 22 core drill holes	Intersected extensive zones of >1g/t gold intervals, initial resource estimates	
ITH	2008-11	550 RC and 72 core drill holes, infill and step-out grid drilling of mineralization, geotechnical drilling, metallurgical testing, environmental baseline data collection	Expanded resource estimates, preliminary economic evaluation of the deposit	

Most recently, in 2006, International Tower Hill (ITH) obtained the approximately 50 mi^2 land package including Livengood Creek, Money Knob, and the surrounding area. Since that time, ITH has conducted surface geochemical sampling, geophysical surveying, and an extensive drilling program. The drill program utilized both reverse circulation and diamond core drilling. Over 160,000 meters from over 700 holes has helped define and substantiate multiple mineralized areas of the Livengood gold and also potential future targets (Figure 3). In August 2011, ITH reported a measured and indicated resource of 16.5Moz at a 0.22g/ton cutoff.

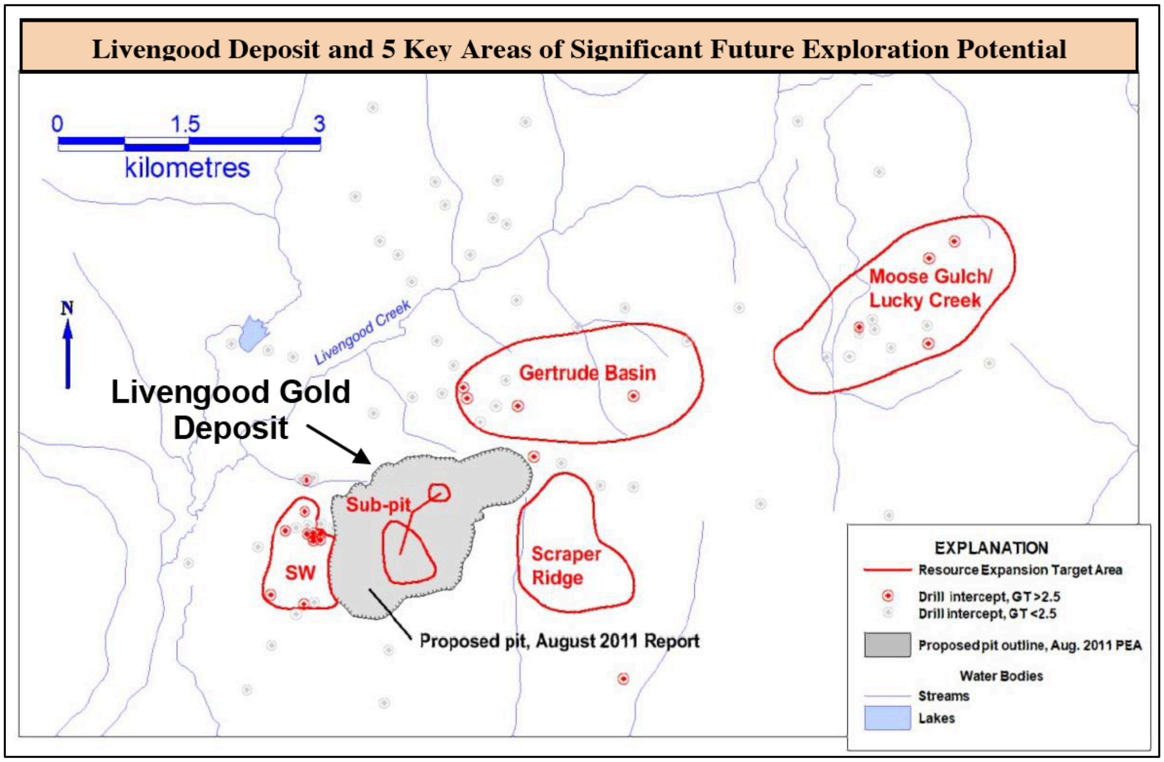

Figure 3: The Livengood gold deposit along with potential future target. Taken from a public ITH fact sheet at www.ithmines.com.

CHAPTER 2

GEOLOGIC SETTING

Regional Geology

East-Central Alaska is made up of several allochthonous terranes (Figure 4) that successively accreted to the North American craton beginning in the Paleozoic and continuing into the early Cenozoic. The age of accretion generally increases from the north to south. One of these terranes, the Livengood terrane, hosts the Livengood deposit. This terrane is a package of deformed and folded rocks of oceanic origin that were accreted in the Devonian and Missisippian. The Livengood terrane is bounded to the north by a steeply dipping reverse fault and the Beaver terrane, and to the south by the Kandik River terrane (Figure 5).

Rocks of the Livengood terrane are early Paleozoic aged shales and cherts overlain unconformably by Devonian volcano-sedimentary package (Churkin et al., 1982). This package was then deformed and folded during the accretion of younger terranes to the south.

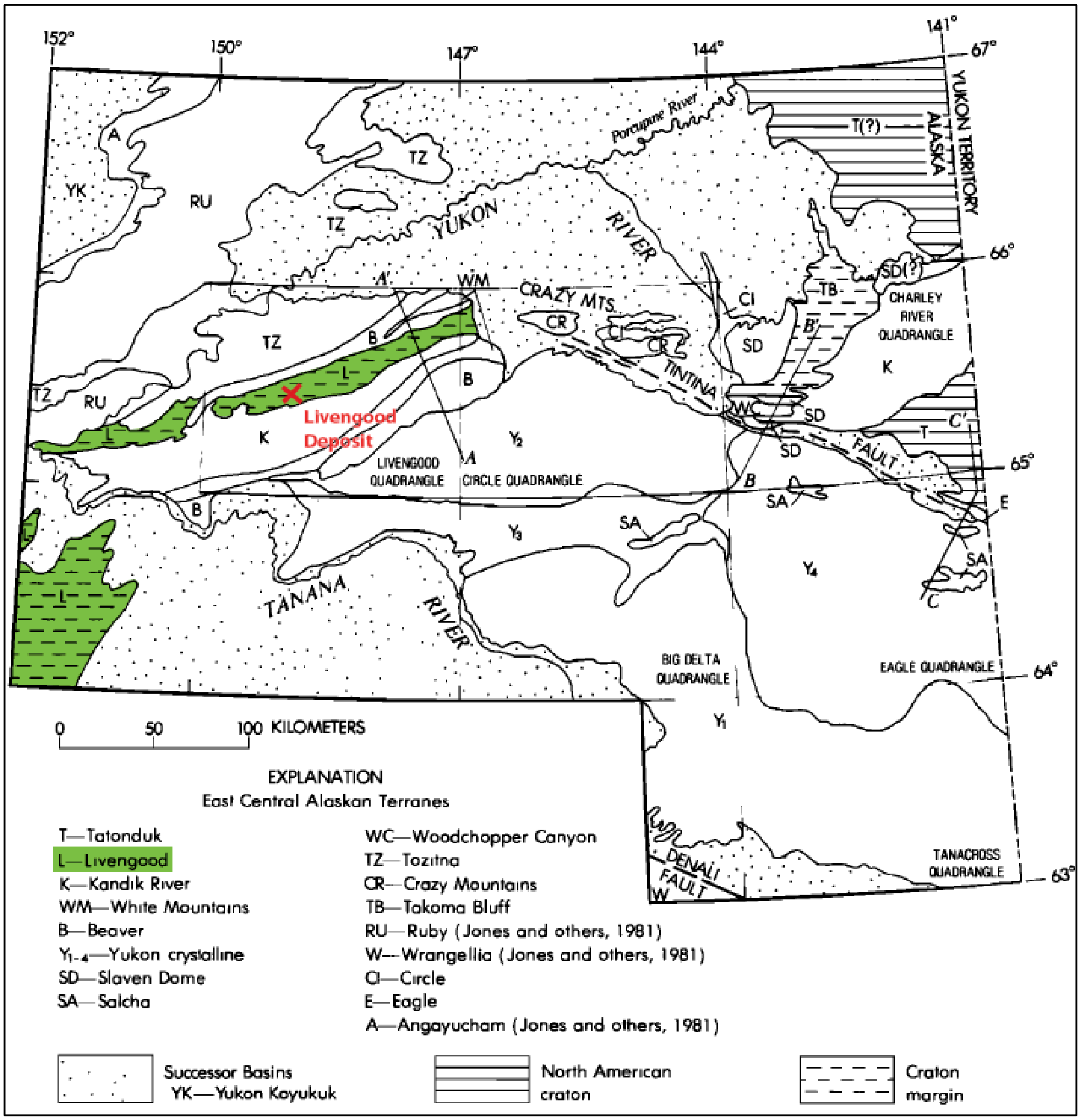

Figure 4: Map of the terranes of East-Central Alaska. Modified from Churkin et al. (1982).

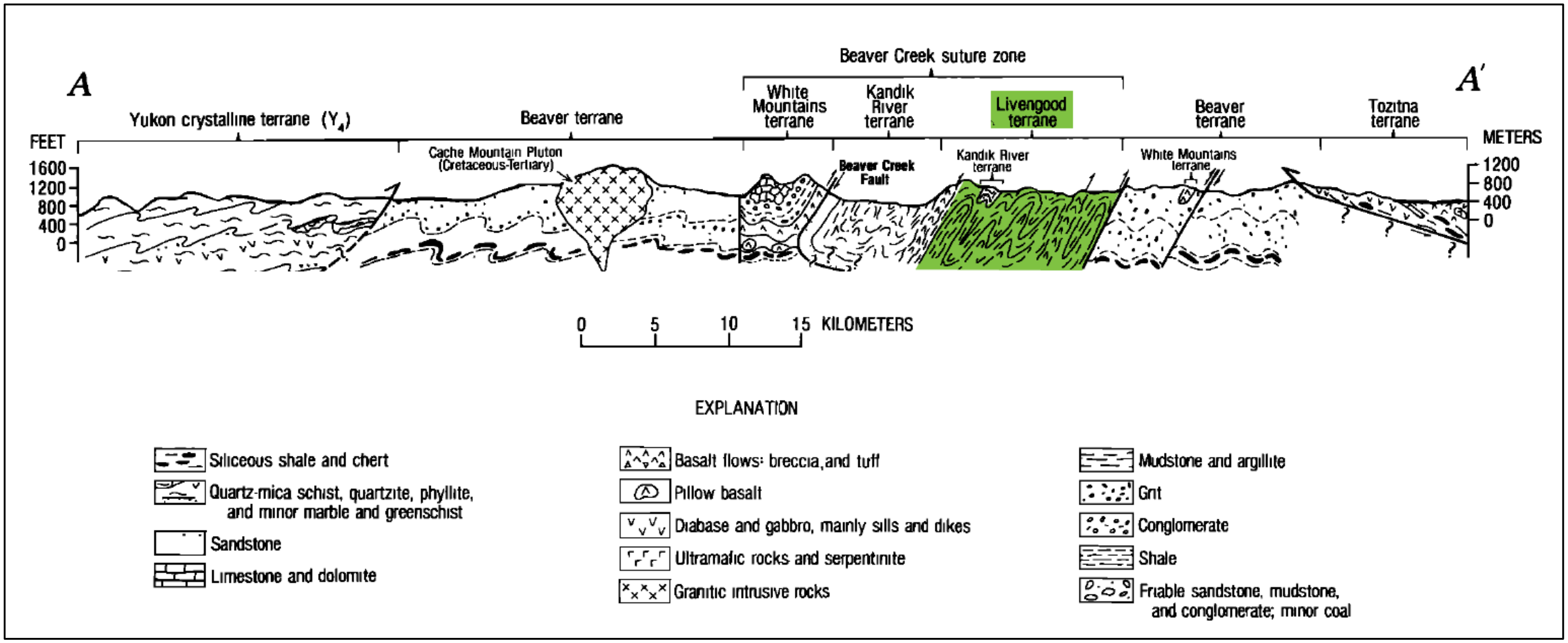

Figure 5: Cross section A-A’ through the terranes of East-Central Alaska. Modified from Churkin et al. (1982).

Deposit Geology

Local geology at Livengood is comprised of multiple thrust stacks of Livengood terrane units. These units include the shallow marine deposits of the Amy Creek assemblage, a Cambrian ophiolite sequence, a Devonian volcano-sedimentary package of clastic sedimentary rocks and volcanic rocks, and Cretaceous plutons, dikes, and sills that intrude and cross cut these units. Each of these units is summarized in the following paragraphs from the mapping of the Livengood Quadrangle by Athey et al. (2004). The stratigraphy of these units is presented in figure 6.

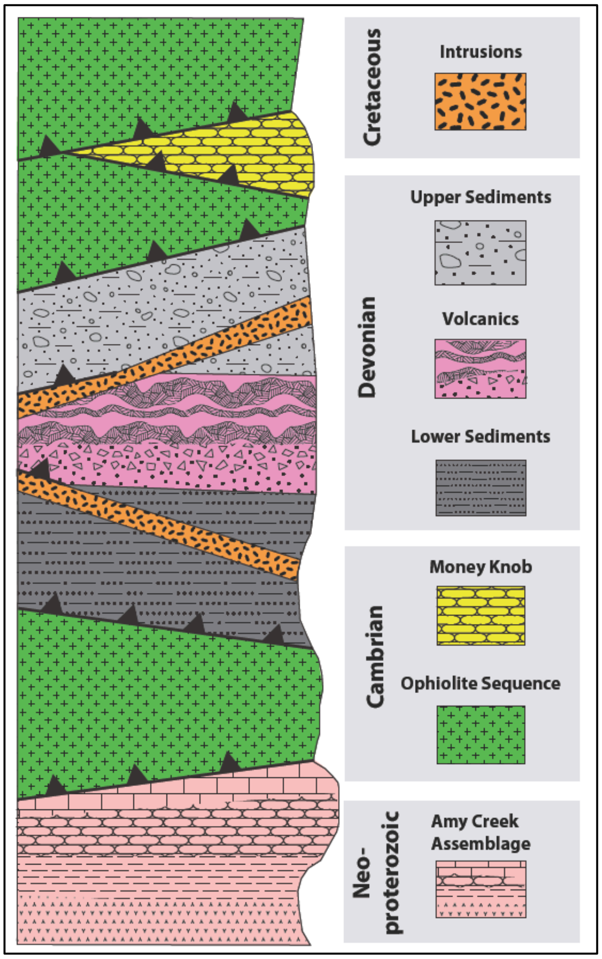

Figure 6: Stratigraphic section of the Livengood area. Modified from Klipfel et al. (2009).

Amy Creek Assemblage

The Amy Creek Assemblage is a >1,160 m thick package of Neoproterozoic to early Paleozoic siliceous mudstone, chert, dolomite, and limestone with interlayered metabasalts. Rocks of this unit were deposited when a shallow-water, inner shelf environment built on a deep-water, outer shelf environment. Occasional, rift-related, within-plate, basaltic flows and sills are interlayered within the unit.

Ophiolite Sequence

The ophiolite sequence is made up of early Cambrian mafic to ultramafic intrusions and metagabbros, most of which are serpentinized. Rocks in this sequence were deposited at a mid-ocean ridge, then metamorphosed to prehnite-pumpellyite facies.

Figure 7: Ophiolite sequence ultramafic rock. Sample shows typical serpentinization and oxidation.

Lower Sediments

The lower sediments are a subgroup of the Devonian volcano-sedimentary package that is Middle Devonian in age. The unit is primarily made up of shales and siltstones with a subordinate amount of sandstone and limestone layers. These rocks were deposited in a shallow water basin near an uplift. The lower sediments are distinguished from the upper sediments because they are generally finer-grained with abundant black shale and digenetic pyrite. The lower sediments are stratigraphically below the main volcanics described in the next section.

Figure 8: Lower sediments shale. Sample shows typical bedding and diagenetic pyrite.

Main Volcanics

The main volcanics are a subgroup of the Devonian volcano-sedimentary package and are Middle Devonian in age. This unit is made up of volcanic tuffs, breccias, and flows.

Figure 9: Main volcanics amygdaloidal flow.

Figure 10: Main volcanics tuff. Sample shows abundant lithic and pumice fragments.

Upper Sediments

The upper sediments are a subgroup of the Devonian volcano-sedimentary Package and are Middle Devonian in age. They are primarily sandstones, but show variable thicknesses of conglomerate, siltstone, and rare shale and limestone. These sediments were deposited in a shallow water basin near an uplift. The upper sediments are distinguished from the lower sediments by being coarser-grained and being stratigraphically above the main volcanics.

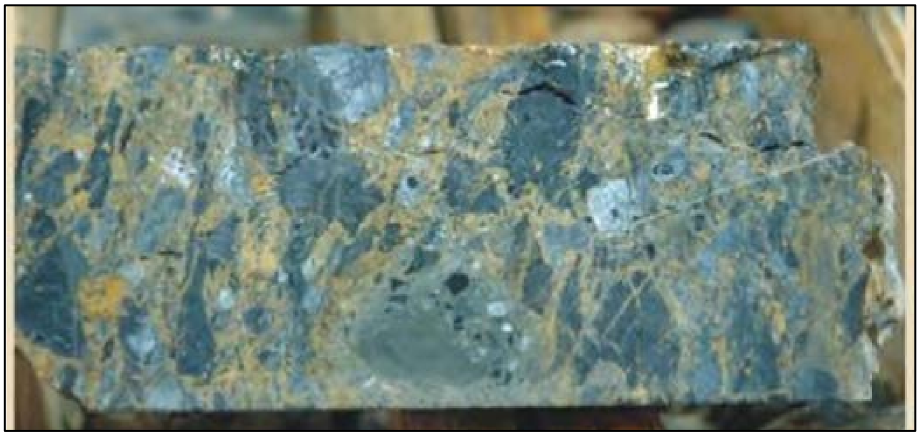

Figure 11: Upper sediments conglomerate.

Figure 12: Upper sediments siltstone with interbedded sandstone.

Plutons, Dikes, and Sills

Cretaceous age plutons, dikes, and sills crosscut the aforementioned stratigraphy. The dikes and sills are 0.1-10m in width with a median thickness of about 1mm. Composition ranges from felsic to intermediate, including monzonites, syenites, granites, and granodiorites. Textures are bimodal, either exhibiting an aphanitic to fine grained texture or a porphyritic texture. These intrusive bodies were emplaced in a back-arc environment at 93Ma and are synchronous with subduction of the Farallon plate and the closure of the Manley Basin.

Figure 13: Dikes and sills. Sample shows porphyritic texture with moderate to strong biotite alteration and oxidation.

The following geologic history of the Livengood area has been developed by Klipfel et al. (2009) based on surface mapping (Athey and Craw, 2004) (Figure 14) and ITH drill hole data. This series of events is illustrated in figure 15.

A volcano-sedimentary package (made up of the lower sediments, main volcanics, and upper sediments) is deposited in the Middle Devonian. A compressional event asymeterically folded the Devonian package signaling the development of a fold-thrust belt. The upper portion of the Devonian package was truncated by a Cambrian age ophiolite sequence as it was thrust on top. Thrust stacking continued causing reverse offset faulting of the Devonian package and major thrust surface. Tectonic relaxation or a tectonic extensional event reactivatee faults and results in normal offset. The Lillian fault, a high-angle normal fault is thought to have formed during this extensional period. Back-arc, Cretaceous intrusions were emplaced, and dikes and sills preferentially infiltrated pre-existing fault zones. Much of the Cambrian ophiolite sequence was truncated during erosion, forming the current topography.

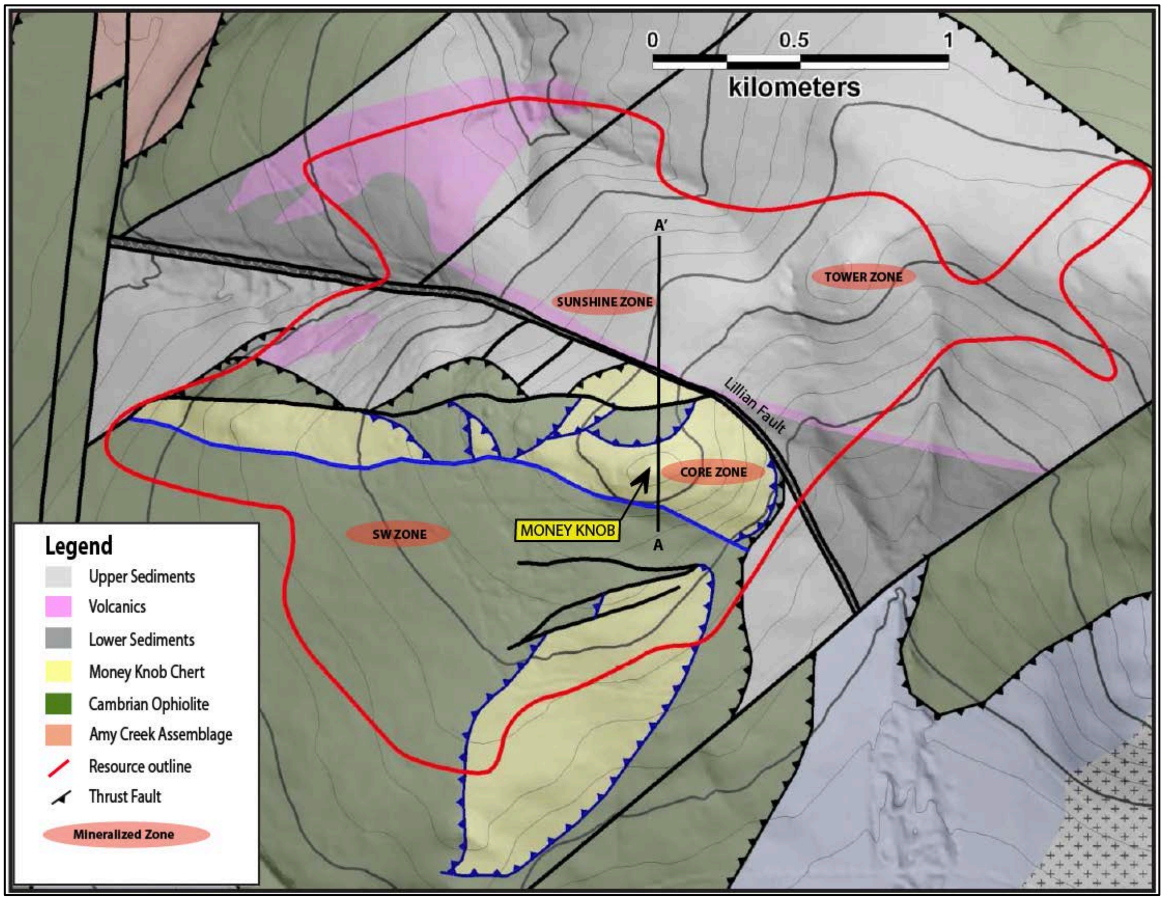

Figure 14: Geologic map of the Livengood area. This map shows geologic units, the high-angle Lillian fault, several sets of thrust faults, the resource area, and identified zones of mineralization. Modified from Klipfel et al., 2009.

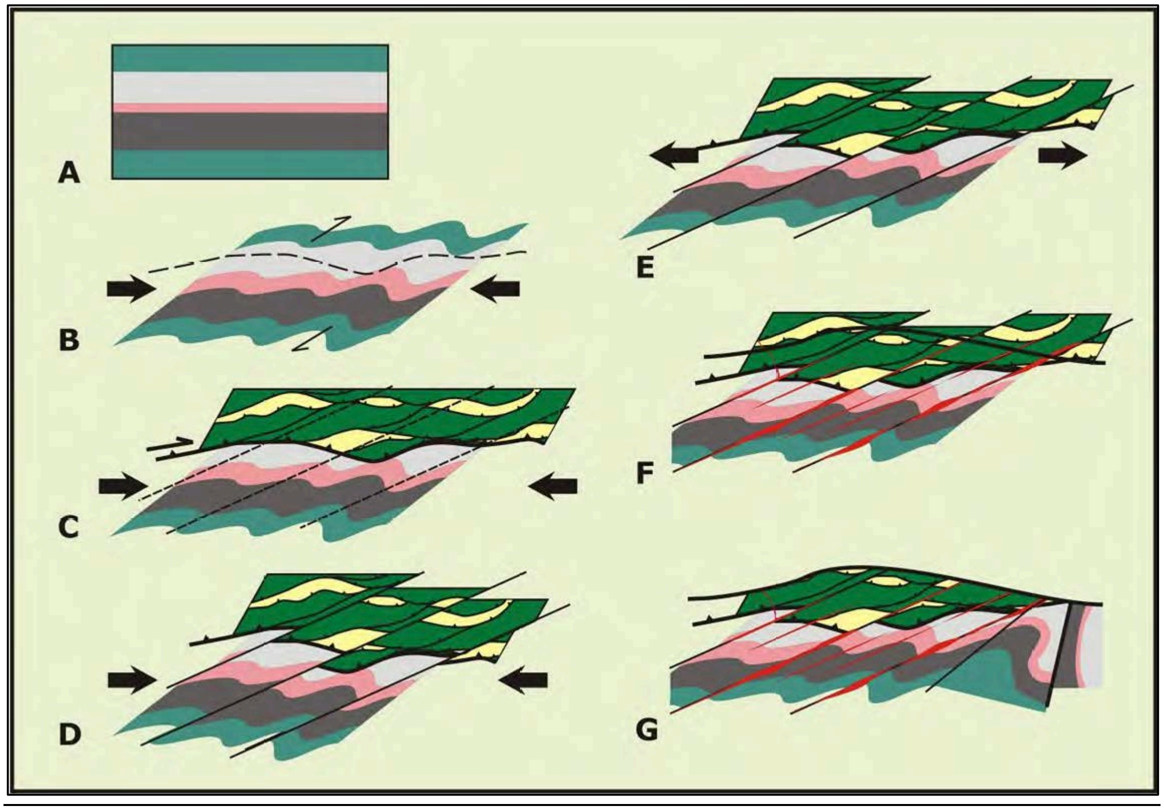

Figure 15: Schematic model of local Livengood geologic history. Taken from Klipfel et al. (2009). A) Devonian volcano-sedimentary sequence is deposited. Pink – main volcanics; light gray – upper sediments; dark gray – lower sediments. B) A compressional event folds the units. Dashed line shows where incipient thrust truncation will develop. C) Cambrian ophiolite sequence is thrust over the folded Devonian volcano-sedimentary sequence. D) Thrusting stacking continues. E) Tectonic relaxation thrusting or a tectonic extensional event reactivates faults and initiates the high-angle, normal Lillian fault. F) Cretaceous dikes (red) are emplaced preferentially along fault surfaces. G) Erosion to current topography.

Mineralization

Gold mineralization in the Livengood deposit takes three main forms (Figure 16): 1) Au associated with the Cretaceous aged dikes and sills that crosscut the stratigraphy; 2) Au hosted within numerous sets of quartz-sulfide-rich veins; and 3) disseminated Au that occurs around the dikes, sills, and veins and preferentially concentrates in the Devonian sediments and volcanic rocks. These mineralization styles are discussed in more detail in the following paragraphs. In all three forms, Au concentration is shown to be positively correlated with As and Sb concentration. The correlation coefficient of Au and As is 0.71 and is shown by figure 16a. The correlation coefficient of Au and Sb is slightly less at 0.47 and is shown by figure 16b.

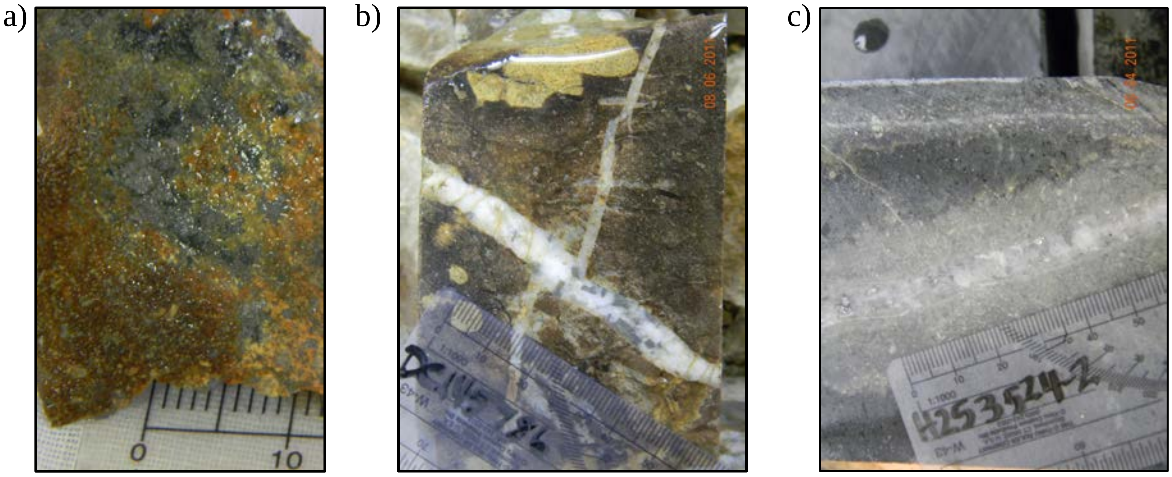

Figure 16: Representative sample of mineralization. a) dikes and sills, b) multiple mineralized vein sets, and c) disseminated mineralization

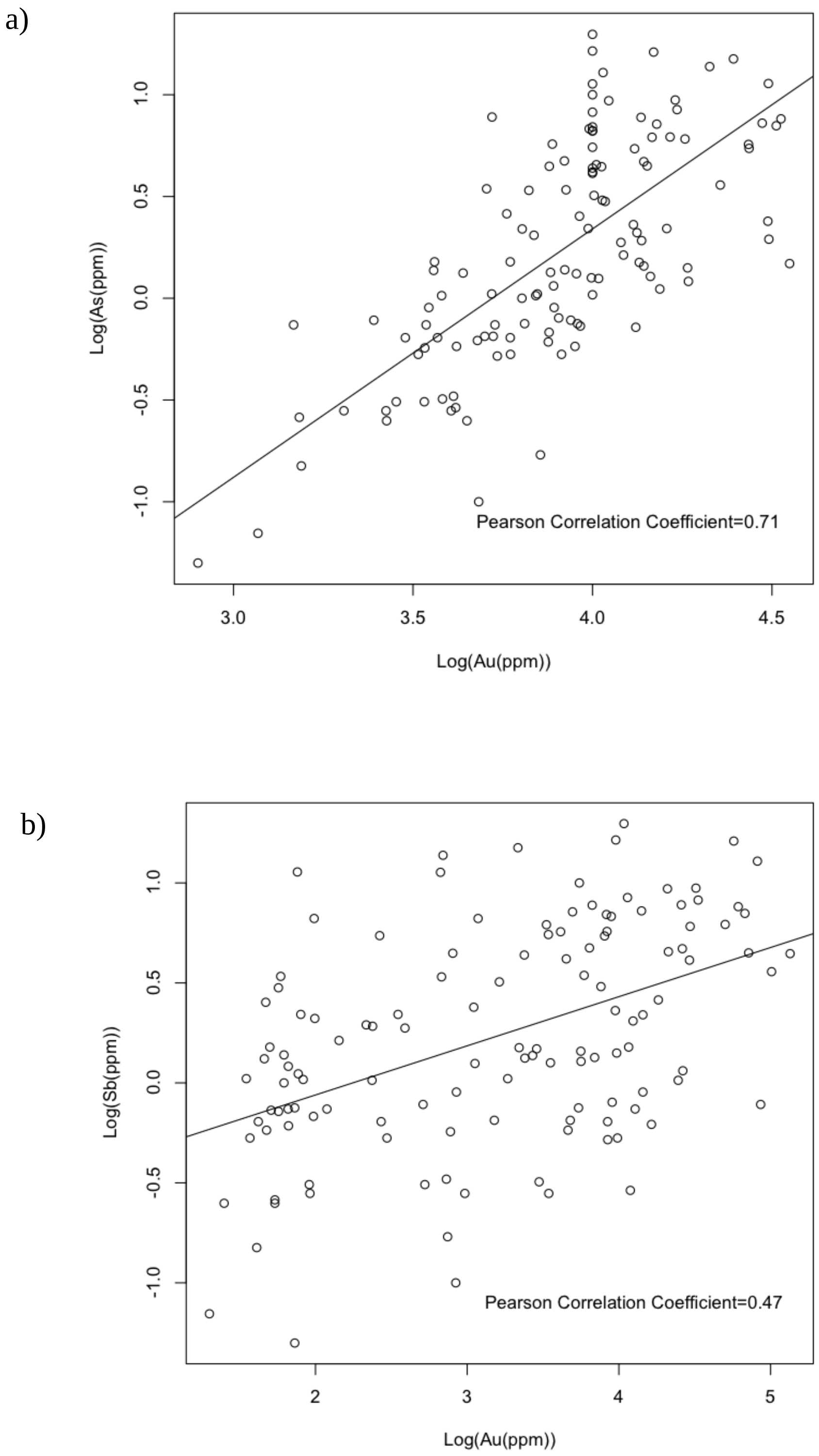

Figure 17: Plot of Au concentration vs a) As and b) Sb. Values are derived from ITH assay chemistry results of drill core. Regression is shown as a solid line. See appendices J and K for data and R code.

Back-arc dikes and sills intruded the Livengood area in the Late Cretaceous (91.7-93.2 m.y.; Athey and Craw, 2004) and host the highest grade material (>1g/ton Au) in the Livengood deposit. Athey and Craw (2004) considered these intrusions to be the primary host of Au ore in the Livengood area. Further exploration showed that vein-hosted and disseminated Au are important as well. The dikes and sills generally dip southward following the trend of the multistage thrust faults, which most likely acted as preferential fluid pathways. These dikes and sills are felsic to intermediate in composition, and plot as monzonite to diorite to syenite. Aphanitic, fine-grained equigranular, and porphyritic textures are seen. Many are heavily altered by biotite and oxidation, but still contain variable amounts of primary feldspar and biotite. Although Au mineralization does occur without any apparent association to the dikes and sills, it has been noted that gold grade generally increases as the density of dikes and sills increases (Puchner, personal communication, 2011).

The mineralized veins contain variable amounts and combinations of quartz, feldspar, calcite, and sulfides: arsenopyrite, pyrite, stibnite, sphalerite, and galena. They range in morphology from small (~1mm) anastomosing veinlets to medium (2cm) sheeted veins to larger (~10cm) veins with abundant open cavities and terminated quartz crystals. Veins of different mineral assemblages and morphologies are seen cross cutting one another, suggesting a prolonged period of emplacement. Visible gold is rarely seen at the Livengood deposit, but when it is, it is seen within quartz-rich veins.

The emplacement of the dikes, sills and veins has also deposited a significant amount of disseminated mineralization in surrounding country rock. The Devonian volcanic rocks have undergone the most substantial mineralization, but ore-grade halos have also been found in the Devonian upper and lower sediments and occasionally in the Cambrian ophiolite sequence, when intrusion density is high.

Currently, the proposed pit of the Livengood deposit is divided up into several zones of mineralization. These zones are shown in map view in figure 18 and in cross section in figure 19. The Core zone includes Money Knob, and the surrounding hillside south of the Lillian Fault. This zone contains mineralization in all three forms, in all stratigraphic units, and shows the most pervasive and variable associated alteration. The Sunshine zone encompasses the hillside to the south of the Lillian fault. This zone is characterized by mineralization in a very thick section of upper sediments and little variability in alteration.

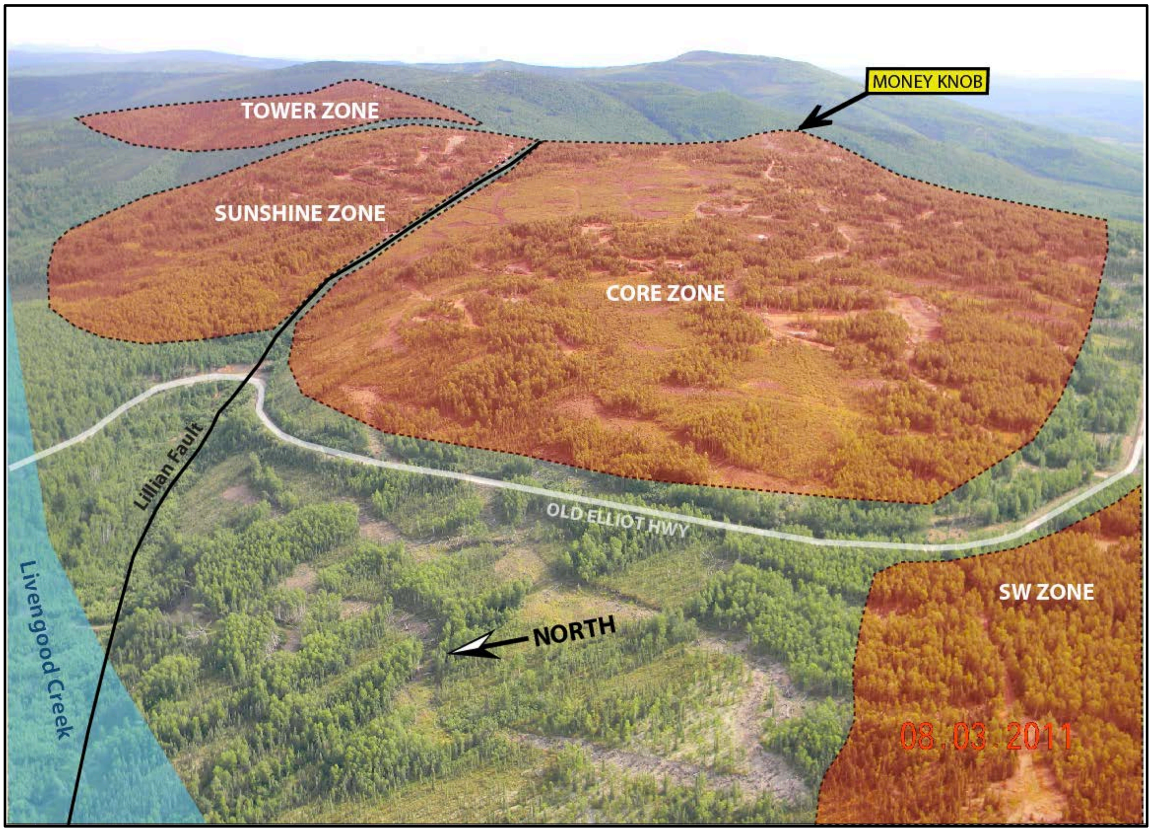

Figure 18: Map of identified zones of mineralization within the Livengood Deposit.

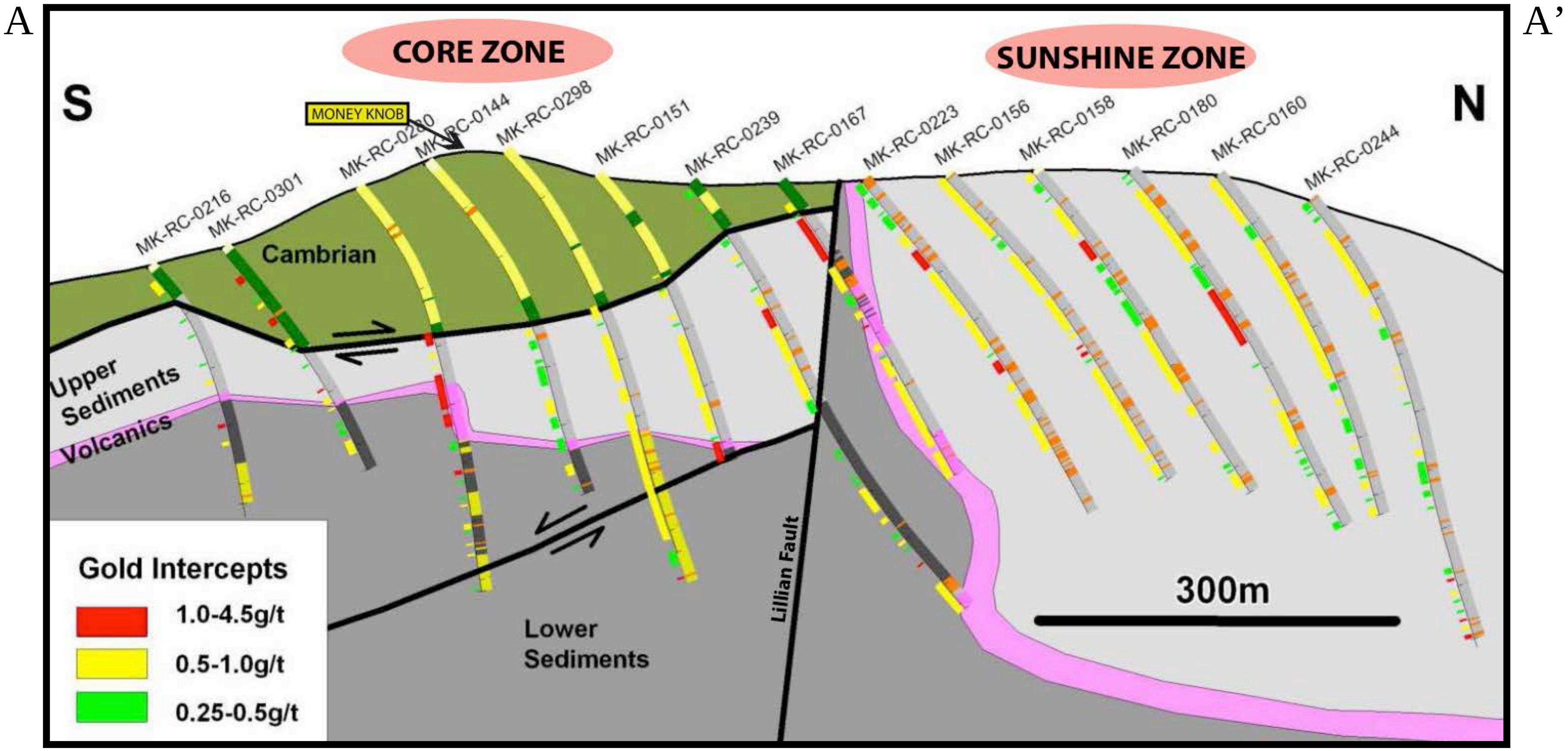

Figure 19: Cross section A-A’ as interpreted from drill holes. This cross section displays geologic units, major faults, and intervals of gold mineralization. Modified from Klipfel et al., 2009.

Alteration

Four dominant alteration stages are recognized in the Livengood deposit: biotite, albite, sericite, and carbonate (Figure 20). Biotite alteration is found as brown to maroon fine-grained patches of biotite (or as phlogopite in the Cambrian mafic-ultramafic rocks). Pyrrhotite, quartz, and arsenopyrite appear to be coeval with this stage. Albite alteration generally destroys all previous rock texture and occurs as massive gray to tan albite-flooded zones. Quartz, carbonate, arsenopyrite and pyrite are sometimes found to be coeval with this stage. Sericite alteration is found as muted green, fine-grained patches of sericite, or as tremolite and fuchsite in Cambrian mafic-ultramafic rocks. Quartz, arsenopyrite and pyrite appear to be coeval with this stage. Carbonate alteration is found as scaly flakes, fine-grained patches, euhedral clusters, of anastomosing veinlets of calcite. Cross cutting relationships of these alteration stages suggest an early biotite stage, followed successively by albite, sericite, and carbonate. Figure 20 shows these relationships.

Figure 20: Cross cutting alterations. Photograph of split core showing early biotite, followed by albite, sericite, then carbonate.

CHAPTER 3

INTRUSION RELATED GOLD SYSTEMS

Classification

The classification and application of the Intrusion Related Gold System (IRGS) model is still widely debated because of ever-changing nomenclature and blurred defining characteristics. Initially, IRGS's were grouped with porphyry systems or orogenic gold deposits, but they were later shown to be associated with a unique type of intrusion and tectonic setting. The distinction of IRGS's from other deposit models has primarily occurred within the last 3 decades, and is still controversial. During this time IRGS's have been lumped, split, and reinterpreted several times. Several authors have worked to define and label these deposits. The development of the nomenclature and concepts are listed in table 3.

Table 3: Historical nomenclature and major concepts of IRGS's. Taken from Hart and Goldfarb (2005).

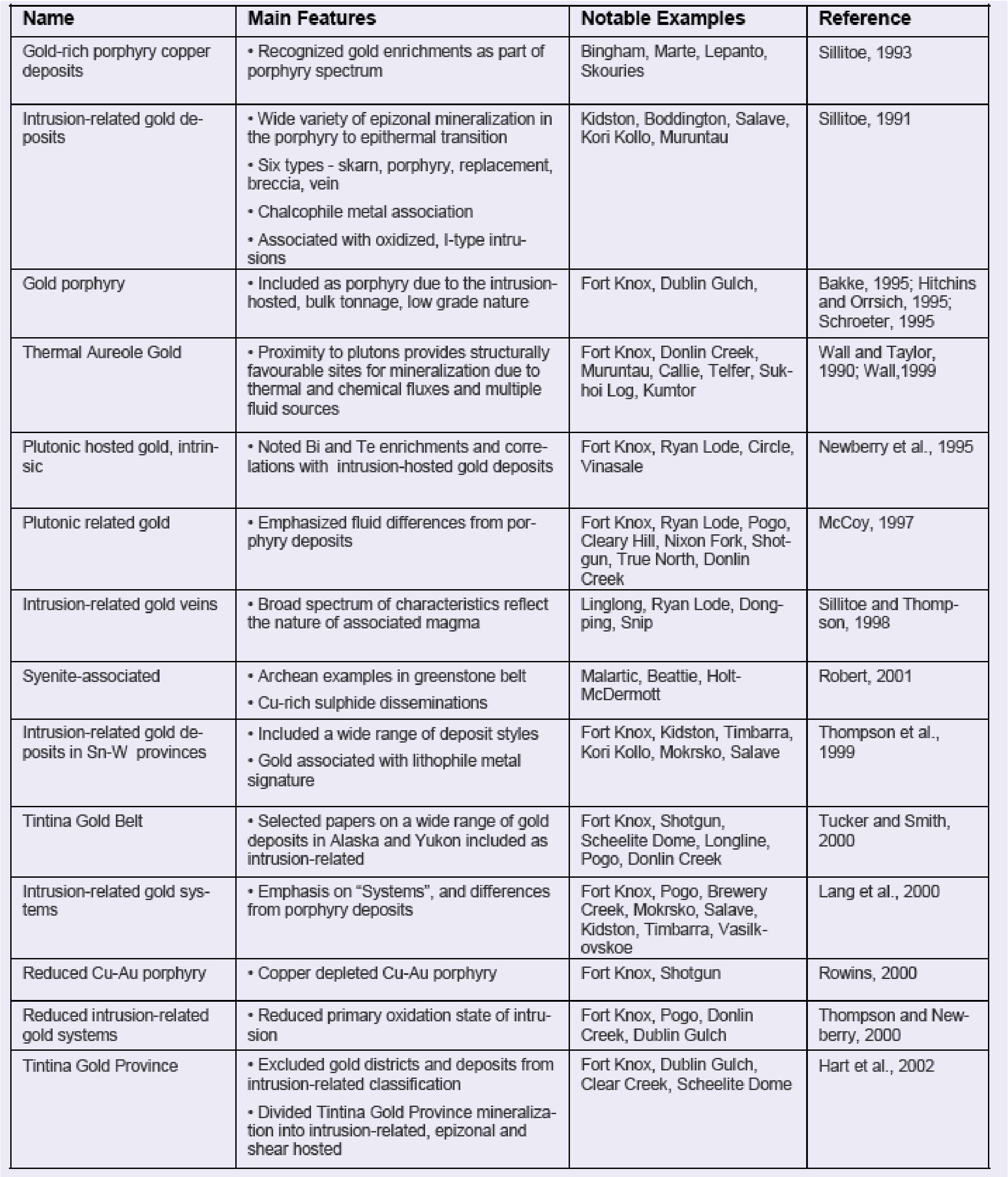

Name	Main Features	Notable Examples	Reference
Gold-rich porphyry copper deposits	• Recognized gold enrichments as part of porphyry spectrum	Bingham, Marte, Lepanto, Skouries	Sillitoe, 1993
Intrusion-related gold deposits	• Wide variety of epizonal mineralization in the porphyry to epithermal transition • Six types - skarn, porphyry, replacement, breccia, vein • Chalcophile metal association • Associated with oxidized, I-type intrusions	Kidston, Boddington, Salave, Kori Kollo, Muruntau	Sillitoe, 1991
Gold porphyry	• Included as porphyry due to the intrusion-hosted, bulk tonnage, low grade nature	Fort Knox, Dublin Gulch,	Bakke, 1995; Hitchins and Orrsich, 1995; Schroeter, 1995
Thermal Aureole Gold	• Proximity to plutons provides structurally favourable sites for mineralization due to thermal and chemical fluxes and multiple fluid sources	Fort Knox, Donlin Creek, Muruntau, Callie, Telfer, Sukhoi Log, Kumtor	Wall and Taylor, 1990; Wall,1999
Plutonic hosted gold, intrinsic	• Noted Bi and Te enrichments and correlations with intrusion-hosted gold deposits	Fort Knox, Ryan Lode, Circle, Vinasale	Newberry et al., 1995
Plutonic related gold	• Emphasized fluid differences from porphyry deposits	Fort Knox, Ryan Lode, Pogo, Cleary Hill, Nixon Fork, Shotgun, True North, Donlin Creek	McCoy, 1997
Intrusion-related gold veins	• Broad spectrum of characteristics reflect the nature of associated magma	Linglong, Ryan Lode, Dongping, Snip	Sillitoe and Thompson, 1998
Syenite-associated	• Archean examples in greenstone belt • Cu-rich sulphide disseminations	Malartic, Beattie, Holt-McDermott	Robert, 2001
Intrusion-related gold deposits in Sn-W provinces	• Included a wide range of deposit styles • Gold associated with lithophile metal signature	Fort Knox, Kidston, Timbarra, Kori Kollo, Mokrsko, Salave	Thompson et al., 1999
Tintina Gold Belt	• Selected papers on a wide range of gold deposits in Alaska and Yukon included as intrusion-related	Fort Knox, Shotgun, Scheelite Dome, Longline, Pogo, Donlin Creek	Tucker and Smith, 2000
Intrusion-related gold systems	• Emphasis on "Systems", and differences from porphyry deposits	Fort Knox, Pogo, Brewery Creek, Mokrsko, Salave, Kidston, Timbarra, Vasilkovskoe	Lang et al., 2000
Reduced Cu-Au porphyry	• Copper depleted Cu-Au porphyry	Fort Knox, Shotgun	Rowins, 2000
Reduced intrusion-related gold systems	• Reduced primary oxidation state of intrusion	Fort Knox, Pogo, Donlin Creek, Dublin Gulch	Thompson and Newberry, 2000
Tintina Gold Province	• Excluded gold districts and deposits from intrusion-related classification • Divided Tintina Gold Province mineralization into intrusion-related, epizonal and shear hosted	Fort Knox, Dublin Gulch, Clear Creek, Scheelite Dome	Hart et al., 2002

Current Model

Seven defining characteristics of reduced IRGS's are listed below. This list was compiled by Lang and Baker (2001), with contributions from Lang et al. (2000) and Thompson and Newberry (2000).

1) Metaluminous, subalkalic intrusion of intermediate to felsic compositions that lie near the boundary between ilmenite and magnetite series igneous rocks;
2) CO_2 bearing hydrothermal fluids;
3) Metal assemblages that variably combine Au with elevated Bi, W, As, Mo, Te, and/or Sb and low concentrations of base metals;
4) A low sulfide mineral content, mostly <5 vol%, with a reduced ore mineral assemblage that typically comprises arsenopyrite, pyrrhotite and pyrite and lacks magnetite or hematite;
5) A very restricted and commonly weak hydrothermal alteration;
6) A back-arc tectonic setting well inboard of convergent plate boundaries (Figure X);
7) A location in magmatic provinces best or formerly known for W and/or Sn deposits.

Hart and Goldfarb (2005) recognized that strong metal zonation is developed around the emplaced pluton (Figure 22). They showed that mineralization and geochemical variations vary predictably outward from the pluton. A model of this zonation is show in figure ***. An assemblage of Au-Bi-Te+-W develops proximal to the pluton, with As-Au, As-Sb-Au, and Ag-Pb-Zn assemblages occurring successively outward. Hart and

Goldfarb (2005) also suggests that skarn deposits can develop when the pluton interacts with carbonate units.

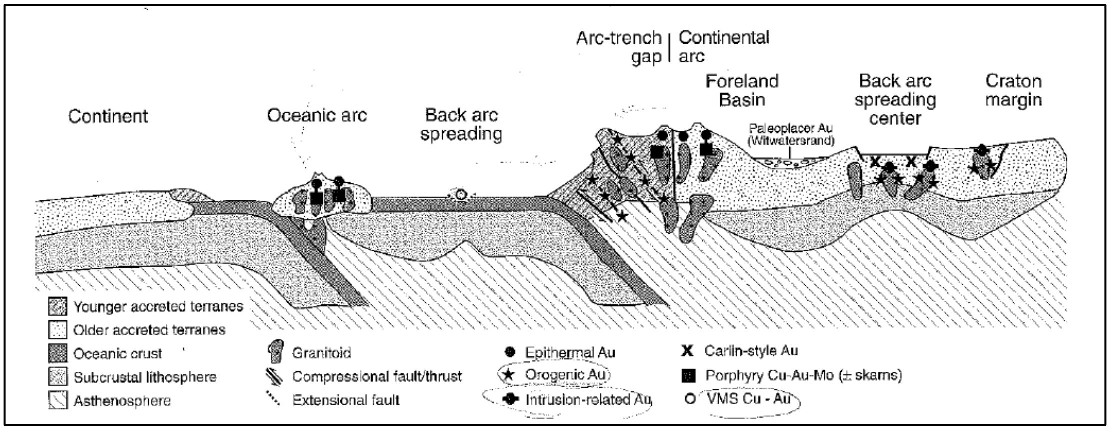

Figure 21: Schematic diagram of tectonic settings of various gold deposits. IRGS deposits from within back-arc spreading centers. Taken from Goldfarb et al., 2005.

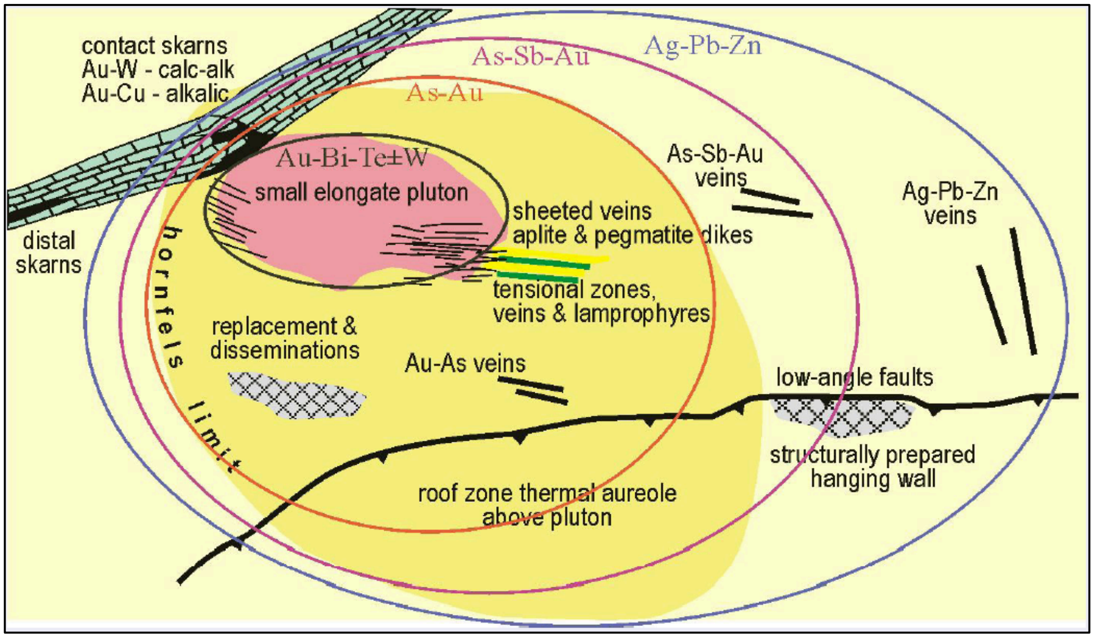

Figure 22: Schematic plan model of IRGS's from the Tintina Gold Province. Taken from Hart et al., 2005.

Fluid Inclusions and Stable Isotope Geochemistry

Fluid chemistry of major Tintina Gold Province deposits is compiled in table 4. The Sheelite Dome, Fort Knox, Pogo, and Donlin Creek deposits listed in the table are all considered to be Reduced Intrusion Related Gold Systems.

Fluid inclusions in IRGS's are typically CO_2-rich and moderately saline. Pressure calculations are variable, and temperature calculations indicate temperature of approximately 300° C to 400° C. Oxygen isotope ratios are consistently enriched pointing to a magmatic or metamorphic hydrothermal fluid, with little to no meteoric influence (Goldfarb et al., 2007). Extremely variable sulfur isotope values indicate contributions from variable crustal reservoirs (Goldfarb et al., 2005).

Table 4: Geochemistry of ore from Tintina Gold province deposits. Scheelite Dome, Fort Knox, Pogo, and Donlin Creek are IRGS. Taken from Goldfarb et al. (2007).

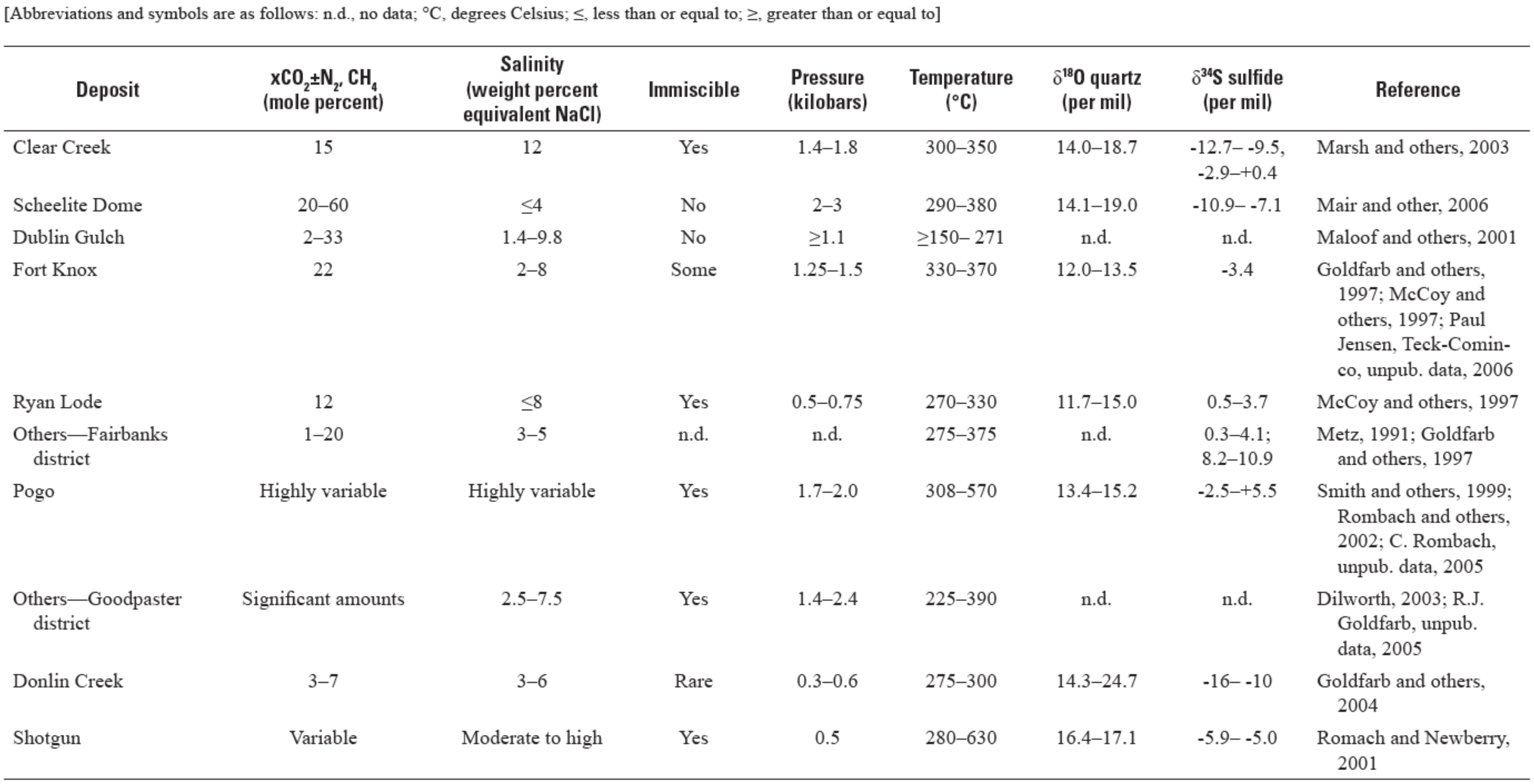

[Abbreviations and symbols are as follows: n.d., no data; °C, degrees Celsius; ≤, less than or equal to; ≥, greater than or equal to]

Deposit	**xCO_2±N_2, CH_4 (mole percent)**	**Salinity (weight percent equivalent NaCl)**	**Immiscible**	**Pressure (kilobars)**	**Temperature (°C)**	**$\delta^{18}O$ quartz (per mil)**	**$\delta^{34}S$ sulfide (per mil)**	**Reference**
Clear Creek	15	12	Yes	1.4–1.8	300–350	14.0–18.7	-12.7– -9.5, -2.9–+0.4	Marsh and others, 2003
Scheelite Dome	20–60	≤4	No	2–3	290–380	14.1–19.0	-10.9– -7.1	Mair and other, 2006
Dublin Gulch	2–33	1.4–9.8	No	≥1.1	≥150– 271	n.d.	n.d.	Maloof and others, 2001
Fort Knox	22	2–8	Some	1.25–1.5	330–370	12.0–13.5	-3.4	Goldfarb and others, 1997; McCoy and others, 1997; Paul Jensen, Teck-Cominco, unpub. data, 2006
Ryan Lode	12	≤8	Yes	0.5–0.75	270–330	11.7–15.0	0.5–3.7	McCoy and others, 1997
Others—Fairbanks district	1–20	3–5	n.d.	n.d.	275–375	n.d.	0.3–4.1; 8.2–10.9	Metz, 1991; Goldfarb and others, 1997
Pogo	Highly variable	Highly variable	Yes	1.7–2.0	308–570	13.4–15.2	-2.5–+5.5	Smith and others, 1999; Rombach and others, 2002; C. Rombach, unpub. data, 2005
Others—Goodpaster district	Significant amounts	2.5–7.5	Yes	1.4–2.4	225–390	n.d.	n.d.	Dilworth, 2003; R.J. Goldfarb, unpub. data, 2005
Donlin Creek	3–7	3–6	Rare	0.3–0.6	275–300	14.3–24.7	-16– -10	Goldfarb and others, 2004
Shotgun	Variable	Moderate to high	Yes	0.5	280–630	16.4–17.1	-5.9– -5.0	Romach and Newberry, 2001

CHAPTER 4

GOALS OF STUDY

This study aims to better understand the vein-hosted style of mineralization and associated alteration of the Livengood deposit.

Because Au grade is known to increase with both As and Sb concentration, quartz-arsenopyrite, quartz-stibnite, quartz-arsenopyrite-stibnite, and stibnite veins were chosen as the focus of the study. Examples of these vein sets are shown in figure 23.

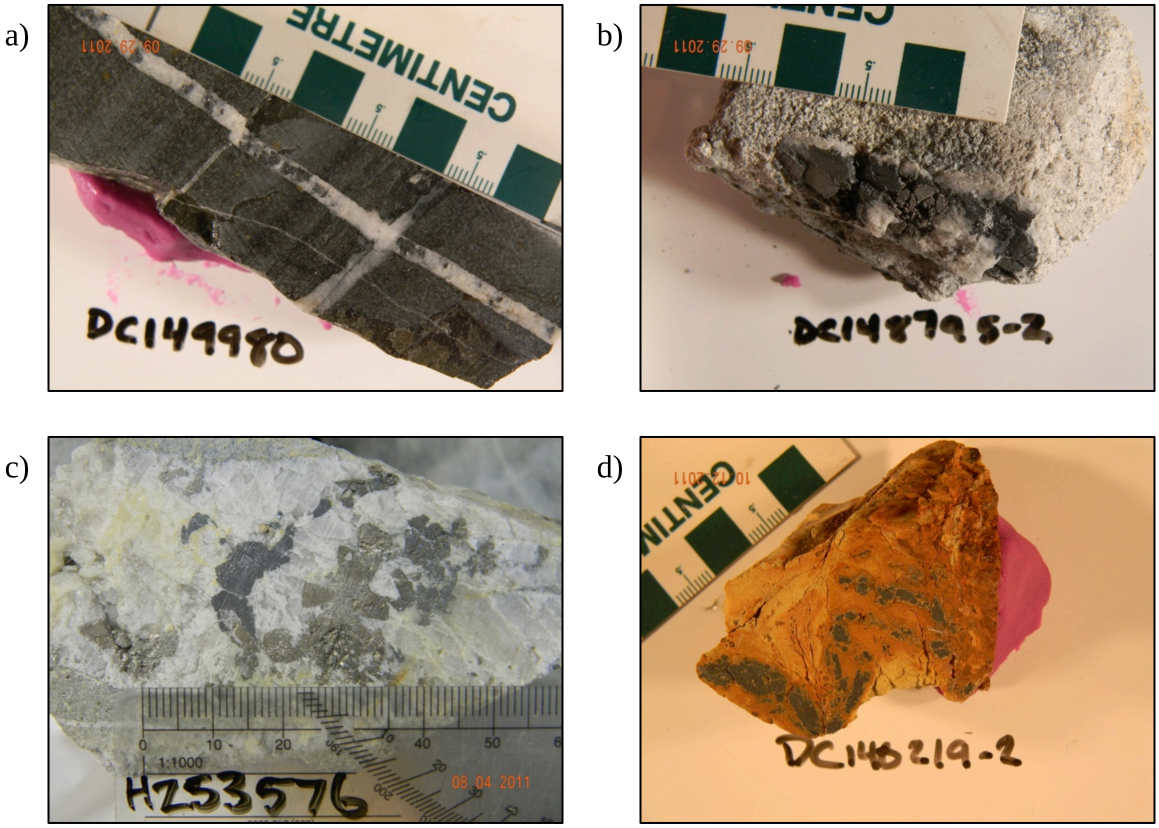

Figure 23: Representative samples of mineralized veins. a) quartz-arsenopyrite, b) quartz-stibnite, c) quartz-arsenopyrite-stibnite, and d) massive stibnite veins.

Four hypotheses were established regarding the vein-hosted mineralization at Livengood. 1) Multiple sets of mineralized vein sets were emplaced during the history of the system. 2) Consistent with Hart and Goldfarb (2005), As- and Sb-associated mineralization occurred at different points in the system's history, with As-associated mineralization occurring earlier, during the hotter stages of the hydrothermal system, and Sb followed during a later, cooler stage. 3) All mineralized veins were emplaced at temperatures similar to other IRGS's, between 275° C and 570° C. 4) the sulfur and oxygen in the mineralizing fluids were mainly derived from a magmatic source.

Because it has been shown that the biotite, albite, and sericite alteration are associated with the Au mineralization at Livengood, three hypotheses were established regarding the alteration. 1) In agreement with cross cutting relationships that show early biotite followed by albite and then sericite, biotite was emplaced during the hottest stage of the system, followed by albite, then sericite. 2) The alteration assemblages were also emplaced at temperatures between 275° C and 570° C. 3) The oxygen in the alteration assemblage silicates was mainly magmatic in origin.

CHAPTER 5

METHODS

Sample Collection

The author collected samples from core holes at the Livengood project (Figure 24). Core had been extracted using a diamond drill between 2006 and 2011. Samples were selected and collected using the following method.

1) Assay results and geologist logs were used to predetermine suitable holes and intervals.
2) From these intervals, samples were chosen based on the presence of mineralized veins or associated alteration. Minerals were identified using a hand lens. Handheld Niton X-ray florescence was used to confirm the presence of As, Sb, Pb, and Zn sulfides.
3) The interval of core being sampled was marked on the core box and photographed. Sample intervals were color coded with Green=thin section, Orange=Sb-rich, Yellow=As-rich, and White=alteration sample.
4) Whole core samples were sawed in half length-wise.
5) Each sample was bagged in a soil sample bag and labeled with the hole number, sample ID, ID extension (if multiple samples were taken with the same sample ID), and interval.
6) A description of each sample was written and added to a file containing the digital geologic log, assay chemistry results, original photos of the uncut core, new photos with marked core boxes, and scanned paper log.

Figure 24: Sample collecting in Livengood, Alaska.

Scanning Electron Microscope

Qualitative compositional analyses of alteration were used to differentiate silicate phases within a single sample. Analyses were performed using a Zeiss 1450EP Scanning Electron Microscope at the University of Georgia Center for Applied Ultrastructural Research.

Petrography

Petrographic descriptions were done on polished thin sections using an Olympus BX40 transmitted and reflected light microscope. Mineralogy, grain size, and mineral relationships were all noted. Photomicrographs were taken with a 10 megapixel Olympus digital camera.

Sulfur Isotopes

Sulfur isotope samples were prepared and analyzed at the University of Georgia Department of Geology Stable Isotope Laboratory. Sulfide samples, including arsenopyrite, pyrite, sphalerite, stibnite, galena and other unknown Sb-minerals, were first powdered using a diamond drill bit. Table 5 shows each sulfide and their corresponding target sample weight based on obtaining 100µmols of SO_2 gas. Unknown Sb-minerals were treated as stibnite.

Table 5: Sulfides analyzed. Table shows each sulfide's molecular weight, theoretical SO_2 released, and target sample weight based on obtaining 100µmol SO_2.

Sulfide	Molecular Weight (g/mol)	SO_2 Released (µmols/mg)	Target Weight (mg) for 100µmol SO_2
Arsenopyrite ($FeAsS_2$)	247.80	4.04	24.75
Pyrite (FeS_2)	119.98	16.67	6.00
Sphalerite (ZnS)	97.43	10.26	9.75
Stibnite (Sb_2S_3)	339.69	8.83	11.33
Galena (PbS)	239.27	4.18	23.92

Powdered sulfides were then mixed with V_2O_5, copper metal powder, and silica powder. V_2O_5 provides the necessary oxygen to react with sulfur to make SO_2 gas. The copper metal powder buffers the oxygen fugacity to suppress the formation of SO and SO_3. The silica powder acts as an abrasive during grinding. The mixture was then ground for 5 minutes with an agate mortar and pestle (Figure 25).

Figure 25: Sample preparation for sulfur isotopes. Powdered sulfides, V_2O_5, copper metal powder, and silica powder ready to be ground.

The ground sample was loaded into a quartz tube and combusted in a 1050° C furnace for 10 minutes. The resultant SO_2 gas was then cryogenically isolated from the other gasses produced (non-condensable gasses, CO_2, and H_2O) on a cryogenic purification line. The amount of isolated SO_2 gas was measured using a calibrated mercury manometer and reported as the actual SO_2 yield. Actual yield was compared to theoretical yield and recorded as percent yield. The SO_2 gas was collected in a Pyrex breakseal tube and analyzed using a Finnigan MAT 252 mass spectrometer. An error of ±0.2 2σ was calculated on replicate analysis of NZ-1 and NBS-123 standards.

Oxygen Isotopes

Oxygen isotope samples were prepared and analyzed at the University of Georgia Department of Geology Stable Isotope Laboratory according to the method presented by Spicuzz et al. (1998). Samples were analyzed using a Finnigan MAT 252 mass spectrometer. An error of ±0.7 2σ was calculated on replicate analysis of NBS-28 standard.

CHAPTER 6

RESULTS

Full results of ITH assay chemistry, Niton XRF, sulfur isotopes of mineralized veins, oxygen isotopes of mineralized veins, oxygen isotopes of alteration, core sample photographs, and ITH geologic descriptions of samples are found in Appendices A-K.

Petrography

Table 6: Petrographic description and photomicrographs of select vein samples.

Sample No.	Description
DC128717-5	Quartz-stibnite-arsenopyrite vein: quartz matrix with ~8pct subhedral to euhedral 1mm arsenopyrite and ~11pct anhedral stibnite that appears to infill voids and envelop preexisting arsenopyrite. Vein is larger than slide, so contact with host rock can not be observed.
H253524-2	Altered Cretaceous dike with small quartz-arsenopyrite-muscovite-calcite vein: 5mm vein of 80% subhedral quartz, 10% subhedral arsenopyrite, 5% anhedral calcite, and 5% fine grained, radiating muscovite cuts the host dike. Contact between vein and dike is sharp. The dike is comprised of phenocrysts of muscovite, biotite, and feldspar in a groundmass of feldspar and arsenopyrite. Outboard of the vein contact is a 10mm envelope of fine grained, secondary muscovite (sericite alteration) replacing the original biotite. Outboard of this envelope the original minerals of the dike are preserved.

Stable Isotopes of Mineralized Veins

Sulfur isotope results of sulfides within mineralized veins are summarized in table 7, with full results in Appendix A. Results were separated based on the vein category and which sulfide was analyzed. The mean and range of $\delta^{34}S_{CDT}$ results are compated in table 7 and plotted in figure 26. Table 7 also shows the mean calculated $\delta^{34}S_{H2S}$ at 300° C and 400° C. These temperatures represent reasonable temperatures for mineralization in an IRGS deposit (see Chapter 3).

Table 7: Summarized results of sulfur isotope analyses of mineralized veins. Fractionation curve by Ohmoto and Rye (1979) was used for fluid composition calculation. Full results are listed in appendix A.

Vein Mineralogy	Sulfide analyzed	# of analyses	Mean $\delta^{34}S_{CDT}$ (‰)	$\delta^{34}S_{CDT}$ range (‰)	$\delta^{34}S_{H2S}$ (‰) (300° C)	$\delta^{34}S_{H2S}$ (‰) (400° C)
Qtz-asp-stib	asp	10	-5.1	-6.1 to -3.9	N/A	N/A
Qtz-asp-stib	Stib	12	-4.4	-5.3 to -3.6	-2.1	-2.7
Qtz-asp	asp	19	-4.9	-6.5 to -3.5	N/A	N/A
Qtz-stib	stib	7	-4.4	-5.7 to -3.0	-2.1	-2.7
Massive stib	stib	5	-3.9	-4.4 to -3.2	-1.6	-2.2

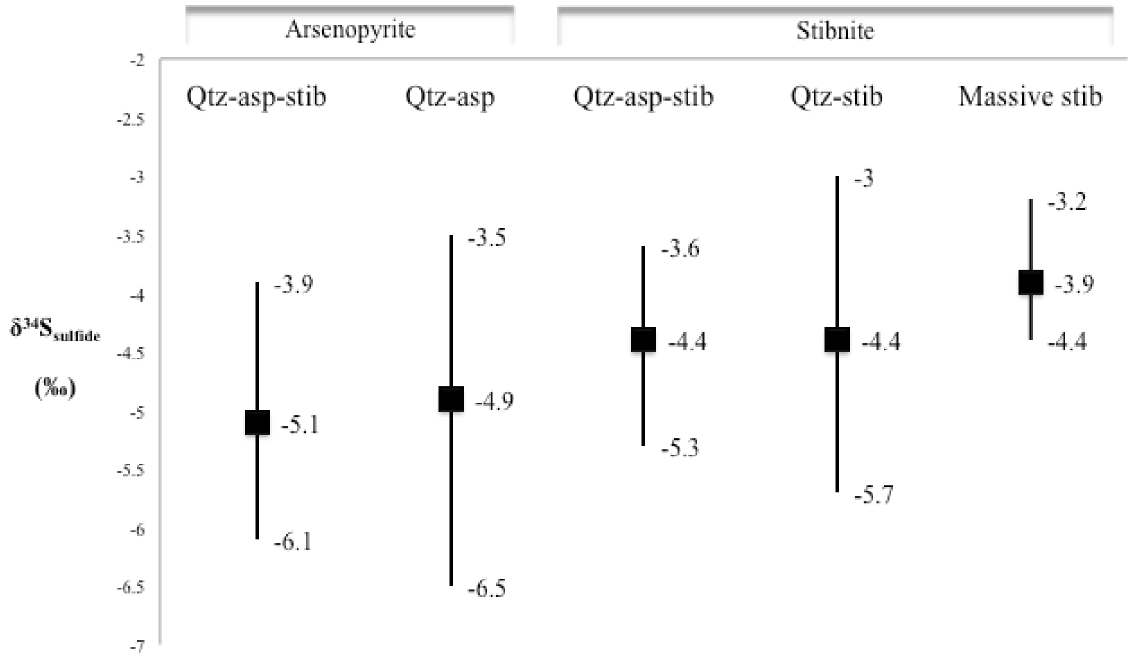

Figure 26: Plot of sulfur isotope results of mineralized veins. The range and mean (black square) of the results are shown for each vein category.

In some of the mineralized veins sampled, multiple sulfide phases coexist (figures 27-31). In these cases, sulfur isotope ratios were measured for all of the sulfides present including sphalerite, pyrite, and galena. Due to the single-stage nature of the veins (see Petrography results), these sulfides were assumed to be in equilibrium with one another, and an equilibrium temperature was calculated. These calculations are shown in table 8.

Table 8: Calculated temperatures of mineralized veins. Fractionation curves by Ohmoto and Rye, 1979 and Li and Liu, 2006 were used. (-) indicates that a temperature could not be calculated.

Sample No.	Mineral A	$\delta^{34}S_A$ (‰)	Mineral B	$\delta^{34}S_B$ (‰)	Δ_{A-B} (‰)	T (°C)
H253528-2	Galena	-5.7	Stibnite	-5.3	-0.4	-
H235882-1	Sphalerite	-6.2	Stibnite	-3.6	-2.4	-
H235882-1	Pyrite	-5.1	Sphalerite	-6.2	1.1	250
H235882-2	Pyrite	-6.6	Stibnite	-4.0	-2.6	-
H253906-2	Pyrite	-7.4	Sphalerite	-6.3	-1.1	-
H253906	Pyrite	-8.5	Sphalerite	-7.6	-0.9	-
H253529	Sphalerite	-8.5	Stibnite	-4.6	-3.9	-

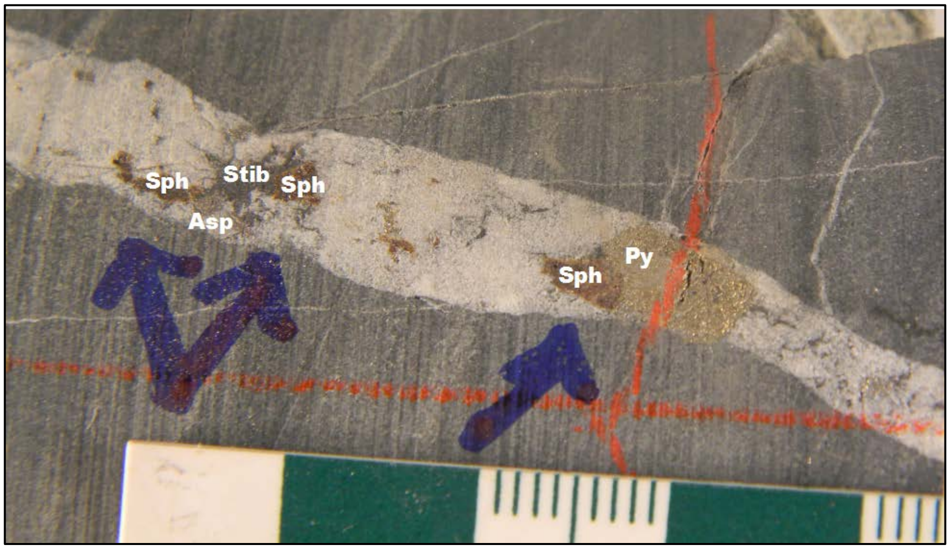

Figure 27: Sample H253529. Quartz-pyrite-sphalerite-stibnite-arsenopyrite vein.

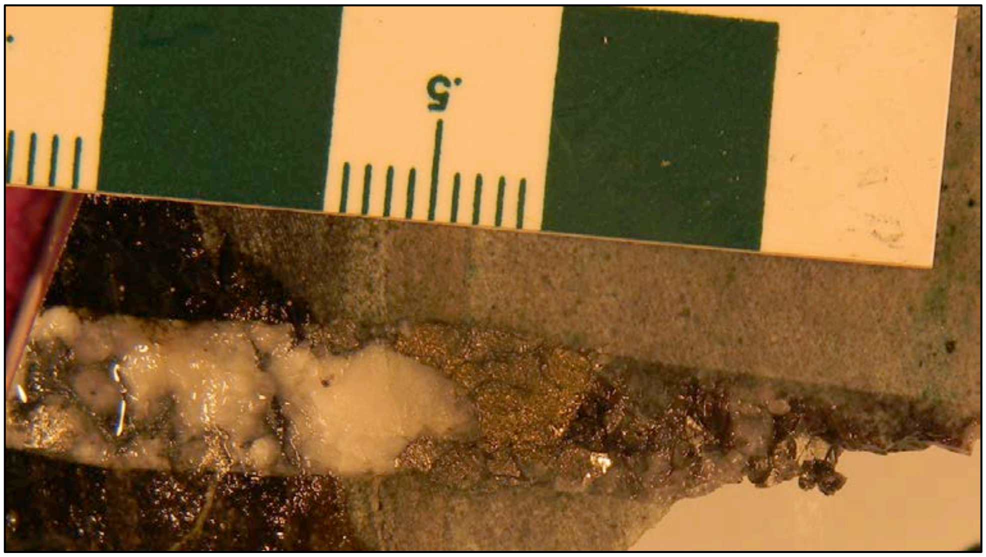

Figure 28: Sample H253528-2. Quartz-arsenopyrite-stibnite-galena-pyrite-sphalerite vein.

Figure 29: Sample H253906. Quartz-arsenopyrite-pyrite-sphalerite vein.

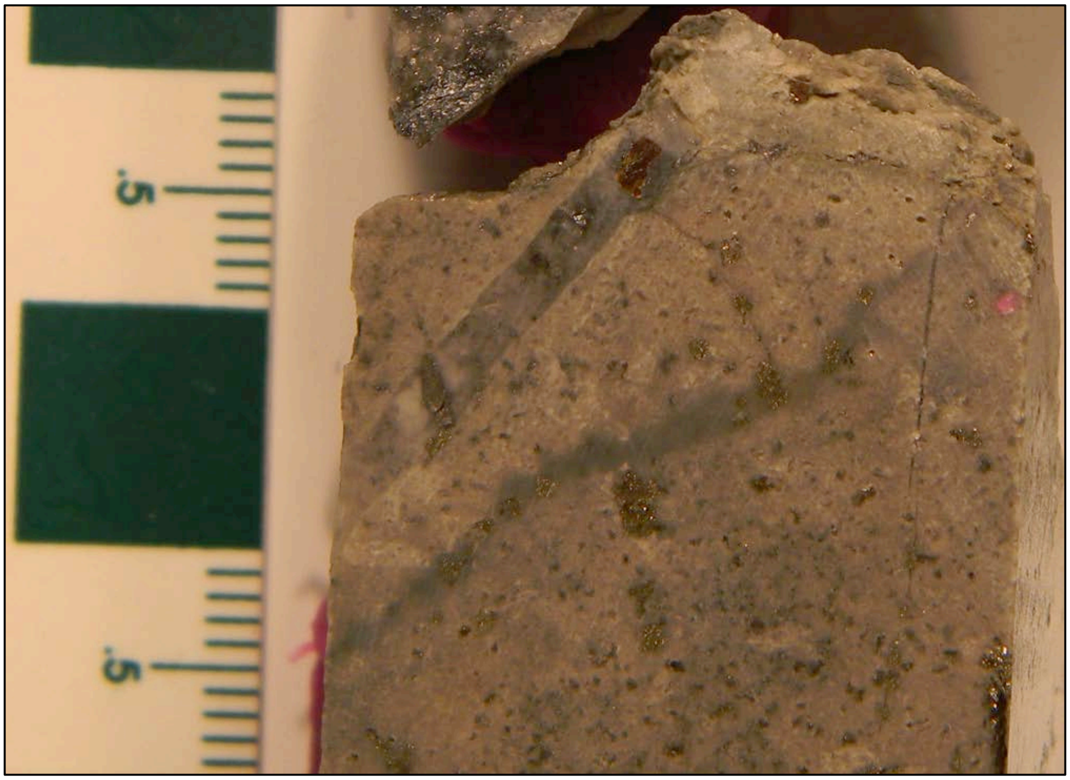

Figure 30: Sample H253906-2. Quartz-arsenopyrite-pyrite-sphalerite vein.

Figure 31: Sample H253882-1. Quartz-arsenopyrite-stibnite-pyrite-sphalerite vein.

Oxygen isotope results of quartz within mineralized veins are summarized in table 8, with full results in Appendix B. Results were separated based on the vein category. The mean and range of $\delta^{18}O_{SMOW}$ results are compared in table 9 and plotted in figure 32. Table 8 also shows the mean calculated $\delta^{18}O_{H2O}$ at 300° C and 400° C. These temperatures represent reasonable temperatures for mineralization in an IRGS deposit (see Chapter 3).

Table 9: Summarized results of oxygen isotope analyses of mineralized veins. Sharp and Kirschner (1994) was used for fluid composition calculation. Full results are listed in appendix B.

Vein Mineralogy	# of analyses	Mean $\delta^{18}O_{SMOW}$ (‰)	$\delta^{18}O_{SMOW}$ range (‰)	$\delta^{18}O_{H2O}$ (‰) (300°C)	$\delta^{18}O_{H2O}$ (‰) (400°C)
Qtz-asp-stib	2	16.8	16.8 to 16.9	8.6	11.6
Qtz-asp	6	16.8	14.0 to 18.9	8.6	11.6
Qtz-stib	1	16.3	16.3	8.1	11.1
Massive stib	N/A	N/A	N/A	N/A	N/A

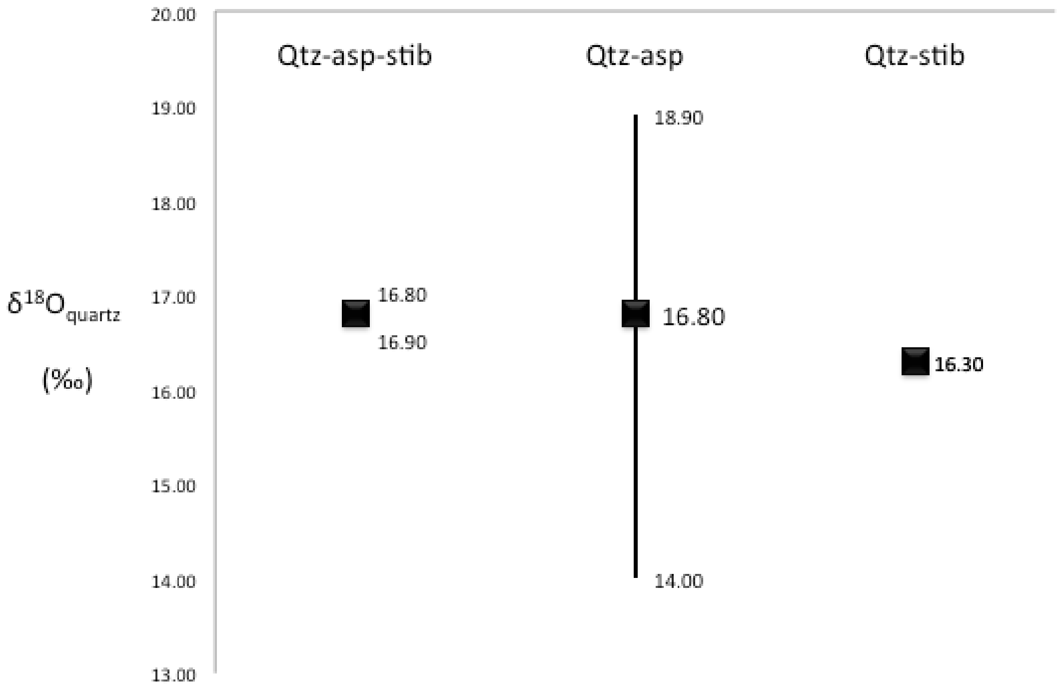

Figure 32: Plot of $\delta^{18}O_{quartz}$ of mineralized veins. The range and mean (black square) of the results are shown for each vein category.

Stable Isotopes of Alteration

Oxygen isotope results of silicate alteration phases are summarized in table 10, with full results in appendix C.

Table 10: Summarized results of oxygen isotope analyses of alteration. Full results are listed in appendix C.

Alteration Mineral	# of analyses	Mean $\delta^{18}O_{SMOW}$ (‰)	$\delta^{18}O_{SMOW}$ range (‰)
Biotite	2	11.3	11.2 to 11.4
Albite	3	14.3	14.1 to 14.6
Sericite	3	13.7	13.1 to 14.4

In the case of each alteration stage, quartz was a coexisting phases (Figures 33-36). These phases were assumed to be in equilibrium and an equilibrium temperature and fluid composition ($\delta^{18}O_{H2O}$) was calculated. The calculations and results are shown in table 11.

Table 11: Calculated temperatures and fluid composition of alteration. Fractionation curves by Bottinga and Javoy (1975), Clayton and Keiffer (1991), and Chacko et al. (1996) were used to calculated temperatures. (-) indicates the pair was not in equilibrium.

Sample No.	Mineral A	$\delta^{18}O_A$ (‰)	Mineral B	$\delta^{18}O_B$ (‰)	Δ_{A-B} (‰)	T (°C)	$\delta^{18}O_{H2O}$ (‰)
DC152389	Biotite	11.2	Quartz	17.0	-5.8	486	13.6
DC152389	Biotite	11.4	Quartz	17.0	-5.6	498	13.8
DC129260	Albite	14.1	Quartz	15.2	-1.1	648	-
DC129260	Albite	14.2	Quartz	15.2	-1.0	695	-
DC128662-1	Albite	14.6	Quartz	18.2	-3.6	205	-
DC129163	Sericite	13.1	Quartz	17.6	-4.5	284	10.1

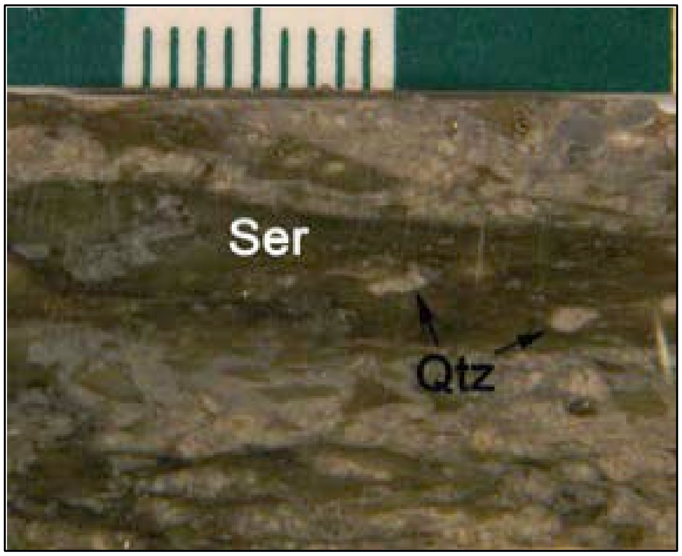

Figure 33: Sample DC129163

Figure 34: Sample DC152389

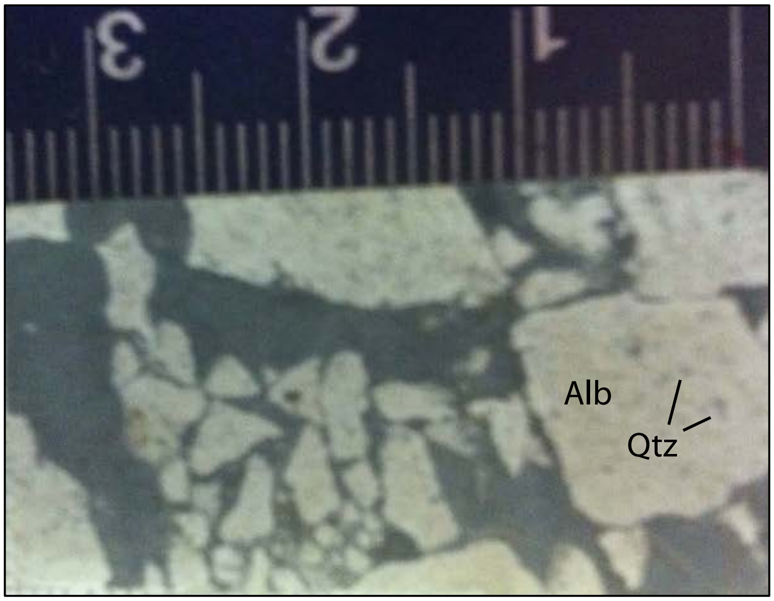

Figure 35: Sample DC128662-1

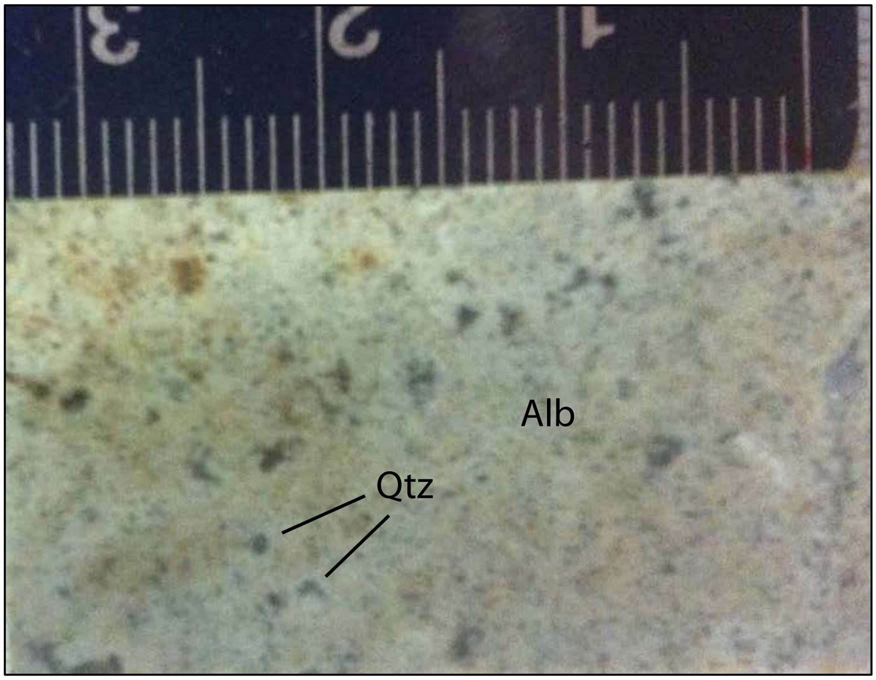

Figure 36: Sample DC129260

CHAPTER 7

DISCUSSION

Petrography

The petrographic study of veins in polished section from the Livengood deposit shows a wide variation in host lithologies, degrees and types of alteration, vein mineral assemblages, and sulfide grain size (Table 6). There was, however, one consistent textural observation: when mineralized veins were present, they appeared to be single stage. The relatively sharp contact with the host rock and the relationship of the minerals within the vein, suggests precipitation during a single hydrothermal fluid event.

Stable Isotopes of Mineralized Veins

During the life of a hydrothermal system, like the one that was responsible for the Au mineralization at the Livengood deposit, conditions typically change over time. Fluid source, temperature, pressure, and water-rock interaction can vary significantly with time as a mineral deposit forms. As minerals precipitate from the hydrothermal fluids, stable isotope ratios will reflect temperature and fluid conditions at the time. In this study, measured sulfur and oxygen isotopic ratios of Au-bearing veins were used to determine the state of the fluid at the time of mineralization. These measurements were used to track changes in fluid conditions over time.

Sulfur isotope analyses of arsenopyrite and stibnite in mineralized veins yielded values of $\delta^{34}S_{asp}$ = -6.5‰ to -3.1‰, and $\delta^{34}S_{stib}$ = -5.7‰ to -3.0‰. Because IRGS's are readily accepted to form between 300° C and 400° C (Table 4), $\delta^{34}S_{H2S}$ calculations were done using the end members of this range. At an assumed temperature of 300° C, calculated $\delta^{34}S_{H2S}$ is -2.1‰ to -1.6‰. At an assumed temperature of 400° C, calculated $\delta^{34}S_{H2S}$ is -2.7‰ to -2.2‰. These values fall within the range of primary magmatic fluids, $\delta^{34}S$ = 0±5‰ (e.g. Ohmoto and Rye, 1979), but are consistently slightly ^{34}S-depleted.

When comparing our sulfur isotope results to other IRGS's within the Tintina Gold Province, we see that ^{34}S-depleted results are common (Table 12 and Figure 37). The Mair et al. (2006) study of arsenopyrite in Au-bearing veins at the Scheelite Dome deposit yielded a similar range of $\delta^{34}S$ values, but with a lightly more negative mean. They attributed the deviation from 0‰ to fluid interaction with metasedimentary country rocks. The Goldfarb et al. (2004) stable isotope study of sulfides in Au-bearing veins at the Donlin Creek deposit yielded significantly more variable and negative $\delta^{34}S$ results for both arsenopyrite and stibnite. They attribute this to be a result of hydrothermal fluid interaction with diagenetic pyrite of the country rock. They also point out that stibnite results show a significantly more negative $\delta^{34}S$ mean, and greater range in values. Their preferred explanation is that there were two distinct hydrothermal events: an early, arsenopyrite-dominated event followed by a later, stibnite-dominated event.

Table 12: $\delta^{34}S_{sulfide}$ of mineralized veins in Tintina Gold Province IRGS deposits.

Deposit	Sulfide analyzed	$\delta^{34}S_{sulfide}$ (‰)	Reference
Livengood	asp	-6.5 to -3.1	This study
Livengood	stib	-5.7 to -3.0	This study
Scheelite Dome	asp	-10.9 to -7.1	Mair et al., 2006
Donlin Creek	asp	-21.2 to -10.0	Goldfarb et al., 2004
Donlin Creek	Stib	-27.2 to -7.5	Goldfarb et al., 2004

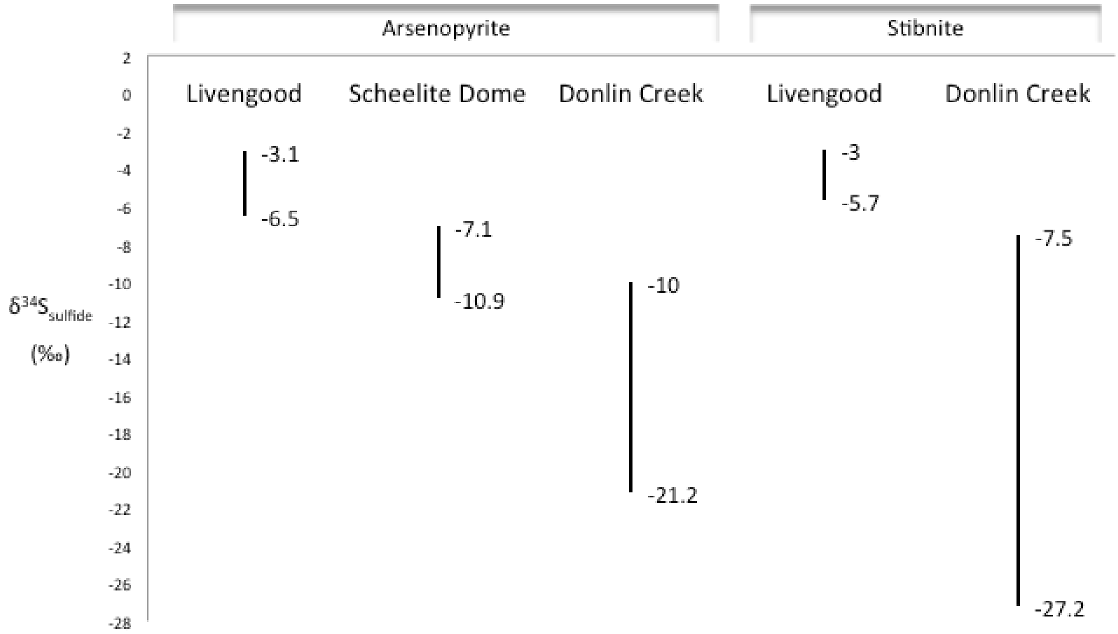

Figure 37: Plot of $\delta^{34}S_{sulfide}$ of mineralized veins in the Tintina Gold Province IRGS deposits.

Given the known, direct relationship of the mineralization of IRGS's to a magmatic intrusion and the results of other isotopic studies of Tintina Gold Province IRGS's, these results suggest that a primary magmatic fluid source was interacting with a

^{34}S-depleted sulfur source at depth. It is likely that the ascending fluid would have interacted with the lower sediments within the Devonian volcano-sedimentary package. These sediments contain abundant black shales with up to 10% diagenetic pyrite. Biologically mineralized pyrite is known to be depleted in ^{34}S (Ohmoto and Rye, 1979) and would draw the $\delta^{34}S$ value of the fluid down.

Oxygen isotope analyses of quartz within mineralized veins yielded results of $\delta^{18}O = 14.0$ to 18.9. At an assumed temperature of 300° C, $\delta^{18}O_{H2O}$ would be 8.1‰ to 8.6‰. At an assumed temperature of 400° C, $\delta^{18}O_{H2O}$ would be 11.1‰ to 11.7‰. These values are consistent with a primary magmatic fluid source, $\delta^{18}O = 5.5‰$ to 10.0‰ (Sheppard, 1986). The results of this oxygen isotope study are very similar to those of other IRGS's in the Tintina gold province (Tables 13, Table 14, Figure 38, and Figure 39). The Goldfarb et al. (2004) study of the Donlin Creek deposit yielded more extreme $\delta^{18}O_{quartz}$ than the Livengood deposit. The more enriched values could be attributed to a shift in fluid composition.

Table 13: δ18O$_{quartz}$ of mineralized veins in Tintina Gold Belt IRGS's.

Deposit	$\delta^{18}O_{quartz}$ (‰)	Reference
Livengood	14.0 to 18.9	This study
Scheelite Dome	14.1 to 19.0	Mair et al., 2006
Fort Knox	12.0 to 13.5	Goldfarb et al., 1997; McCoy et al., 1995
Pogo	13.4 to 15.2	Smith et al., 1999; Rombach et al., 2002
Donlin Creek	14.3 to 24.7	Goldfarb et al., 2004

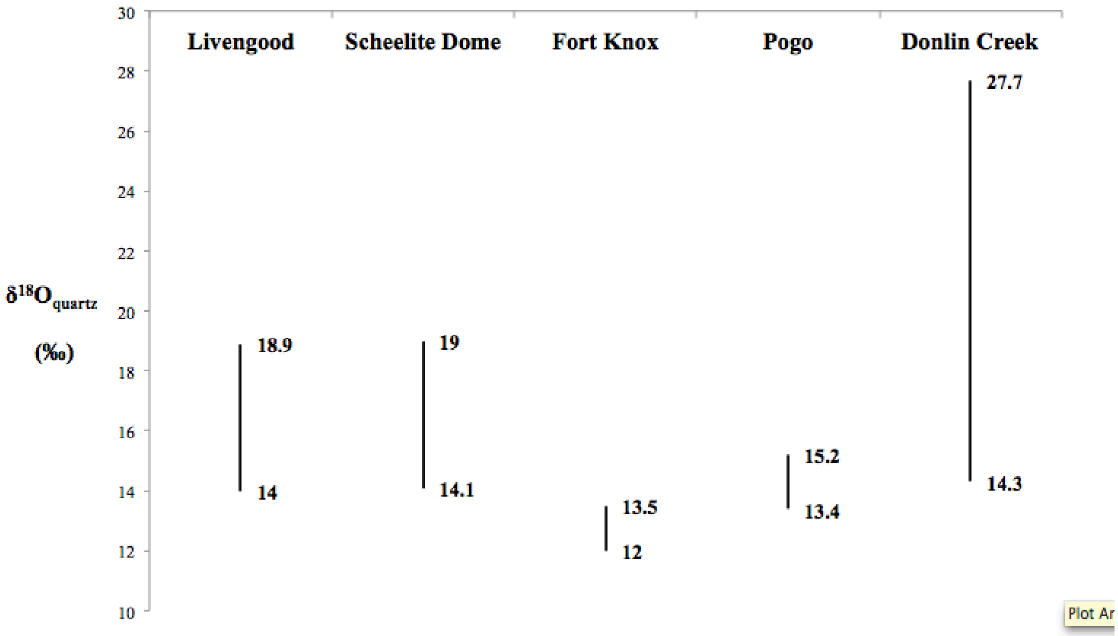

Figure 38: Plot of $\delta^{18}O_{quartz}$ of mineralized veins in Tintina Gold Province IRGS's.

Table 13: $\delta18O_{H2O}$ of mineralized veins in Tintina Gold Belt IRGS's.

Deposit	$\delta^{18}O_{H2O}$ (‰)	Reference
Livengood	8.1 to 11.7	This study
Scheelite Dome	7.1 to 13.0	Mair et al., 2006
Donlin Creek	7.0 to 12.0	Goldfarb et al., 2004

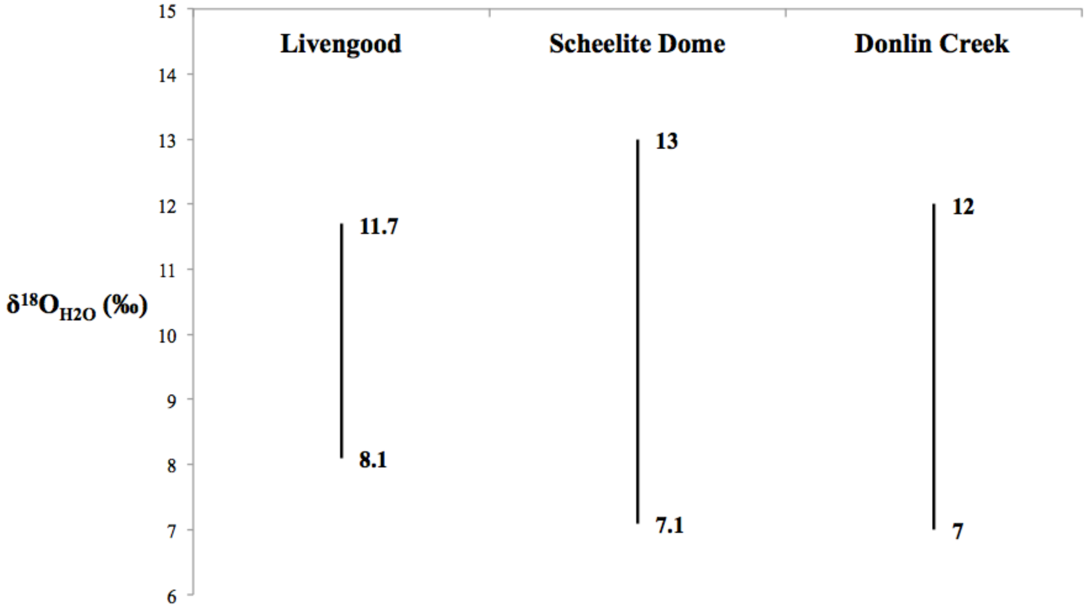

Figure 39: Plot of $\delta18O_{H2O}$ of mineralized veins in Tintina Gold Belt IRGS's.

In the instances when accessory sulfides (pyrite, galena, sphalerite) were present in a mineralized vein, stable isotope ratios of these sulfides were measured. From these measurements, a closure temperature calculation was attempted. In all but one case, unreasonable temperatures were calculated. In sample H235882-1, a pyrite-sphalerite pair yielded a reasonable temperature of 250° C, while a sphalerite-stibnite pair within the same vein boundaries was not in equilibrium. This could indicate that there was one mineralizing event that precipitated the pyrite and sphalerite, and a separate event that precipitated the stibnite. This, however, seems unlikely because other veins with pyrite-sphalerite pairs were not in equilibrium. It is likely that the temperature that was calculated was serendipitous. In all other samples, the results indicate that sulfides within a single vein's boundaries were not in equilibrium, and imply that they were not precipitated from the same fluid.

The results of $\delta^{34}S_{sulfide}$ analyses were consistent between arsenopyrite, stibnite, and quartz: there was no significant variation seen in either the mean or range of the sulfur or oxygen isotopes when comparing these minerals in the four vein sets. These consistent isotopic ratios could imply that the vein sets were coevally emplaced, and that As- and Sb-associated mineralization occurred at the same point during hydrothermal circulation. This, however, seems unlikely because of the abundant cross cutting sets of veins and disequilibrium between coexisting sulfides within veins. It could also be argued that the similarity among the stable isotopes for different mineralizing vein sets does not preclude the vein sets from being emplaced at different times or conditions.

Stable Isotopes of Alteration

Because biotite, albite, and sericite alteration facies are shown to be associated with Au mineralization at the Livengood deposit, oxygen isotope ratios were measured to help constrain the fluid conditions. $\delta^{18}O_{biotite}$ = 11.2‰ to11.4‰, $\delta^{18}O_{albite}$ = 14.1‰ to

14.6‰, and $\delta^{18}O_{sericite}$ = 13.1‰ to 14.4‰. Since quartz appears to occur coevally with all three phases, quartz was also analyzed, and an equilibrium temperature of each alteration was calculated. For biotite-quartz, temperatures of 486° C to 498° C were calculated. These temperatures are reasonable for the higher temperature portions of IRGS's and correlates with observed early biotite in hand sample and thin section. For albite-quartz, temperatures of 695° C, 648° C, and 205° C were calculated. These temperatures are inconsistent and are likely too extreme to occur in an IRGS deposit. Most likely, these unreasonable temperatures signify that the albite and quartz were not in isotopic equilibrium, and therefore, are unreliable as a thermometer. For sericite-quartz, a temperature of 284° C was calculated. This temperature is reasonable for the cooler stages of an IRGS's and correlates with observed cross cutting relationships.

Using the temperatures for biotite and sericite alteration facies, $\delta^{18}O_{H2O}$ was calculated. For sericite, $\delta^{18}O_{H2O}$ is 10.1‰. The value of sericite are consistent with a primary magmatic fluid source, $\delta^{18}O$ = 5.5‰ to 10.0‰ (Sheppard, 1986). The value is also very similar to isotopic fluid compositions calculated for mineralized veins at Livengood and other IRGS deposits (Table 13). This could imply that the fluids responsible for vein-hosted mineralization are the same that were responsible for sericite alteration.

For biotite, calculated $\delta^{18}O_{H2O}$ is 13.6‰ and 13.8‰. These values are slightly more ^{18}O-enriched than primary magmatic fluids. Biotite is also more ^{18}O-enriched than fluid compositions of mineralized veins at Livengood. This indicates that biotite alteration was sourced from a slightly more ^{18}O-enriched source, and implies that it precipitated from a different fluid than the mineralization and sericite alteration. $\delta^{18}O_{H2O}$

for biotite is, however, within the range of $\delta^{18}O_{H2O}$ of vein-hosted mineralization for two other IRGS deposits, Scheelite Dome and Donlin Creek (Table 13).

CHAPTER 8

CONCLUSIONS

Results of petrography and stable isotope analyses help to reach the goals of this study and address the numerous hypotheses. We are now able to better understand the vein-hosted Au mineralization of the Livengood deposit, as well as its associated alteration.

The vein-hosted mineralization history of Livengood is complicated and poorly understood. Although vein sets could not be distinguished from one another based on their $\delta^{34}S$ or $\delta^{18}O$ values, observed hand sample and petrographic relationships allow us to confirm that there were multiple sets of mineralized veins emplaced during the history of the Livengood hydrothermal system. Since sulfides within a single vein are not in isotopic equilibrium, we can conclude that either, 1) veins were reopened and filled by mineralizing fluids at a different temperature and/or $\delta^{34}S_{H2S}$ composition, or 2) during a single stage of vein filling, the temperature and/or $\delta^{34}S_{H2S}$ composition changed. Because of this a temperature could not be calculated. Therefore, we can neither confirm nor refute that vein-hosted mineralization occurred at temperatures similar to other IRGS's or that As- and Sb-associated mineralization occurred at different times and temperatures during the hydrothermal system. $\delta^{34}S_{H2S}$ and $\delta^{18}O_{H2O}$ calculations support the hypothesis that vein-hosted mineralization sulfur and oxygen was primarily sourced from magmatic fluids.

Prior research and observations showed that biotite, albite, and sericite alteration facies were associated with the vein-hosted mineralization at Livengood. $\delta^{18}O_{H2O}$ calculations of these alteration events and comparison to $\delta^{18}O_{H2O}$ of the mineralization substantiate this for the sericite alteration. However, fluid composition differences between biotite alteration and vein-hosted mineralization suggest that they may not have been derived from fluids at the same conditions. $\delta^{18}O_{H2O}$ of alteration is within the range of, or only slightly higher than magmatic fluids, and allows us to confirm that this is the primary source of oxygen of the biotite and sericite alterations. Temperature calculations of biotite and sericite alteration facies allow us to confirm what was observed in cross-cutting relationships: early, hotter biotite facies followed by later, cooler sericite facies fluids. Calculated temperatures also allow us to confirm that the alteration formed at temperatures similar to other IRGS's (275° C to 570° C).

REFERENCES

Albanese, M., 1983, Geochemical Reconnaissance of the Livengood B-3, B-4, C-3, and C-4 Quadrangles, Alaska: Summary of the Data on Stream-sediment, Pan-concentrate, and Rock Samples, Alaska Division of Geological and Geophysical Surveys.

Arbogast, B., Lee, G., and Light, T., 1991, Analytical results and sample locality map of stream-sediment and heavy, mineral-concentrate samples from the Livengood 1 degree X 3 degree Quadrangle: Alaska: US Geological Survey, Open file Report OF.

Athey, J.E., and Craw, P.A., 2004, Geologic Map of the Livengood SW C-3 and SE C-4 Quadrangles, Tolovana Mining District, Alaska, State of Alaska, Department of Natural Resources, Division of Geological & Geophysical Surveys.

Bakke, A., 1995, The Fort Knox ‘porphyry’gold deposit—Structurally controlled stockwork and shear quartz vein, sulfide-poor mineralization hosted by a Late Cretaceous pluton, east-central Alaska.: Porphyry Deposits of Northwestern Cordillera of North America. Canadian Institute of Mining and Metallurgy.

Brechtel, C., Carew, T., Myers, R., Pennstrom, W., Puchner, C., and Wilson, S., August 2011, Summary Report on the Livengood Project, Tolovana District, Alaska.

Brooks, A., 1915, Mineral Resources of Alaska, Report on Progress of Investigations in 1915: US Geological Survey Bulletin, v. 642.

Chacko, T., Hu, X., Mayeda, T.K., Clayton, R.N., and Goldsmith, J.R., 1996, Oxygen isotope fractionations in muscovite, phlogopite, and rutile: Geochimica et Cosmochimica Acta, v. 60, p. 2595-2608.

Chapman, R., and Weber, F., 1972, Geochemical analyses of bedrock and stream sediment samples from the Livengood Quadrangle: Alaska: US Geological Survey Open-file report, p. 72-67.

Chapman, R.M., Weber, F.R., and Taber, B., 1971, Preliminary geologic map of the Livengood Quadrangle, Alaska, Geological Survey.

Churkin, M., Foster, H., Chapman, R., and Weber, F., 1982, Terranes and suture zones in east central Alaska: Journal of Geophysical Research: Solid Earth (1978‚Äì2012), v. 87, p. 3718-3730.

Clayton, R.N., and Kieffer, S., 1991, Oxygen isotopic thermometer calibrations: Stable isotope geochemistry: A tribute to Samuel Epstein, v. 3, p. 3-10.

Cobb, E.H., 1972, Metallic mineral resources map of the Tanana Quadrangle: Alaska: US Geological Survey Miscellaneous Field Studies Map MF-371, v. 1.

Dilworth, K.M., 2003, Geological setting, nature and evolution of reduced intrusions and gold bearing quartz veins of the 4021 prospect, Goodpaster District, east-central Alaska.

Foster, R.L., 1968, Potential for lode deposits in the Livengood gold placer district, east-central Alaska, US Department of the Interior.

Goldfarb, R.J., Farmer, G.L., Cieutat, B.A., and Meier, A.L., 1997, Major-element, Trace Element, and Strontium-Isotope Systematics of Natural Waters in the Fairbanks Mining District: Constraints from Local Geology: Geological studies in Alaska by the US Geological Survey, p. 139-150.

Goldfarb, R., Baker, T., Dube, B., Groves, D.I., Hart, C.J., and Gosselin, P., 2005, Distribution, character and genesis of gold deposits in metamorphic terranes.

Goldfarb, R., Hart, C., Miller, M., Miller, L., Farmer, G.L., and Groves, D., 2000, The Tintina gold belt: A global perspective: British Columbia and Yukon Chamber of Mines, Special Volume, v. 2, p. 5-34.

Goldfarb, R.J., Ayuso, R., Miller, M.L., Ebert, S.W., Marsh, E.E., Petsel, S.A., Miller, L.D., Bradley, D., Johnson, C., and McClelland, W., 2004, The late Cretaceous Donlin Creek gold deposit, Southwestern Alaska: Controls on epizonal ore formation: Economic Geology, v. 99, p. 643-671.

Goldfarb, R.J., Marsh, E.E., Hart, C.J., Mair, J.L., Miller, M., and Johnson, C., 2007, Geology and Origin of Epigenetic Lode Gold Deposits, Tintina Gold Province, Alaska and Yukon: Recent US Geological Survey Studies in the Tintina Gold Province, Alaska, United States, and Yukon, Canada: US Geological Survey Scientific Investigations Report, p. A1-A18.

Groves, D.I., Goldfarb, R.J., Robert, F.O., and Hart, C.J., 2003, Gold deposits in metamorphic belts: overview of current understanding, outstanding problems, future research, and exploration significance: Economic Geology, v. 98, p. 1-29.

Hart, C., and Goldfarb, R., 2005, Distinguishing intrusion-related from orogenic gold systems, New Zealand Minerals Conference Proceedings, p. 125-133.

Hart, C., McCoy, D., Goldfarb, R., Smith, M., Roberts, P., Hulstein, R., Bakke, A., and Bundtzen, T., 2002, Geology, exploration, and discovery in the Tintina Gold Province, Alaska and Yukon: Special Publication-Society Of Economic

Geologists, v. 9, p. 241-274.

Hart, C., Villeneuve, M., Mair, J., Goldfarb, R., Selby, D., Creaser, R., and Wijns, C., 2004, Comparative U Pb, Re, Os and Ar, Ar geochronology of mineralizing plutons in Yukon and Alaska, SEG.

Hart, C.J., 2007, Reduced intrusion-related gold systems: Mineral deposits of Canada: A synthesis of major deposit types, district metallogeny, the evolution of geological provinces, and exploration methods: Geological Association of Canada, Mineral Deposits Division, Special Publication, p. 95-112.

Hitchens, A.C., Orssich C.N., 1995. The Eagle zone gold–tungsten sheeted vein porphyry deposit and related mineralization, Dublin Gulch, Yukon Territory. In: Schroeter, T.G. (Ed.), Porphyry Deposits of the Northwestern Cordillera of North America. Canadian Institute of Minerals and Metallogeny, Special Volume 37, p. 245–254.

International Tower Hill Mines, I., 2011, ITH Fact Sheet. www.ithmines.com

Klipfel, P., Carew, T., and Pennstrom, W., October 2009, Summary Report on the Livengood Project, Tolovana District, Alaska: Livengood.

Lang, J.R., and Baker, T., 2001, Intrusion-related gold systems: the present level of understanding: Mineralium Deposita, v. 36, p. 477-489.

Lang, J.R., Baker, T., Hart, C., and Mortensen, J.K., 2000, An exploration model for intrusion-related gold systems: SEG Newsletter, v. 40, p. 6-15.

Li, Y., and Liu, J., 2006, Calculation of sulfur isotope fractionation in sulfides: Geochimica et Cosmochimica Acta, v. 70, p. 1789-1795.

Mair, J.L., Goldfarb, R.J., Johnson, C.A., Hart, C.J., and Marsh, E.E., 2006, Geochemical constraints on the genesis of the Scheelite Dome intrusion-related gold deposit, Tombstone gold belt, Yukon, Canada: Economic Geology, v. 101, p. 523-553.

Maloof, T.L., Baker, T., and Thompson, J.F., 2001, The Dublin Gulch intrusion-hosted gold deposit, Tombstone plutonic suite, Yukon Territory, Canada: Mineralium Deposita, v. 36, p. 583-593.

Marsh, E.E., Goldfarb, R.J., Hart, C.J., and Johnson, C.A., 2003, Geology and geochemistry of the Clear Creek intrusion-related gold occurrences, Tintina Gold Province, Yukon, Canada: Canadian Journal of Earth Sciences, v. 40, p. 681-699.

McCoy, D., Newberry, R.J., Layer, P., DiMarchi, J.J., Bakke, A., Masterman, J.S., and Minehane, D.L., 1997, Plutonic-related gold deposits of interior Alaska: Economic Geology Monograph, v. 9, p. 191-241.

McCoy, D., and Olsen, I., 1997, Thermochronology, mineralogy, elemental and microprobe analysis of the Fort Knox, Dolphin and selected Golden Summit deposits, Geology of bulk-mineable, plutonic-hosted and plutonic-related gold deposits of the north Pacific: Short Course Notes, Alaska Miner's Association Annual Convention and Trade Fair, Anchorage, Alaska.

Metz, P.A., 1991, Metallogeny of the Fairbanks mining district: Alaska and Adjacent Areas, University of Alaska, School of Mineral Engineering, Minerals Research Industry Laboratory Report, v. 90, p. 370.

Newberry, R., Field Trip Guide: Lodes, placers, faults, gold, and how they tie together in the Livengood area. <http://www.uaf.edu/files/aqc/FOP2010_RL_lo.pdf>

Newberry, R., and McCoy, D., Exploration Models For Mid And Late Cretaceous Intrusion-Related Gold Deposits In Alaska And The Yukon Territory, Canada.

Newberry, R., McCoy, D., and Brew, D., 1995, Plutonic-hosted gold ores in Alaska:

igneous vs. metamorphic origins: Resource Geology Special Issue, p. 57-100.

Ohmoto, H., and Rye, R., 1979, Isotopes of sulfur and carbon: Geochemistry of hydrothermal ore deposits, p. 509-567.

Ohmoto, H., Rye, R., and Barnes, H., 1979, Geochemistry of hydrothermal ore deposits: H, v. 1.

Plafker, G., Berg, H.C., 1994. Overview of the geology and tectonic evolution of Alaska. In: Plafker G., Berg, H.C. (Eds.), The Geology of Alaska. Geol. Soc. Am., The Geology of North America, G-1, pp. 989–1021.

Puchner, C., and Myers, R., 2008, Geology And Mineralization Of The Livengood Gold Deposit, Alaska: Mining, P. 39.

Robert, F., and Poulsen, K., 2001, Vein formation and deformation in greenstone gold deposits: Reviews in Economic Geology, v. 14, p. 111-155.

Robinson, M., 1983, Bedrock Geologic Map of the Livengood C-4 Quadrangle Alaska: Alaska Division of Geological and Geophysical Surveys: Report of Investigations, p. 83-4.

Rombach, C.S., and Newberry, R.J., 2001, Shotgun deposit: granite porphyry-hosted gold-arsenic mineralization in southwestern Alaska, USA: Mineralium Deposita, v. 36, p. 607-621.

Rombach, C., Newberry, R., Goldfarb, R., and Smith, M., 2002, Geochronology and mineralization of the Liese zones, Pogo deposit, Alaska [abs.], Geological Society of America Abstracts with Programs, Volume 34, p. A114.

Rowins, S.M., 2000, Reduced porphyry copper-gold deposits: A new variation on an old theme: Geology, v. 28, p. 491-494.

Schroeter, T.G., 1995, Porphyry deposits of the northwestern cordillera of North America.

Sharp, Z., and Kirschner, D., 1994, Quartz-calcite oxygen isotope thermometry: A calibration based on natural isotopic variations: Geochimica et Cosmochimica Acta, v. 58, p. 4491-4501.

Sheppard, S.M., 1986, Characterization and isotopic variations in natural waters: Reviews in Mineralogy and Geochemistry, v. 16, p. 165-183.

Sillitoe, R., and Thompson, J., 1998, Intrusion-Related Vein Gold Deposits: Types, Tectono-Magmatic Settings and Difficulties of Distinction from Orogenic Gold Deposits: Resource Geology, v. 48, p. 237-250.

Sillitoe, R., 1993, Gold-rich porphyry copper deposits: Geological model and exploration implications: Geological Association of Canada Special Paper, v. 40, p. 465-478.

Sillitoe, R.H., And Thompson, J.F., 1998, Intrusion-Related Vein Gold Deposits: Types, Tectono-Magmatic Settings and Difficulties of Distinction from Orogenic Gold Deposits: Resource Geology, v. 48, p. 237-250.

Smith, M., Thompson, J., Bressler, J., Layer, P., Mortensen, J., Abe, I., and Takaoka, H., 1999, Geology of the Liese zone: Pogo property, east-central Alaska: Society of Economic Geologists Newsletter, v. 38, p. 12-21.

Smith, M., Thompson, J.F., Moore, K.H., Bressler, J.R., Layer, P., Mortensen, J.K., Abe, I., and Takaoka, H., 2000, The Liese zone, Pogo property: A new high-grade gold deposit in Alaska: The Tintina Gold Belt: Concepts, exploration and discoveries: British Columbia, Yukon Chamber of Mines, Cordilleran Round-Up Special, v. 2, p. 131-144.

Spicuzza, M., Valley, J., Kohn, M., Girard, J., and Fouillac, A., 1998, The rapid heating, defocused beam technique: a CO2-laser-based method for highly precise and accurate determination of delta18O values of quartz: Chemical Geology, v. 144, p. 195-203.

Thompson, J., and Newberry, R., 2000, Gold deposits related to reduced granitic intrusions: Reviews in Economic Geology, v. 13, p. 377-400.

Thompson, J., Sillitoe, R., Baker, T., Lang, J., and Mortensen, J., 1999, Intrusion-related gold deposits associated with tungsten-tin provinces: Mineralium Deposita, v. 34, p. 323-334.

Tucker, T.L., and Smith, M.T., 2000, The Tintina Gold Belt: concepts, exploration, and discoveries, British Columbia and Yukon Chamber of Mines.

Wall, V., 1999, Pluton-related (thermal Aureole) gold, Short Course Notes, Yukon Geoscience Forum.

Wall, V., and Taylor, J., 1991, Thermal aureole gold: Victoria and elsewhere, Annual Selwyn Memorial Symposium 1991 Abstracts.

Waythomas, C., Ten Brink, N., and Ritter, D., 1984, Surficial geologic map of the Livengood B-3: B-4, C-3 and C-4 quadrangles, Yukon, Tanana Upland, Alaska: Alaska Division of Geological & Geophysical Surveys Report of Investigations, p. 84-6.

APPENICES

Appendix A: Sulfur isotopes of mineralized veins. Standard deviation is the internal precision of each analytical analysis.

Lab ID	Sample No.	Sulfide analyzed	Vein Mineralogy	Raw $\delta^{34}S/^{32}S$ Mean	$\delta^{34}S$ /^{32}S Std. Dev.	$\delta^{34}S_{CDT}$ (‰)
S1202203	DC140214-1	stib	massive stib	-18.26	0.032	-4.37
S1202202	DC140218-2-1	stib	massive stib	-18.07	0.012	-4.17
S1202200	DC140219-1-1	stib	massive stib	-17.74	0.013	-3.82
S1109079	DC140219-2-1	stib	massive stib	-17.90	0.014	-3.23
S1202201	DC144215-1-1	stib	massive stib	-17.80	0.025	-3.88
S1110080	DC128694-1	asp	qtz-asp	-19.44	0.016	-4.79
S1112167	DC128724-1-1	asp	qtz-asp	-19.05	0.013	-5.21
S1112168	DC128724-1-2	asp	qtz-asp	-19.69	0.036	-5.89
	DC128724-2	asp	qtz-asp	-19.45	0.01	-4.80
S1202205	DC128732-1	asp	qtz-asp	-19.51	0.012	-5.69
S1112170	Dc129054-1	asp	qtz-asp	-19.25	0.019	-5.42
	DC129058-2	asp	qtz-asp	-20.060	0.018	-5.41
S1202206	DC145786-1	asp	qtz-asp	-19.980	0.02	-6.19
S1202207	DC145786-2	asp	qtz-asp	-20.240	0.019	-6.47
	DC145790-1-1	asp	qtz-asp	-18.740	0.015	-4.08
	DC145790-1-2	asp	qtz-asp	-19.16	0.019	-4.50
S1202204	DC145800-1	asp	qtz-asp	-19.11	0.022	-5.27
	DC145800-2	asp	qtz-asp	-18.84	0.02	-4.18
S1112183	DC149959-1	asp	qtz-asp	-18.15	0.034	-4.25
	DC149980-1	asp	qtz-asp	-18.650	0.009	-3.98
S1111116	H253887-1	asp	qtz-asp	-18.67	0.017	-4.01
S1111135	H253898-1	asp	qtz-asp	-19.560	0.01	-4.90
S1110081	H253903-1	asp	qtz-asp	-19.830	0.011	-5.18
S1111137	H253910-1	asp	qtz-asp	-19.50	0.026	-4.84
S1111136	J180571-2	asp	qtz-asp	-18.13	0.026	-3.46
S1112189	DC148145-1-1	asp	qtz-asp-stib	-18.380	0.051	-4.49
S1112189	DC148145-1-1	asp	qtz-asp-stib	-18.41	0.015	-4.52
S1110083	DC148145-2-1	asp	qtz-asp-stib	-19.83	0.023	-5.18

Lab ID	Sample No.	Sulfide analyzed	Vein Mineralogy	Raw $\delta^{34}S/^{32}S$ Mean	$\delta^{34}S$ /^{32}S Std. Dev.	$\delta^{34}S_{CDT}$ (‰)
S1109076	DC148795-2-1	asp	qtz-asp-stib	-18.59	0.01	-3.93
S1109078	H253528-1-1	asp	qtz-asp-stib	-19.71	0.011	-5.06
S1202199	H253528-2-4	asp	qtz-asp-stib	-19.45	0.018	-5.63
S1111156	H253576-2	asp	qtz-asp-stib	-18.72	0.027	-4.86
S1112177	H253882-2-2	asp	qtz-asp-stib	-19.84	0.026	-5.19
S1112180	H253906-2-3	asp	qtz-asp-stib	-20.07	0.03	-5.42
S1112192	J180565-2	asp	qtz-asp-stib	-19.40	0.016	-5.58
S1110082	J180616-1	asp	qtz-asp-stib	-20.76	0.014	-6.12
S1202198	H253528-2-3	gal	qtz-asp-stib	-19.51	0.012	-5.69
S1111166	DC148792-3-1	py	qtz-asp-stib	-18.29	0.01	-3.62
S1112195	H253868-2-2	py	qtz-asp-stib	-30.79	0.008	-17.66
S1111118	H253882-1-3	py	qtz-asp-stib	-19.74	0.022	-5.08
S1112178	H253882-2-3	py	qtz-asp-stib	-21.24	0.023	-6.61
S1111157	H253906-1	py	qtz-asp-stib	-22.17	0.029	-8.52
S1112175	H253906-2-2	py	qtz-asp-stib	-22.03	0.021	-7.40
S1111127	H253529-1	sphal	qtz-asp-stib	-20.46	0.011	-5.82
S1110085	H253882-1-1	sphal	qtz-asp-stib	-20.82	0.02	-6.18
S1111158	H253906-2	sphal	qtz-asp-stib	-22.24	0.017	-7.61
S1111159	H253906-2-1	sphal	qtz-asp-stib	-20.90	0.014	-6.26
S1112190	DC148145-1-2	stib	qtz-asp-stib	-18.24	0.021	-4.34
S1110084	DC148145-2-2	stib	qtz-asp-stib	-18.99	0.01	-4.33
S1109077	DC148795-2-2	stib	qtz-asp-stib	-18.28	0.015	-3.61
S1111154	H253518-1-1	stib	qtz-asp-stib	-18.48	0.013	-3.81
S1112179	H253528-2-1	stib	qtz-asp-stib	-19.90	0.012	-5.25
S1111139	H253529-3	stib	qtz-asp-stib	-19.23	0.016	-4.58
S1111155	H253576-1	stib	qtz-asp-stib	-19.81	0.014	-5.16
S1112194	H253868-2-1	stib	qtz-asp-stib	-18.55	0.034	-4.67
S1111117	H253882-1-2	stib	qtz-asp-stib	-18.31	0.036	-3.64
S1112176	H253882-2-1	stib	qtz-asp-stib	-18.70	0.026	-4.03
S1112193	J180586-1	stib	qtz-asp-stib	-17.67	0.01	-3.74
S1112191	J180565-1	stib	qtz-asp-stib	-18.29	0.019	-4.40
S1111138	J180616-2	stib	qtz-asp-stib	-19.80	0.011	-5.15
S1110088	DC128717-2-1	stib	qtz-stib	-20.30	0.019	-5.65
S1111152	DC128718-1	stib	qtz-stib	-19.51	0.019	-4.86
S1110087	DC128718-2-1	stib	qtz-stib	-19.28	0.01	-4.62
S1111150	DC128726-1	stib	qtz-stib	-17.67	0.029	-3.00
S1111151	DC128726-2	stib	qtz-stib	-18.74	0.022	-4.08
S1110086	DC128727-1	stib	qtz-stib	-19.03	0.025	-4.37
S1111153	DC128738-1	stib	qtz-stib	-19.00	0.026	-4.31

Appendix B: Oxygen isotopes of mineralized veins. Standard deviation is the internal precision of each analysis.

Lab ID	Sample No.	Mineral Analyzed	Vein Mineralogy	Raw $\delta^{18}O/^{16}O$ Mean	$\delta^{18}O/^{16}O$ Std. Dev.	$\delta^{18}O_{SMOW}$ (‰)
LF1205097	DC128694-2	Quartz	qtz-asp	17.01	0.043	17.40
LF1205090	DC128718-2	Quartz	qtz-asp	13.94	0.057	14.88
LF1205101	DC145786-3	Quartz	qtz-asp	18.53	0.045	18.92
LF1205099	DC145986-4	Quartz	qtz-asp	16.61	0.066	17.00
LF1205098	DC149980-3	Quartz	qtz-asp	18.44	0.059	18.83
LF1205096	J180571-2-2	Quartz	qtz-asp	13.63	0.044	14.02
LF1205114	J180565-4	Quartz	qtz-asp-stib	16.26	0.073	16.85
LF1205111	J180586-2	Quartz	qtz-asp-stib	16.18	0.049	16.77
LF1205091	DC128717-2-2	Quartz	qtz-stib	15.310	0.04	16.25

Appendix C: Oxygen Isotopes of Alteration. Standard deviation is the internal precision of each analysis.

Lab ID	Sample No.	Mineral Analyzed	Raw $\delta^{18}O/^{16}O$ Mean	$\delta^{18}O/^{16}O$ Std. Dev.	$\delta^{18}O_{SMOW}$ (‰)
LF1202010	DC152389	biotite	11.51	0.05	11.16
LF1202011	DC152389	biotite	11.76	0.03	11.41
LF1202016	DC152389	quartz	16.09	0.03	17.03
LF1203015	DC129260	albite	13.56	0.062	14.10
LF1203022	DC129260	albite	13.62	0.052	14.20
LF1202020	DC129260	quartz	14.95	0.14	15.24
LF1203020	DC129170	sericite	13.88	0.044	14.40
LF1203017	DC129169	sericite	13.04	0.044	13.60
LF1203016	DC129163	sericite	12.56	0.079	13.10
LF1202018	DC129163	quartz	16.63	0.07	17.58
LF1203021	DC128662-1	albite	14.01	0.061	14.60
LF1202017	DC128662-1	quartz	17.27	0.07	18.21

Appendix D: Sample Geologic Log Descriptions. These results were provided by ITH.

SampleID	IDext	HoleID	From_m	To_m	Host Unit	Geologic Description
DC128694		MK-06-07	154.04	154.04	Main Volcanics	in situ vol-"puzzle" bx; monomicitic; angular;felsic-vol clasts=blk altd fspr-plag phenos w/ round-spheroid vesicles qtz fill; hypoxtallin-porphyritic plag-bio latitic clasts in gry "cherty" chalcedonic qtz cement matrix;autoclastic
DC128724	1	MK-06-07	171.88	171.88	Main Volcanics	in situ vol-"puzzle" bx becomes conglomeratic-polymicitic;picks up granular-grit; m-c.g siliciclastic sand clasts + latitic vol vesciular w/ blk-altd plg; loose gry "cherty" chalcedonic qtz cement matrix to siliceous rhyolitic xtal-tuff mtx;pyroclastic?
DC128724	2	MK-06-07	172.49	172.49	Main Volcanics	in situ vol-"puzzle" bx becomes conglomeratic-polymicitic;picks up granular-grit; m-c.g siliciclastic sand clasts + latitic vol vesciular w/ blk-altd plg; loose gry "cherty" chalcedonic qtz cement matrix to siliceous rhyolitic xtal-tuff mtx;pyroclastic?
DC128732		MK-06-07	177.39	178.92	Main Volcanics	in situ vol-"puzzle" bx picks up siliciclastic sedimentary lithic clasts mixed w/ felsic-vol clasts=blk altd fspr-plag phenos w/ round-spheroid vesicles qtz fill; hypoxtallin-porphyritic plag-bio latitic clasts in gry lt. gry rhy-siliceous tuff cement mat
DC128717	3	MK-06-07	166.92	166.92	Main Volcanics	in situ vol-"puzzle" bx monomicitic felsic-vol clasts=blk altd fspr-plag phenos w/ round-spheroid vesicles qtz fill; hypoxtallin-porphyritic plag-bio latitic clasts in gry "cherty" chalcedonic qtz cement matrix; autoclastic
DC128718		MK-06-07	167.34	168.19	Main Volcanics	in situ vol-"puzzle" bx monomicitic felsic-vol clasts=blk altd fspr-plag phenos w/ round-spheroid vesicles qtz fill; hypoxtallin-porphyritic plag-bio latitic clasts in gry "cherty" chalcedonic qtz cement matrix; autoclastic
DC128726		MK-06-07	172.36	173.13	Main Volcanics	in situ vol-"puzzle" bx becomes conglomeratic-polymicitic;picks up granular-grit; m-c.g siliciclastic sand clasts + latitic vol vesciular w/ blk-altd plg; loose gry "cherty" chalcedonic qtz cement matrix to siliceous rhyolitic xtal-tuff mtx;pyroclastic?
DC128727		MK-06-07	173.13	174.04	Main Volcanics	in situ vol-"puzzle" bx becomes conglomeratic-polymicitic;picks up granular-grit; m-c.g siliciclastic sand clasts + latitic vol vesciular w/ blk-altd plg; loose gry "cherty" chalcedonic qtz cement matrix to siliceous rhyolitic xtal-tuff mtx;pyroclastic?
DC128738		MK-06-07	181.81	181.81	Main Volcanics	in situ vol-"puzzle" bx; momomicitic; angular felsic-vol clasts=blk altd fspr-plag phenos w/ round-spheroid vesicles qtz fill; hypoxtallin-porphyritic plag-bio latitic clasts in gry "cherty" chalcedonic qtz cement matrix
DC129054		MK-07-13	132.70	133.25	Main Volcanics	vol bx. < 10 cm sub ang to sub rounded clasts. 20 % matrix of 1mm py silica and feox. < 3cm dilation. 1 clast type. Aphanitic gmass buff tan to ornage color hard; mod albite and blk silica. 10% 2-5mm round qtz phenos. 5% 2-6mm blocky kspar phenos and 3%
DC129058		MK-07-13	135.09	135.09	Main Volcanics	vol bx. < 10 cm sub ang to sub rounded clasts. 20 % matrix of 1mm py silica and feox. < 3cm dilation. 1 clast type. Aphanitic gmass buff tan to ornage color hard; mod albite and blk silica. 10% 2-5mm round qtz phenos. 5% 2-6mm blocky kspar phenos and 3%
DC140214		MK-07-18	94.55	94.55	Upper Seds	lt-dark red/brown-med.gry; v.f.-f.g. calc.ss; str.patchy arg.alt- bx "look"
DC140218	2	MK-07-18	96.75	96.75	Upper Seds	med-drk grn/gry - lt-drk.red/brown; v.f.-f.g.; str.ser+arg.alt; abundant str. Ox'd blk-drk.redbrown sulfide vns-stwk-stand out in relief;
DC140219	1	MK-07-18	97.40	98.10	Upper Seds	med-drk grn/gry - lt-drk.red/brown; v.f.-f.g.; str.ser+arg.alt; abundant str. Ox'd blk-drk.redbrown sulfide vns-stwk-stand out in relief;
DC140219	2	MK-07-18	98.10	98.85	Upper Seds	med-drk grn/gry - lt-drk.red/brown; v.f.-f.g.; str.ser+arg.alt; abundant str. Ox'd blk-drk.redbrown sulfide vns-stwk-stand out in relief;
DC144215		MK-07-20	128.36	129.00	Upper Seds	lead gry-yllw-steel gry; strong alt overprint
DC145786		MK-08-30	130.02	130.02	Main Volcanics	Dvol bx. Clast supported 1-20cm subrounded to sub angular. 5% matrix of qtz + py/aspy. Gmass of clasts is aphanitic but str TD altered w/ rare preserved phenos of Plag to 5mm. 5% diss 1mm aspy. Few bx clasts alb alt. hard and white
DC145790	1	MK-08-30	132.82	132.82	Main Volcanics	Dvol bx. Clat supported subrouned clasts 1-10cm in size. Clast have TD creamy green ser alt but appear to be aphantic w/ kspar phenos v rarely preserved. Gray qtz/feox/py matrix few vfg gray qtzvns offset by fracs. Kspar phenos balck silica alt.
DC145790	2	MK-08-30	132.99	132.99	Main Volcanics	Dvol bx. Clat supported subrouned clasts 1-10cm in size. Clast have TD creamy green ser alt but appear to be aphantic w/ kspar phenos v rarely preserved. Gray qtz/feox/py matrix few vfg gray qtzvns offset by fracs. Kspar phenos balck silica alt.
DC145800	1	MK-08-30	144.80	144.80	Main Volcanics	Dvol bx. Clast supported str alt clasts 5-30cm rounded to subrounded clasts str alt varies by clast appears to be aphantic gmass w/ str alb or ser alt w/ 3% 1-3mm plag 1% 1-2 mm Kspar phenos and 1-2mm qtz filled vesicles. Feld phenos are replaced with qtz
DC148145	1	MK-09-36	386.05	387.70	Lower Sand	Fine sandstone. Strong argillic alteration; bleaching locally visible bedding definedby brownish color (biotite?)
DC148145	2	MK-09-36	387.30	387.30	Lower Sand	Fine sandstone. Strong argillic alteration; bleaching locally visible bedding definedby brownish color (biotite?)
DC148795	2	MK-09-37	440.44	441.38	Kint	Light grey/white; fine grained; non-porphyritic; sulfidized; argillized. Stibnit is 1-5cm irregular blobs; possibly deformed veins; with gouge and minor qtz.
DC148792	3	MK-09-37	438.40	438.40	Lower Seds	Black argillite as previous. Faulted to rubble gouge or broken rock with gouge seams running through. Mineralized with stib "veins" +/- qtz. Fault fabric low angle to core axis
DC149959		MK-09-40	471.73	472.22	Lower Sand	469.39-472.22 FAULT; highly fractured broken core with frequent flt zones with gouge through highly altered mineralized siltstone. Siltstone increasingly softer and more sericitic with depth in interval.
DC149980		MK-09-40	486.46	486.65	Lower Seds	black mineralized shale; both vfg and blebby pyrite. Cross-cutting mineralized quartz veins. Still see dolomite alteration.
H253528	1	MK-11-108	368.18	368.42	Lower Sand	368.18 to 368.80 Lower Sands - Siltstone & Conglomerate; Quartz pebble conglomerate with fuchite disseminated along bedding in upper sample and black siltstone in lower sample. Quartz-arsenopyrite-sphalerite-pyrite-jamesonite vein crosses sample break and
H253528	2	MK-11-108	368.40	368.40	Lower Sand	368.18 to 368.80 Lower Sands - Siltstone & Conglomerate; Quartz pebble conglomerate with fuchite disseminated along bedding in upper sample and black siltstone in lower sample. Quartz-arsenopyrite-sphalerite-pyrite-jamesonite vein crosses sample break and
H253576		MK-11-108	339.10	339.10	kint	399.05 to 399.41 Kint - Biotite Feldspar; Biotite feldspar dike with arsenopyrite rich quartz vein and disseminated arsenopyrite and pyrite. Pervasive weak sericite. Stibnite in vein.
H253529		MK-11-108	368.42	368.80	Lower Sand	368.18 to 368.80 Lower Sands - Siltstone & Conglomerate; Quartz pebble conglomerate with fuchite disseminated along bedding in upper sample and black siltstone in lower sample. Quartz-arsenopyrite-sphalerite-pyrite-jamesonite vein crosses sample break and
H253518	1	MK-11-108	361.80	362.44	kint	361.80 to 362.44 Faulted Kint & Lower Seds; Fault gouge with kint and seds clasts. Gouge supported. White/gray. Massive stibnite mineralization with arsenopyrite. Stibnite apperas to be related to syn-deformational fluid flow by broken vein textures as we

Appendix D (continued)

SampleID	IDext	HoleID	From_m	To_m	Host Unit	Geologic Description
H253528	2	MK-11-108	368.40	368.40	Lower Sand	368.18 to 368.80 Lower Sands - Siltstone & Conglomerate; Quartz pebble conglomerate with fuchite disseminated along bedding in upper sample and black siltstone in lower sample. Quartz-arsenopyrite-sphalerite-pyrite-jamesonite vein crosses sample break and
H253529		MK-11-108	368.42	368.80	Lower Sand	368.18 to 368.80 Lower Sands - Siltstone & Conglomerate; Quartz pebble conglomerate with fuchite disseminated along bedding in upper sample and black siltstone in lower sample. Quartz-arsenopyrite-sphalerite-pyrite-jamesonite vein crosses sample break and
H253576		MK-11-108	339.10	339.10	kint	399.05 to 399.41 Kint - Biotite Feldspar; Biotite feldspar dike with arsenopyrite rich quartz vein and disseminated arsenopyrite and pyrite. Pervasive weak sericite. Stibnite in vein.
H253877	1	MK-11-116	177.55	178.40	Lower Seds	177.55 to 178.40; Greater concentration of quartz and feldspar sand grains.
H253898		MK-11-116	192.96	193.16	Main Volcanics	188.67 to 194 87 Main Volcanics - Amygdiodal Flow; Mottled green and grey amygdiodal flow with disseminated pyrite and pyrite pooling along textures. Fine disseminated arsenopyrite throughout. Albite and sericite alteration in varying intensities througho
H253903		MK-11-116	195.83	195.90	Main Volcanics	194.87 to 196.44 Main Volcanics - Amygdiodal Flow; Faulted amygdiodal flow described above. Stronger disseminated mineralization in gouge zones.
H253910		MK-11-116	199.79	200.56	Main Volcanics	198.58 to 199.49; Poor recovery of quartz arsenopyrite vein. 50% of recovery is bull quartz arsenopyrite (5%) vein in gouge.
J180571	2	MK-11-116	341.79	341.79	Lower Sand	341.07 to 356.31 Lower Sands - Siltstone & Sandstone; greenish grey interbedded sericitized siltstone and sandstone. Moderate to strong silica overprint and banded fuchsite along bedding in sandstone. Weak calcite also selective to sandstone. Local stibni
H253882	2	MK-11-116	182.30	182.30	Lower Seds	182.12 to 183.90 Main Volcanics - Epiclastic Siltstone; Light green/grey siltstone. Fractured to rubble. Disseminated pyrite and fine grained arsenopyrite. Trace stibnite on fractures. Moderate sericite alteration on fractures and moderate pervasive albit
H253906		MK-11-116	197.16	197.30	Lower Seds	196.44 to 197.95 Main Volcanics - Epiclastic Siltstone; Grey massive epiclastic siltstone with trace bedding selective sericite alteration. Overprinting strong silica. Stockwork quartz veining in upper sample and strong sericite in lower sample. Lower sam
J180565		MK-11-116	338.19	338.50	Kint	338.19 to 338.50 Kint - Feldspar Porphyry & Vein; Intact dike (see above) with mineralized veining. One quartz-arsenopyrite (30%) vein above two (or one with splay?) quartz-stibnite veins that appear fractured with stibite infill. Upper vein has vein-perp
J180616		MK-11-116	375.98	376.20	Lower Sand	374.60 to 377.03 Siltstone & Sandstone; Increasing sericite alteration in siltstone downhole. Strong silica overprint and trace banded biotite alteration. Quartz veining parallel to bedding as well as quartz veinlets parallel to quartz and quartz-stibnite
H253868	2	MK-11-116	173.12	173.12	Main Volcanics	182.87 to 173.43 Main Volcanics - Tuff; Grey crystal lithic tuff with disseminated pyrite and fine grained arsenopyrite. Stibnite-quartz vein at 173.12 m. Two calcareous sections with distinct dark bands at contacts and possible kint texture. Black silica
H253882	1	MK-11-116	182.12	182.42	Lower Seds	182.12 to 183.90 Main Volcanics - Epiclastic Siltstone; Light green/grey siltstone. Fractured to rubble. Disseminated pyrite and fine grained arsenopyrite. Trace stibnite on fractures. Moderate sericite alteration on fractures and moderate pervasive albit
H253882	2	MK-11-116	182.30	182.30	Lower Seds	182.12 to 183.90 Main Volcanics - Epiclastic Siltstone; Light green/grey siltstone. Fractured to rubble. Disseminated pyrite and fine grained arsenopyrite. Trace stibnite on fractures. Moderate sericite alteration on fractures and moderate pervasive albit
H253906		MK-11-116	197.16	197.30	Lower Seds	196.44 to 197.95 Main Volcanics - Epiclastic Siltstone; Grey massive epiclastic siltstone with trace bedding selective sericite alteration. Overprinting strong silica. Stockwork quartz veining in upper sample and strong sericite in lower sample. Lower sam
H253868	2	MK-11-116	173.12	173.12	Main Volcanics	182.87 to 173.43 Main Volcanics - Tuff; Grey crystal lithic tuff with disseminated pyrite and fine grained arsenopyrite. Stibnite-quartz vein at 173.12 m. Two calcareous sections with distinct dark bands at contacts and possible kint texture. Black silica
H253882	2	MK-11-116	182.30	182.30	Lower Seds	182.12 to 183.90 Main Volcanics - Epiclastic Siltstone; Light green/grey siltstone. Fractured to rubble. Disseminated pyrite and fine grained arsenopyrite. Trace stibnite on fractures. Moderate sericite alteration on fractures and moderate pervasive albit
J180586		MK-11-116	351.90	352.05	Lower Sand	351.74 to 358.45; Sandstone beds more common than above. Could explain any higher arsenic values seen in these samples.
J180565		MK-11-116	338.19	338.50	Kint	338.19 to 338.50 Kint - Feldspar Porphyry & Vein; Intact dike (see above) with mineralized veining. One quartz-arsenopyrite (30%) vein above two (or one with splay?) quartz-stibnite veins that appear fractured with stibite infill. Upper vein has vein-perp
J180616		MK-11-116	375.98	376.20	Lower Sand	374.60 to 377.03 Siltstone & Sandstone; Increasing sericite alteration in siltstone downhole. Strong silica overprint and trace banded biotite alteration. Quartz veining parallel to bedding as well as quartz veinlets parallel to quartz and quartz-stibnite

Appendix E: Sample Geologic Log Alteration. These results were provided by ITH.

Sample ID	ID ext	Hole ID	From (m)	To (m)	ox intensity	ox style	Alb intensity	Alb style	cal intensity	cal style	ser intensity	ser style	sil intensity	sil style
DC128694		MK-06-07	154.04	154.04										
DC128724	1	MK-06-07	171.88	171.88	complete									
DC128724	2	MK-06-07	172.49	172.49	complete									
DC128732		MK-06-07	177.39	178.92	partial									
DC128717	3	MK-06-07	166.92	166.92	complete									
DC128718		MK-06-07	167.34	168.19	complete									
DC128726		MK-06-07	172.36	173.13	complete									
DC128727		MK-06-07	173.13	174.04	complete									
DC128738		MK-06-07	181.81	181.81										
DC129054		MK-07-13	132.70	133.25	trace									
DC129058		MK-07-13	135.09	135.09	trace									
DC140214		MK-07-18	94.55	94.55	partial				strong					
DC140218	2	MK-07-18	96.75	96.75	partial				strong					
DC140219	1	MK-07-18	97.40	98.10	partial				strong					
DC140219	2	MK-07-18	98.10	98.85	partial				strong					
DC144215		MK-07-20	128.36	129.00	partial				strong					
DC145786		MK-08-30	130.02	130.02	moderate	pervasive	moderate	pervasive			intense	texture destructive		
DC145790	1	MK-08-30	132.82	132.82	moderate	on fractures					strong	texture destructive		
DC145790	2	MK-08-30	132.99	132.99	moderate	on fractures					strong	texture destructive		
DC145800	1	MK-08-30	144.80	144.80	strong	pervasive					moderate	pervasive		
DC148145	1	MK-09-36	386.05	387.70	none									
DC148145	2	MK-09-36	387.30	387.30	none									
DC148795	2	MK-09-37	440.44	441.38	none									
DC148792	3	MK-09-37	438.40	438.40	none									
DC149959		MK-09-40	471.73	472.22	none						strong	pervasive	very weak	selective
DC149980		MK-09-40	486.46	486.65	none						very weak	pervasive		
H253528	1	MK-11-108	368.18	368.42	none						weak	pervasive	strong	pervasive
H253528	2	MK-11-108	368.40	368.40	none						very weak	banded	strong	pervasive
H253576		MK-11-108	339.10	339.10	none						weak	disseminated		
H253529		MK-11-108	368.42	368.80	none						very weak	banded	strong	pervasive
H253518	1	MK-11-108	361.80	362.44	none									
H253528	2	MK-11-108	368.40	368.40	none						very weak	banded	strong	pervasive
H253529		MK-11-108	368.42	368.80	none						very weak	banded	strong	pervasive

Appendix E (continued)

Sample ID	ID ext	Hole ID	From (m)	To (m)	ox intensity	ox style	Alb intensity	Alb style	cal intensity	cal style	ser intensity	ser style	sil intensity	sil style
H253576		MK-11-108	339.10	339.10	none						weak	disseminated		
H253877	1	MK-11-116	177.55	178.40	none				weak	patchy				
H253898		MK-11-116	192.96	193.16	none		strong	patchy	weak	on fractures	moderate	patchy	strong	patchy
H253903		MK-11-116	195.83	195.90	none		weak	patchy	moderate	pervasive	weak	patchy	strong	pervasive
H253910		MK-11-116	199.79	200.56	none		strong	patchy	weak	pervasive	weak	patchy	moderate	patchy
J180571	2	MK-11-116	341.79	341.79	none						weak	pervasive	weak	overprint
H253882	2	MK-11-116	182.30	182.30	none		moderate	pervasive	weak	on fractures	very weak	pervasive		
H253906		MK-11-116	197.16	197.30	none						moderate	banded	strong	pervasive
J180565		MK-11-116	338.19	338.50	none									
J180616		MK-11-116	375.98	376.20	none						moderate	banded	strong	overprint
H253868	2	MK-11-116	173.12	173.12	none				weak	pervasive	very weak	disseminated		
H253882	1	MK-11-116	182.12	182.42	none		moderate	pervasive	weak	on fractures	very weak	pervasive		
H253882	2	MK-11-116	182.30	182.30	none		moderate	pervasive	weak	on fractures	very weak	pervasive		
H253906		MK-11-116	197.16	197.30	none						moderate	banded	strong	pervasive
H253868	2	MK-11-116	173.12	173.12	none				weak	pervasive	very weak	disseminated		
H253882	2	MK-11-116	182.30	182.30	none		moderate	pervasive	weak	on fractures	very weak	pervasive		
J180586		MK-11-116	351.90	352.05	none						moderate	banded	strong	overprint
J180565		MK-11-116	338.19	338.50	none									
J180616		MK-11-116	375.98	376.20	none						moderate	banded	strong	overprint

Appendix F: Sample Geologic Log Sulfides. These results were provided by ITH.

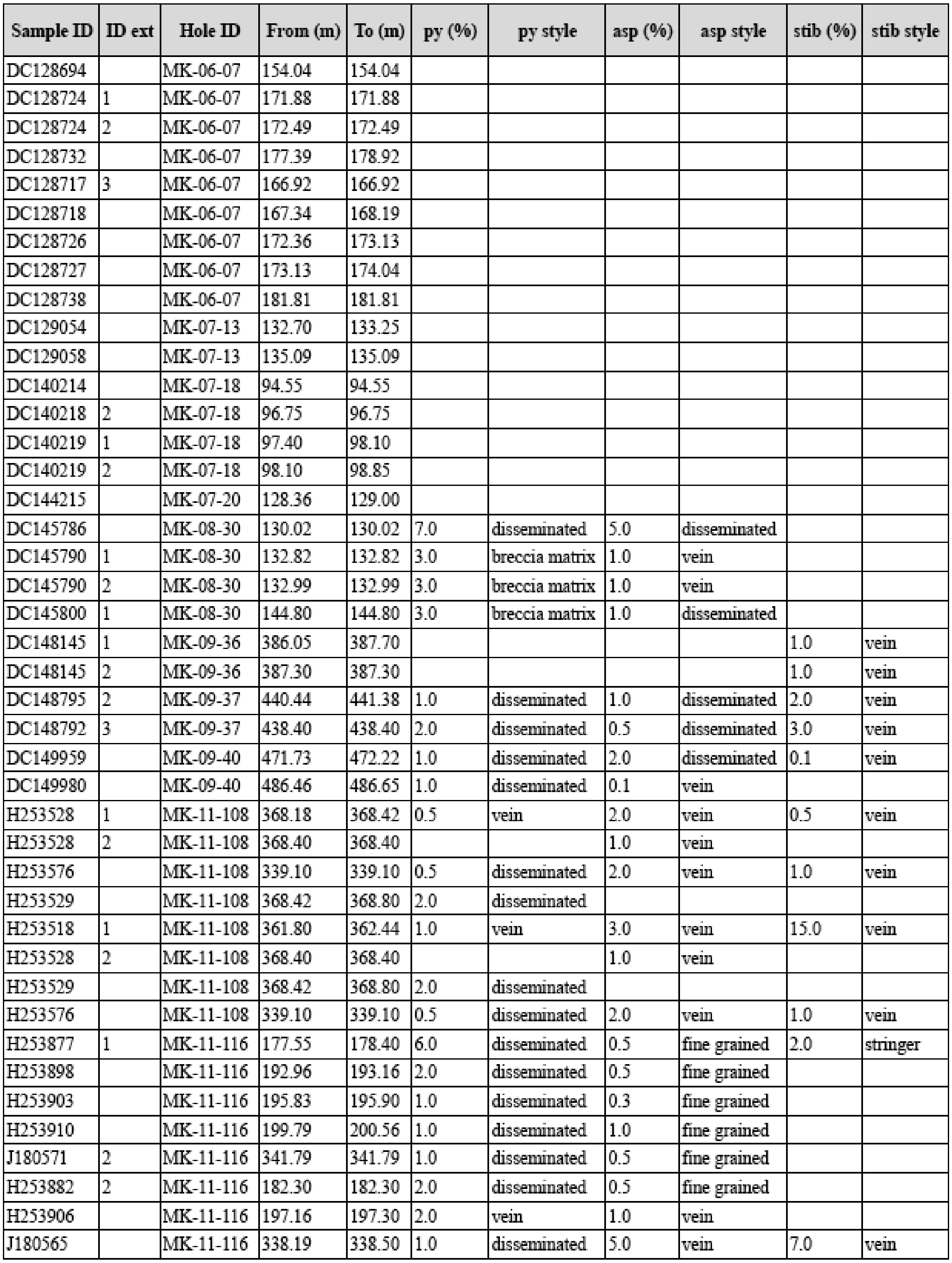

Sample ID	ID ext	Hole ID	From (m)	To (m)	py (%)	py style	asp (%)	asp style	stib (%)	stib style
DC128694		MK-06-07	154.04	154.04						
DC128724	1	MK-06-07	171.88	171.88						
DC128724	2	MK-06-07	172.49	172.49						
DC128732		MK-06-07	177.39	178.92						
DC128717	3	MK-06-07	166.92	166.92						
DC128718		MK-06-07	167.34	168.19						
DC128726		MK-06-07	172.36	173.13						
DC128727		MK-06-07	173.13	174.04						
DC128738		MK-06-07	181.81	181.81						
DC129054		MK-07-13	132.70	133.25						
DC129058		MK-07-13	135.09	135.09						
DC140214		MK-07-18	94.55	94.55						
DC140218	2	MK-07-18	96.75	96.75						
DC140219	1	MK-07-18	97.40	98.10						
DC140219	2	MK-07-18	98.10	98.85						
DC144215		MK-07-20	128.36	129.00						
DC145786		MK-08-30	130.02	130.02	7.0	disseminated	5.0	disseminated		
DC145790	1	MK-08-30	132.82	132.82	3.0	breccia matrix	1.0	vein		
DC145790	2	MK-08-30	132.99	132.99	3.0	breccia matrix	1.0	vein		
DC145800	1	MK-08-30	144.80	144.80	3.0	breccia matrix	1.0	disseminated		
DC148145	1	MK-09-36	386.05	387.70					1.0	vein
DC148145	2	MK-09-36	387.30	387.30					1.0	vein
DC148795	2	MK-09-37	440.44	441.38	1.0	disseminated	1.0	disseminated	2.0	vein
DC148792	3	MK-09-37	438.40	438.40	2.0	disseminated	0.5	disseminated	3.0	vein
DC149959		MK-09-40	471.73	472.22	1.0	disseminated	2.0	disseminated	0.1	vein
DC149980		MK-09-40	486.46	486.65	1.0	disseminated	0.1	vein		
H253528	1	MK-11-108	368.18	368.42	0.5	vein	2.0	vein	0.5	vein
H253528	2	MK-11-108	368.40	368.40			1.0	vein		
H253576		MK-11-108	339.10	339.10	0.5	disseminated	2.0	vein	1.0	vein
H253529		MK-11-108	368.42	368.80	2.0	disseminated				
H253518	1	MK-11-108	361.80	362.44	1.0	vein	3.0	vein	15.0	vein
H253528	2	MK-11-108	368.40	368.40			1.0	vein		
H253529		MK-11-108	368.42	368.80	2.0	disseminated				
H253576		MK-11-108	339.10	339.10	0.5	disseminated	2.0	vein	1.0	vein
H253877	1	MK-11-116	177.55	178.40	6.0	disseminated	0.5	fine grained	2.0	stringer
H253898		MK-11-116	192.96	193.16	2.0	disseminated	0.5	fine grained		
H253903		MK-11-116	195.83	195.90	1.0	disseminated	0.3	fine grained		
H253910		MK-11-116	199.79	200.56	1.0	disseminated	1.0	fine grained		
J180571	2	MK-11-116	341.79	341.79	1.0	disseminated	0.5	fine grained		
H253882	2	MK-11-116	182.30	182.30	2.0	disseminated	0.5	fine grained		
H253906		MK-11-116	197.16	197.30	2.0	vein	1.0	vein		
J180565		MK-11-116	338.19	338.50	1.0	disseminated	5.0	vein	7.0	vein

Appendix F (continued)

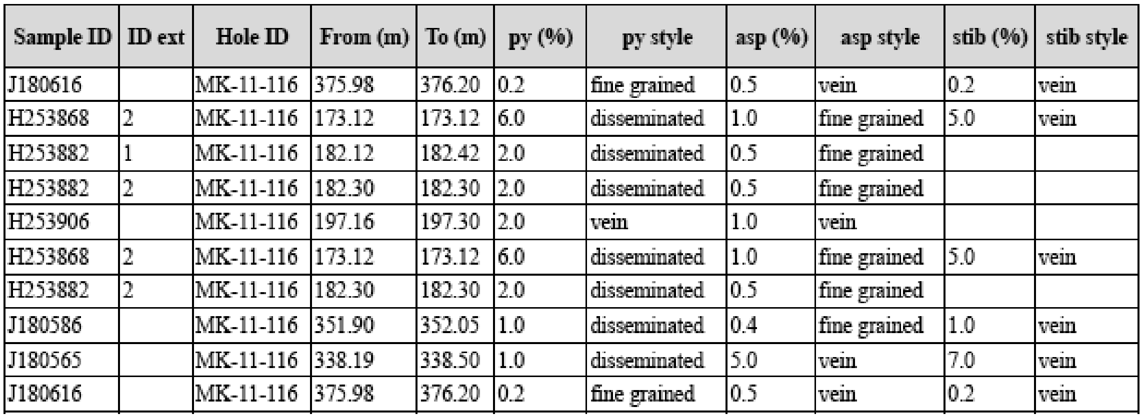

Sample ID	ID ext	Hole ID	From (m)	To (m)	py (%)	py style	asp (%)	asp style	stib (%)	stib style
J180616		MK-11-116	375.98	376.20	0.2	fine grained	0.5	vein	0.2	vein
H253868	2	MK-11-116	173.12	173.12	6.0	disseminated	1.0	fine grained	5.0	vein
H253882	1	MK-11-116	182.12	182.42	2.0	disseminated	0.5	fine grained		
H253882	2	MK-11-116	182.30	182.30	2.0	disseminated	0.5	fine grained		
H253906		MK-11-116	197.16	197.30	2.0	vein	1.0	vein		
H253868	2	MK-11-116	173.12	173.12	6.0	disseminated	1.0	fine grained	5.0	vein
H253882	2	MK-11-116	182.30	182.30	2.0	disseminated	0.5	fine grained		
J180586		MK-11-116	351.90	352.05	1.0	disseminated	0.4	fine grained	1.0	vein
J180565		MK-11-116	338.19	338.50	1.0	disseminated	5.0	vein	7.0	vein
J180616		MK-11-116	375.98	376.20	0.2	fine grained	0.5	vein	0.2	vein

Appendix G: Sample Assay Chemistry. These results were generated by ALS Chemex in Vancouver, CA and provided by ITH.

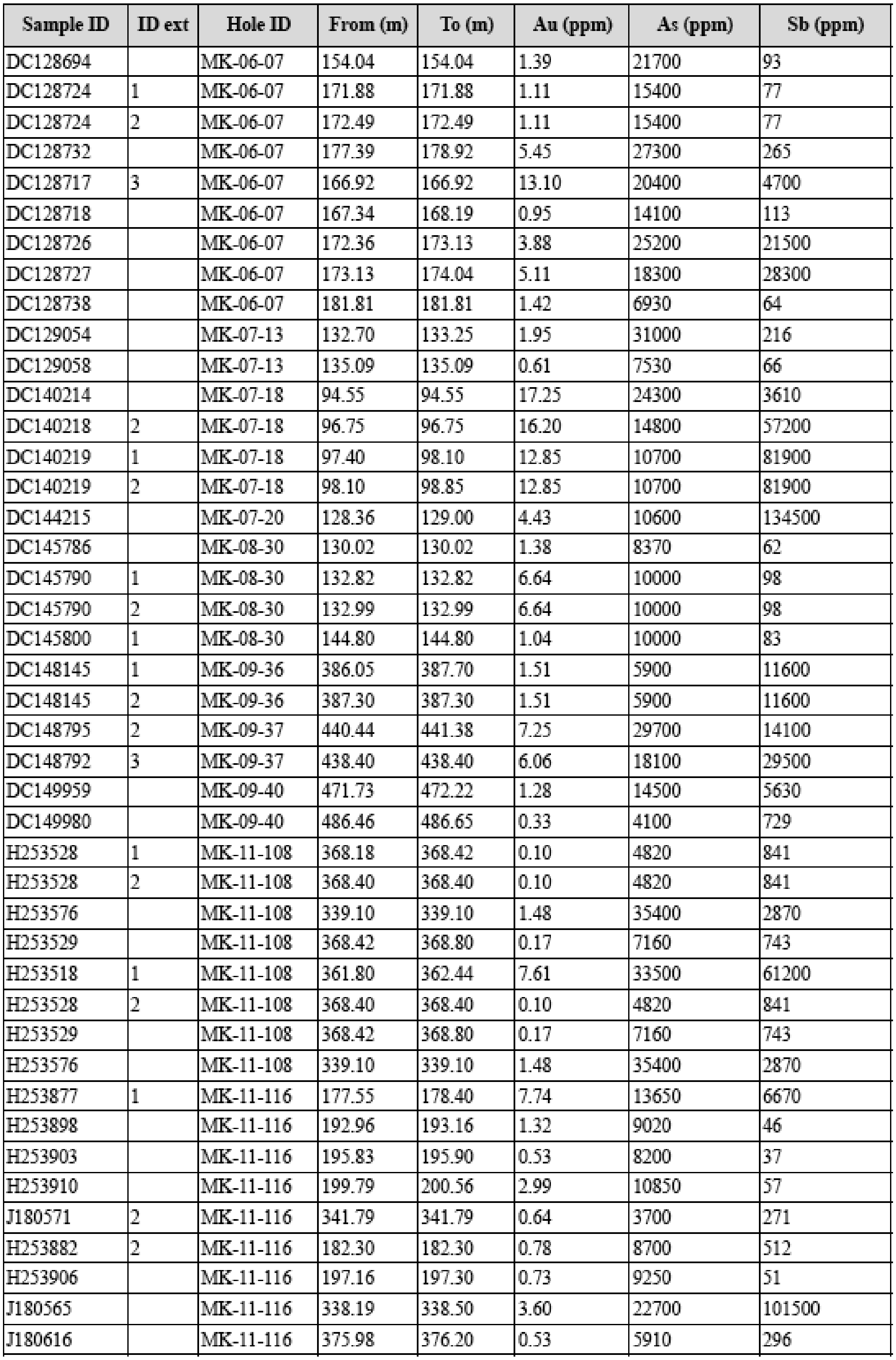

Sample ID	ID ext	Hole ID	From (m)	To (m)	Au (ppm)	As (ppm)	Sb (ppm)
DC128694		MK-06-07	154.04	154.04	1.39	21700	93
DC128724	1	MK-06-07	171.88	171.88	1.11	15400	77
DC128724	2	MK-06-07	172.49	172.49	1.11	15400	77
DC128732		MK-06-07	177.39	178.92	5.45	27300	265
DC128717	3	MK-06-07	166.92	166.92	13.10	20400	4700
DC128718		MK-06-07	167.34	168.19	0.95	14100	113
DC128726		MK-06-07	172.36	173.13	3.88	25200	21500
DC128727		MK-06-07	173.13	174.04	5.11	18300	28300
DC128738		MK-06-07	181.81	181.81	1.42	6930	64
DC129054		MK-07-13	132.70	133.25	1.95	31000	216
DC129058		MK-07-13	135.09	135.09	0.61	7530	66
DC140214		MK-07-18	94.55	94.55	17.25	24300	3610
DC140218	2	MK-07-18	96.75	96.75	16.20	14800	57200
DC140219	1	MK-07-18	97.40	98.10	12.85	10700	81900
DC140219	2	MK-07-18	98.10	98.85	12.85	10700	81900
DC144215		MK-07-20	128.36	129.00	4.43	10600	134500
DC145786		MK-08-30	130.02	130.02	1.38	8370	62
DC145790	1	MK-08-30	132.82	132.82	6.64	10000	98
DC145790	2	MK-08-30	132.99	132.99	6.64	10000	98
DC145800	1	MK-08-30	144.80	144.80	1.04	10000	83
DC148145	1	MK-09-36	386.05	387.70	1.51	5900	11600
DC148145	2	MK-09-36	387.30	387.30	1.51	5900	11600
DC148795	2	MK-09-37	440.44	441.38	7.25	29700	14100
DC148792	3	MK-09-37	438.40	438.40	6.06	18100	29500
DC149959		MK-09-40	471.73	472.22	1.28	14500	5630
DC149980		MK-09-40	486.46	486.65	0.33	4100	729
H253528	1	MK-11-108	368.18	368.42	0.10	4820	841
H253528	2	MK-11-108	368.40	368.40	0.10	4820	841
H253576		MK-11-108	339.10	339.10	1.48	35400	2870
H253529		MK-11-108	368.42	368.80	0.17	7160	743
H253518	1	MK-11-108	361.80	362.44	7.61	33500	61200
H253528	2	MK-11-108	368.40	368.40	0.10	4820	841
H253529		MK-11-108	368.42	368.80	0.17	7160	743
H253576		MK-11-108	339.10	339.10	1.48	35400	2870
H253877	1	MK-11-116	177.55	178.40	7.74	13650	6670
H253898		MK-11-116	192.96	193.16	1.32	9020	46
H253903		MK-11-116	195.83	195.90	0.53	8200	37
H253910		MK-11-116	199.79	200.56	2.99	10850	57
J180571	2	MK-11-116	341.79	341.79	0.64	3700	271
H253882	2	MK-11-116	182.30	182.30	0.78	8700	512
H253906		MK-11-116	197.16	197.30	0.73	9250	51
J180565		MK-11-116	338.19	338.50	3.60	22700	101500
J180616		MK-11-116	375.98	376.20	0.53	5910	296

Appendix G (continued)

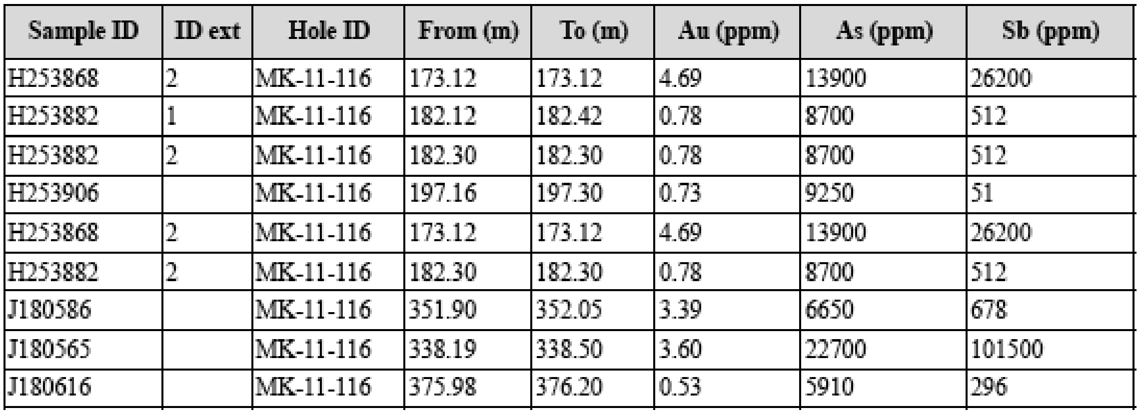

Sample ID	ID ext	Hole ID	From (m)	To (m)	Au (ppm)	As (ppm)	Sb (ppm)
H253868	2	MK-11-116	173.12	173.12	4.69	13900	26200
H253882	1	MK-11-116	182.12	182.42	0.78	8700	512
H253882	2	MK-11-116	182.30	182.30	0.78	8700	512
H253906		MK-11-116	197.16	197.30	0.73	9250	51
H253868	2	MK-11-116	173.12	173.12	4.69	13900	26200
H253882	2	MK-11-116	182.30	182.30	0.78	8700	512
J180586		MK-11-116	351.90	352.05	3.39	6650	678
J180565		MK-11-116	338.19	338.50	3.60	22700	101500
J180616		MK-11-116	375.98	376.20	0.53	5910	296

Appendix H: Sample Core Photographs

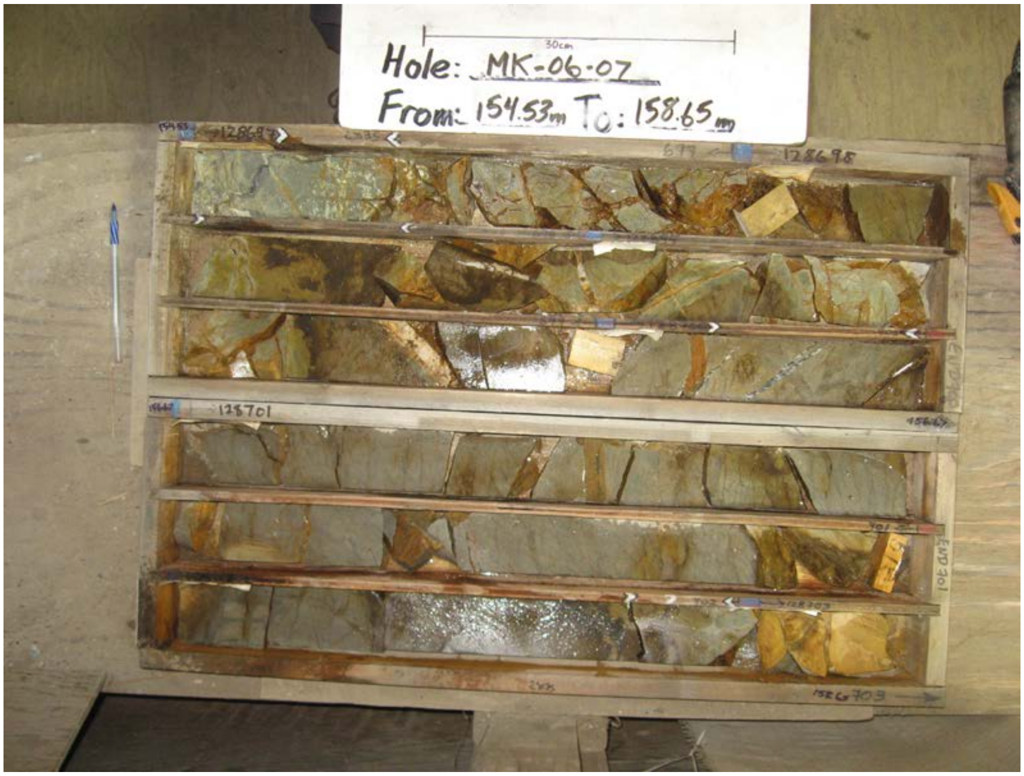

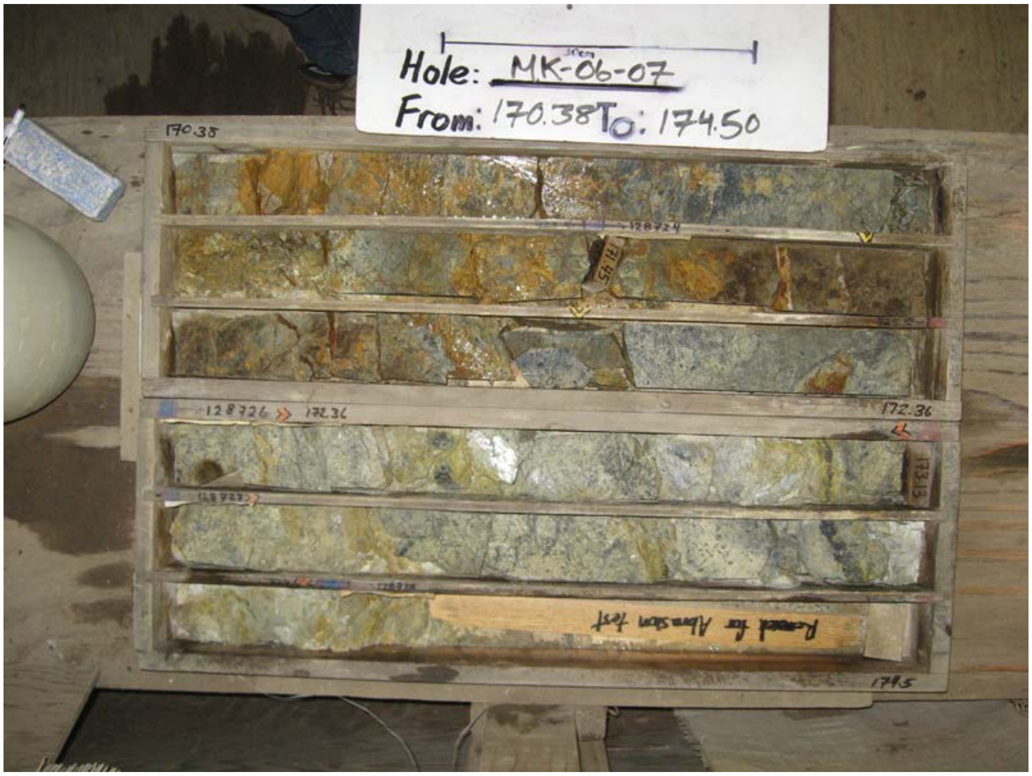
Hole: MK-06-07
From: 170.38 To: 174.50
170.38
171.45
128726
172.36
172.36
173.15
Removed for Abrasion test
174.5


Hole: MK-06-07
From: 174.50 To: 178.31
128729
174.5
128730
176.98
Removed for Abrasion test
Rem for Abrasion test
128733
178.31

30cm
Hole: MK-06-07
From: 178.31 To: 182.42m
178.31
128736 180.14
128737
180.14
128738
128739
182.42

08.07.2011
0
10
20
30
40
50
1:1000
DC128717.5
W-43
THE C-THRU RULER COMPANY
Bloomfield, CT 06002, U.S.A.
C-Thru Custom Products Div.
(860) 243-0303

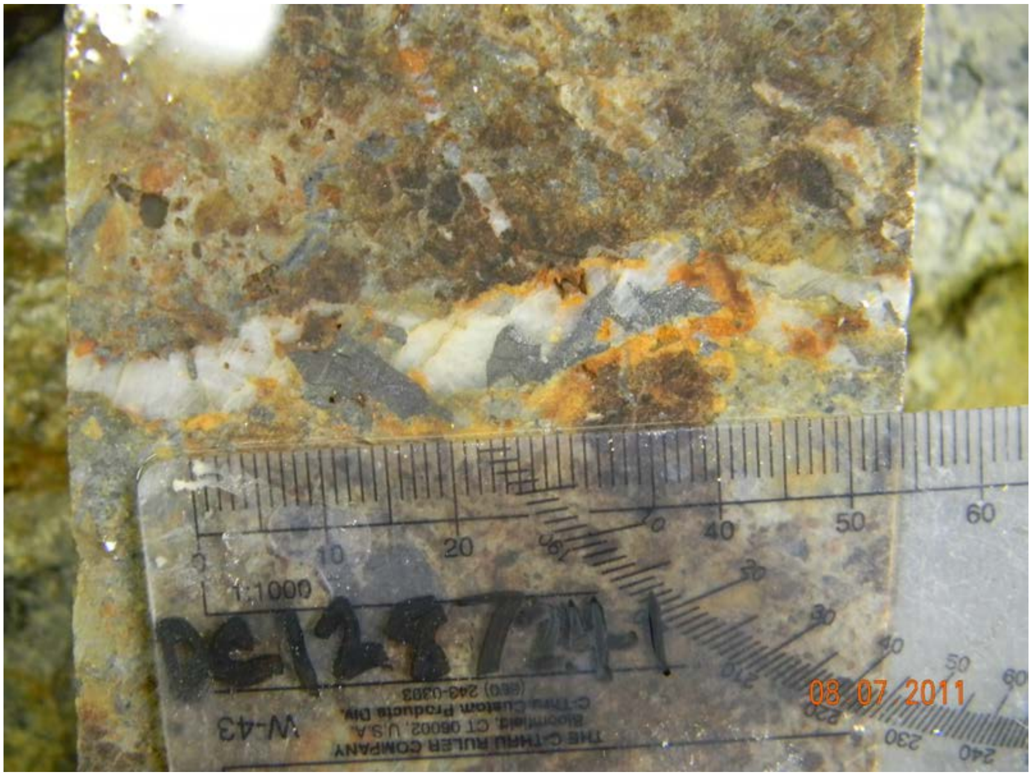
DC128724-1
08 07 2011


DC128724
08 07 2011


08 07 2011
1:1000

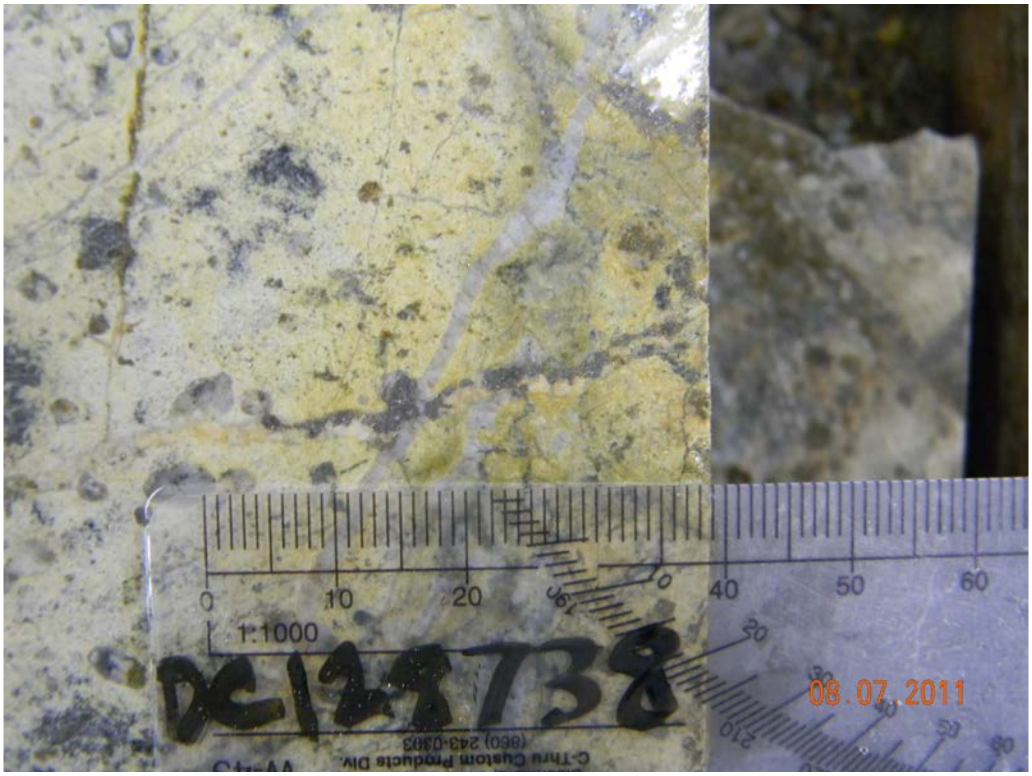
DC128738
1:1000
08 07 2011


DC128727
08 07 2011


30cm
Hole: MK-07-13
From 132.28 To: 134.11m
132.28
134.11
134.11
DONT SAMPLE

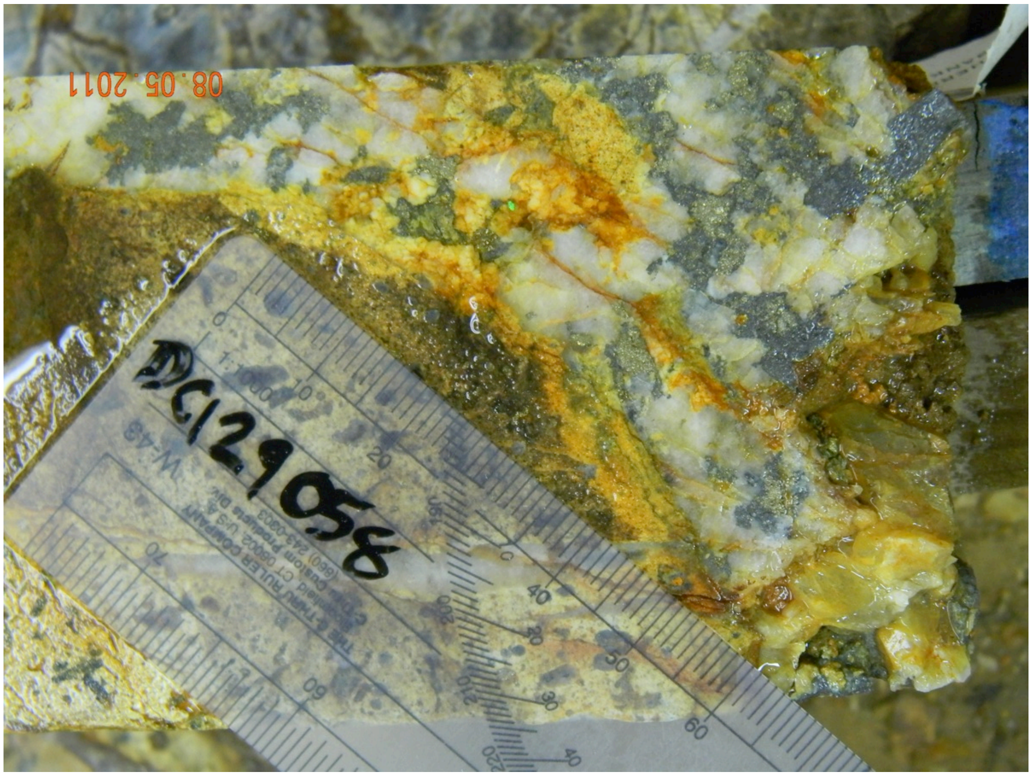
08 05 2011
DC129058


30cm
Hole: MK-07-18
From: 93.67 To: 97.54
93.67
93.70-99.00 140213
99.00-99.68 140214
CORE REMOVED FOR COLUMN TESTING
140215
95.40
95.40
140218
96.23-97.40 140218
97.54


30cm
Hole: MK-07-18
From: 97.40 To: 101.50
97.40-98.85 140219
140220
99.52
99.52
140221
100.00-102.20 140222
CORE REMOVED FOR COLUMN TESTING
101.50

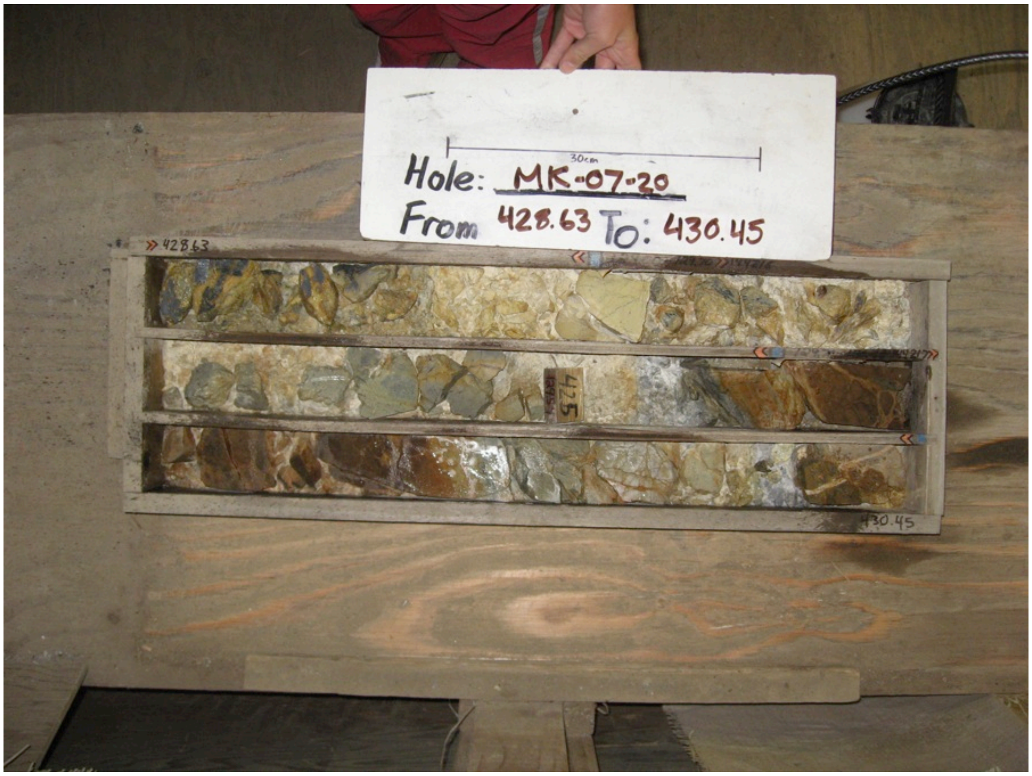

30cm
Hole: MK-07-20
From 428.63 To: 430.45
428.63
425
430.45

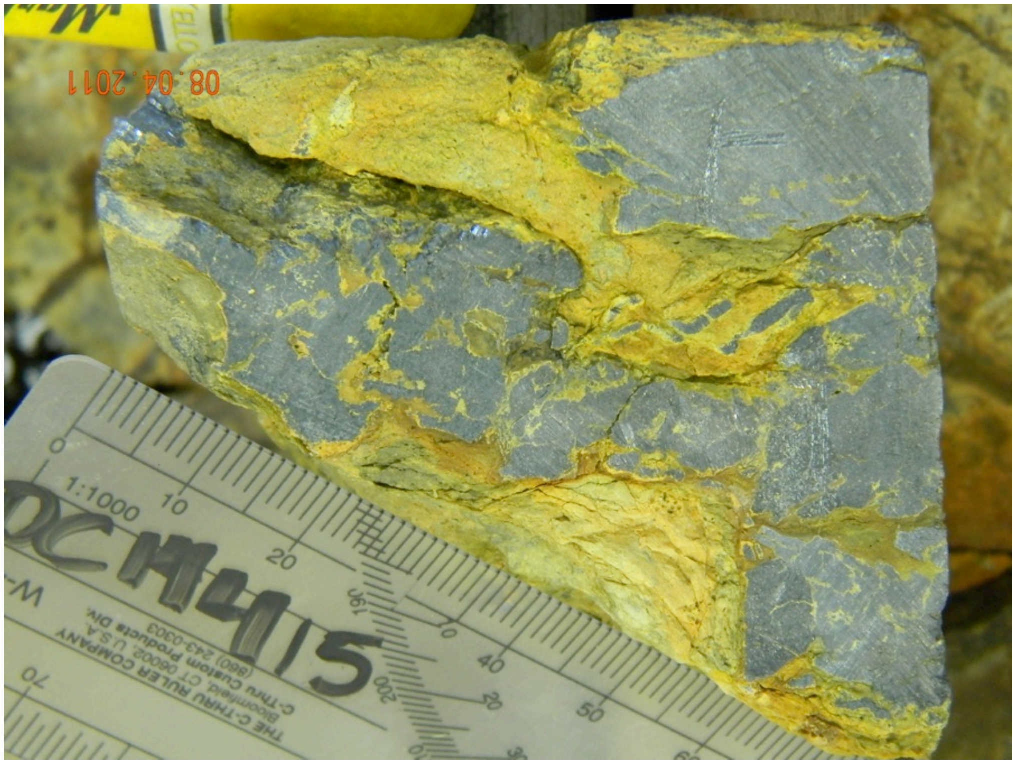

08 04 2011
DCH415


30cm
Hole: MK-08-30
From 127.30 To: 131.13
127.80
129.26
129.26
131.13


30cm
Hole: MK-08-30
From 131.13 To: 134.92
132.94
132.94
134.92


30cm
Hole: MK-08-30
From 142.52 To. 146.56
142.54
144.54
144.54
146.56


08 06 2011
DC 145 786

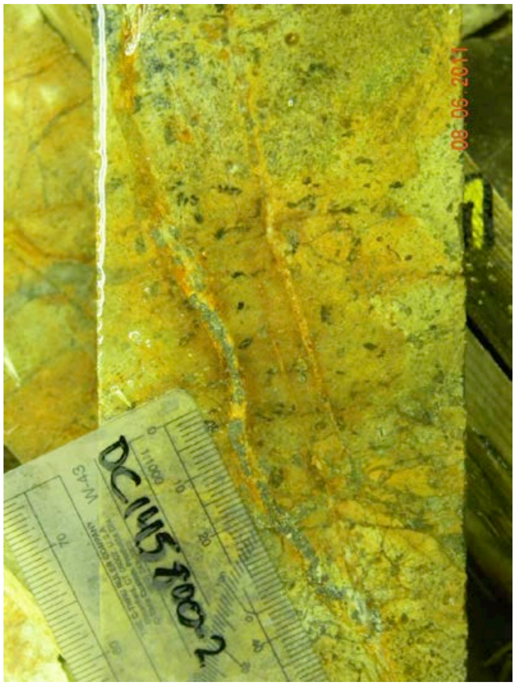
08 06 2011
DC 145 700 2

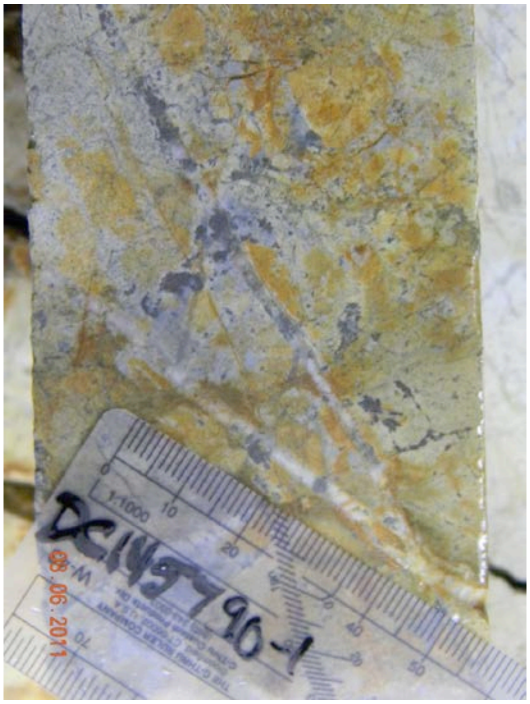
DC1457 90-1
08.06.2011

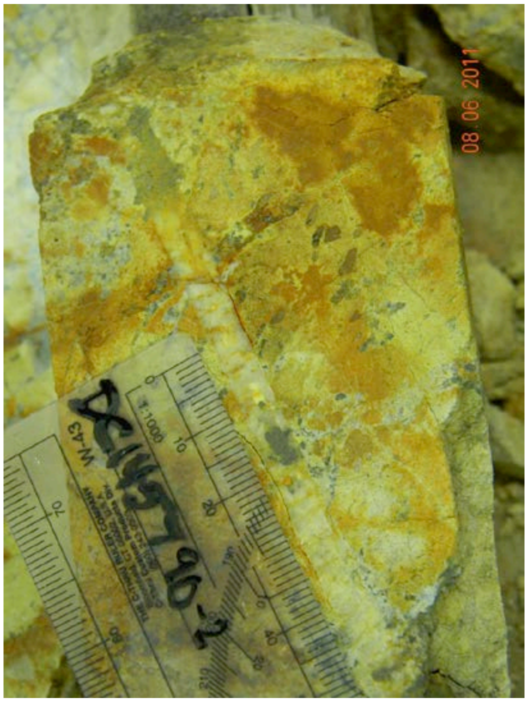
DC1457 90-2
08.06.2011


30cm
Hole: MK-09-36
From 383.27 To: 389.06
148146
1271


30cm
Hole: MK-09-37
From 437.69 To. 441.58
148792
148793
1440
437.47
148794
439.97
441.58


08.03.2011


0
10
20
40
50
1:1000
08.03.2011


30cm
Hole: MK-09-40
From 472.00 To: 475.66
472.00
149960
149961, 149962
149963
473.88
475.66


30cm
Hole: MK-09-40
From 483.59 To: 487.48
483.59
149977
485.42
485.42
149980
487.48


30cm
Hole: MK-11-108
From 361.13 To: 363.84
361.13
362.20
363.89


H253518-3
08.04.2011

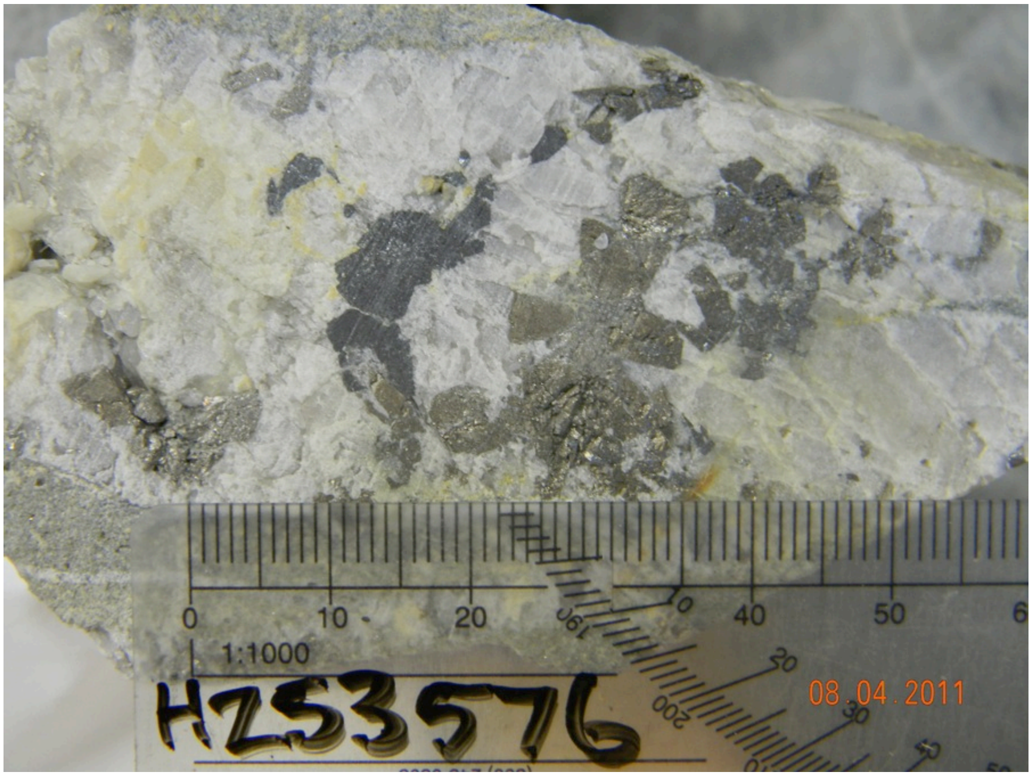
0
10
20
40
50
1:1000
HZ53576
08.04.2011


30cm
Hole: MK-11-11b
From: 162.76m To: 166.17 m
162.76
H253853
164.64
164.64
H253857
H253858
H253859
166.17


30cm
Hole: MK-11-11b
From: 166.17 m To: 170.98 m
166.17
H253860
168.77
168.77
170.98


30cm
Hole: MK-11-116
From: 170.98 m To: 174.92 m
170.98
H253864 + H253865
173.24
173.24
H253870
174.92


30cm
Hole: MK-11-116
From: 174.92 m To: 179.18 m
174.92
177.30
177.30
179.18


30cm
Hole: MK-11-11b
From: 179.18 m To: 183.64 m
179.18
181.90
181.90
H253882
H253883


30cm
Hole: MK-11-11b
From: 183.64 m To: 187.50 m
H253886
184.98
184.98
H253890
187.50


30cm
Hole: MK-11-11b
From: 187.50 m To: 191.25 m
187.50
H253892
189.52
189.52
H253894 + H253895
H253896
191.25


30cm
Hole: MK-11-11b
From: 191.25 m To: 194.41 m
191.25
H253897
H253898
193.19
H253899
193.19
H253900
This slot is on strike... fight the man!
194.41


30cm
Hole: MK-11-11b
From: 194.41 To: 198.29 m
194.41
H253902
H253903
196.44
H253904 + H253905
196.44
H253906
H253907
198.29


30cm
Hole: MK-11-11b
From: 198.29 m To: 202.61 m
198.29
H253908
H253909
H253910
200.56
H253911
H253912
H253913
202.61


30cm
Hole: MK-11-116
From: 334.21 m To: 338.19 m
J180560 334.21
J180561
J180562 336.50
336.50
J180563 + J180564
338.19


30cm
Hole: MK-11-116
From: 338.19 m To: 341.79 m
J180565 338.19
J180566
J180567
J180568
J180569
340.29
340.24
J180570
J180571
341.79


30cm
Hole: MK-11-116
From: 341.79 m To: 345.01 m
341.79
343.40
J180573 J180574
345.01


30cm
Hole: MK-11-116
From: 345.01 m To: 348.89 m
345.01
347.03
J180580
348.89


30cm
Hole: MK-11-116
From: 348.89 m To: 352.76 m
348.89
J180582
J180583-J180584
J180585
J180586
J180587
352.76


30cm
Hole: MK-11-116
From: 359.05 m To: 363.74 m
359.05
J180596
J180597
J180598
J180599
363.74


30cm
Hole: MK-11-116
From: 363.74 m To: 367.29 m
363.74
J180600
J180601
365.53
365.53
J180602
J180603
J180604
J180605
367.29


30cm
Hole: MK-11-116
From: 367.29 m To: 371.03 m
367.29
J180606
J180607
J180608
369.21
369.21
J180609
J180610
J180611
371.03


30cm
Hole: MK-11-116
From: 371.03 m To: 374.75 m
371.03
J180612
J180613 + J180614
372.86
372.88
J180615
J180616
374.75


30cm
Hole: MK-11-116
From: 374.75 m To: 378.06 m
374.75
J180617
J180618
376.56
376.50
J180619
J180620
377.95
378.06


30cm
Hole: MK-11-116
From: 378.06 m To: 386.90 m
378.06
J180621
J180622
J180623 – J180624
379.75


30cm
Hole: MK-11-116
From: 381.9 m To: 384.02 m
381.90
J180625
J180626
J180627


MK-11-116
H253881-2
CM
07.21.2011


MK-11-116
H253868-2
CM
07.21.2011


MK-11-116
H253868-3
CM
INCH
07.21.2011

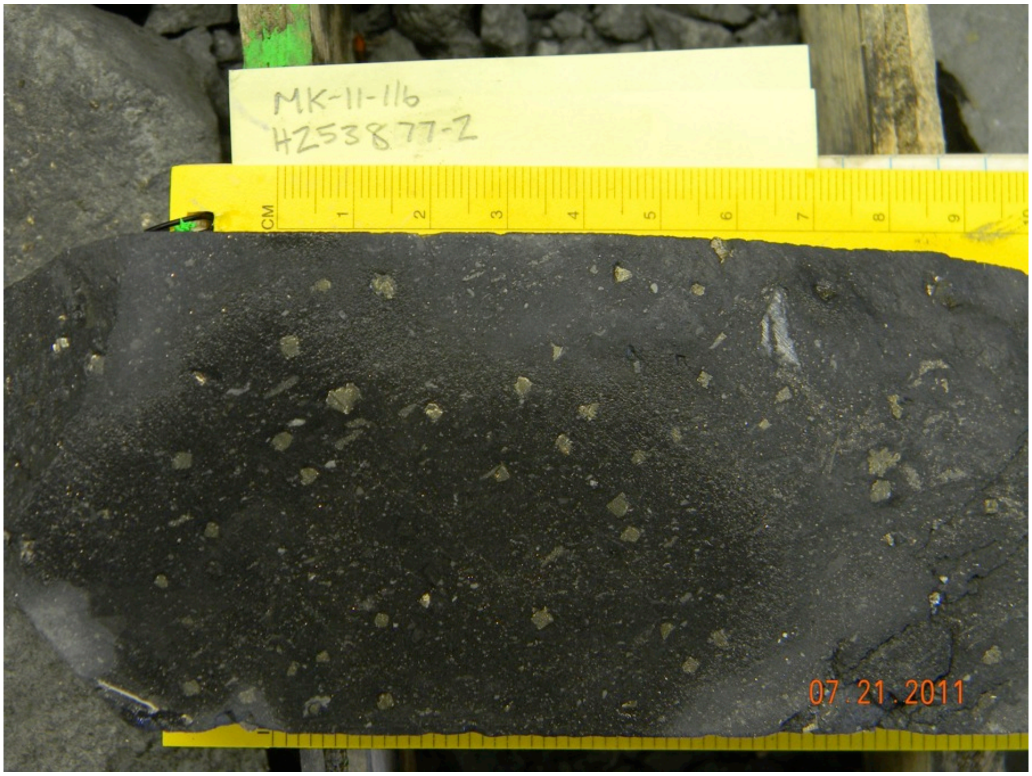
MK-11-116
H253877-2
CM
07.21.2011


MK-11-116
H253882-2
07.21.2011


MK-11-116
H253884-2
07.21.2011


MK-11-116
H253898-2
CM
07.21.2011

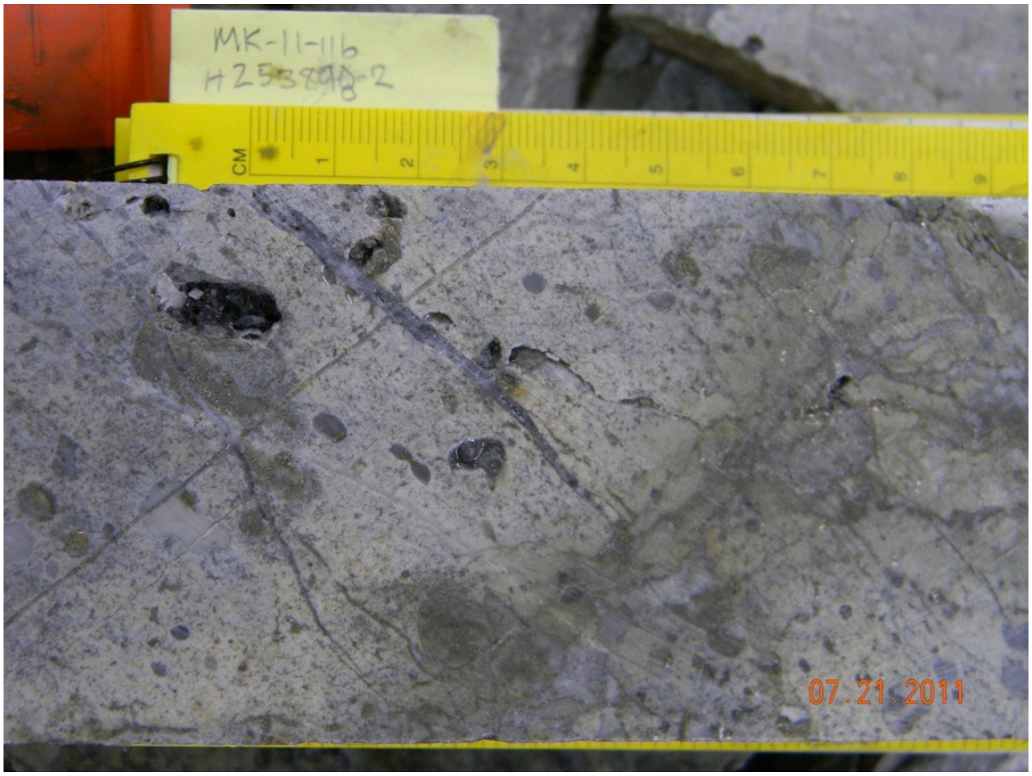
MK-11-116
H253898-2
CM
07.21.2011

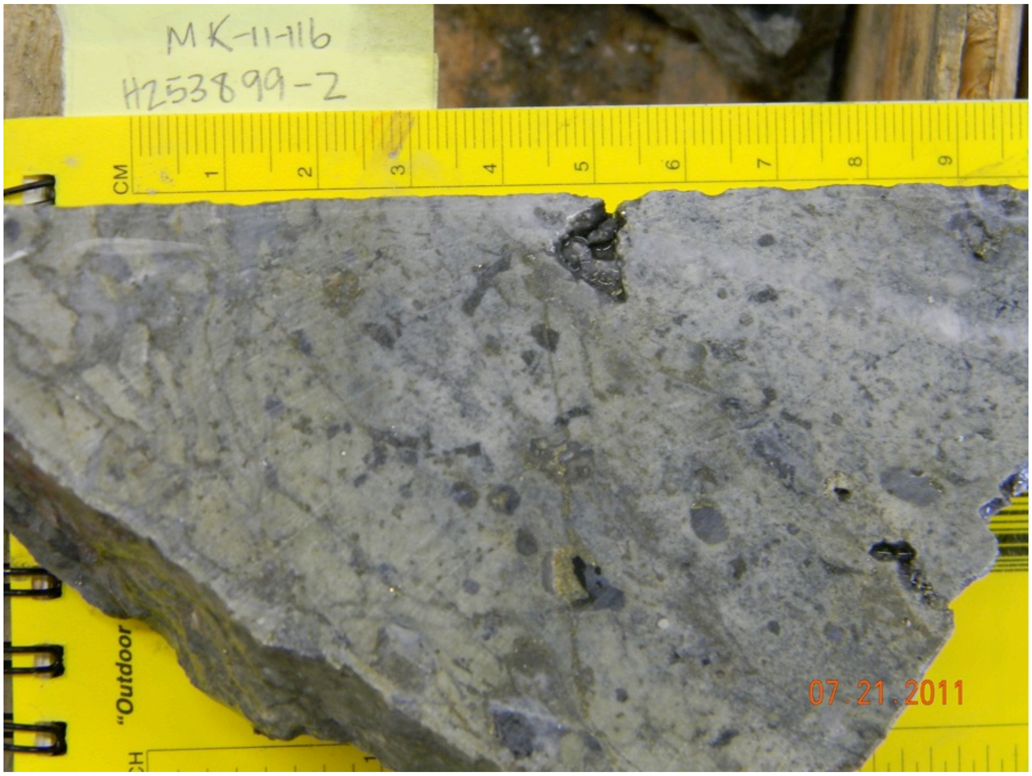
MK-11-116
H253899-2
CM
1
2
3
4
5
6
7
8
9
"Outdoor
07.21.2011


MK-11-116
H180616-2
07.21.2011

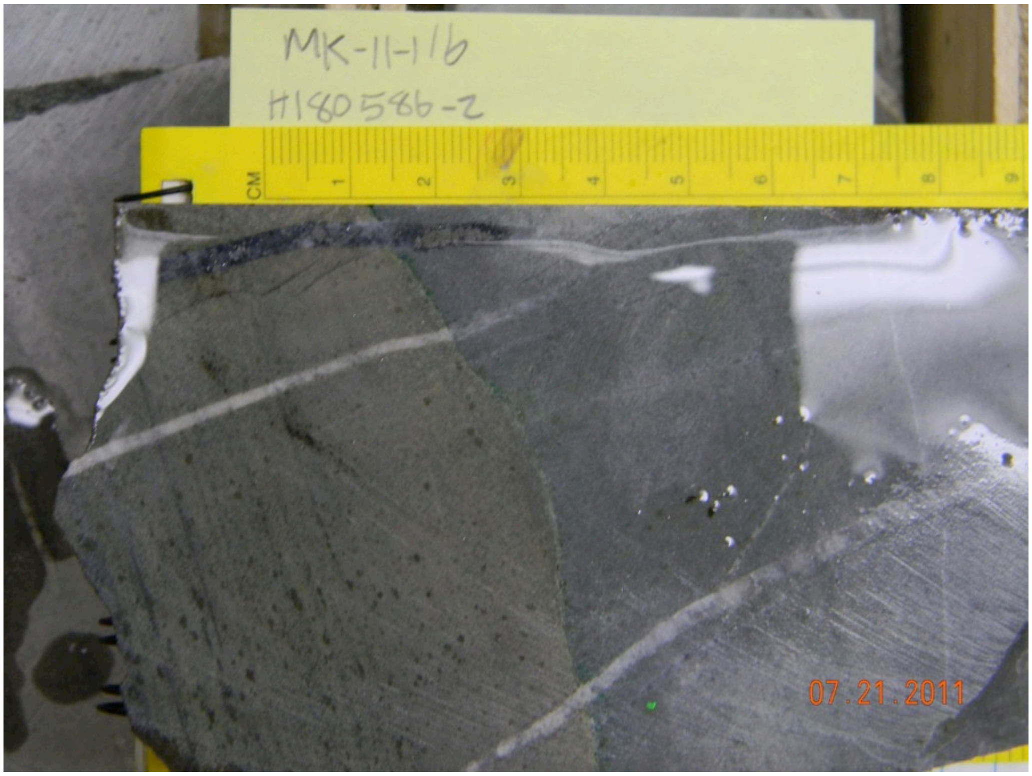
MK-11-116
H180586-2
CM
07.21.2011


MK-11-116
H180600-2
CM
07.21.2011

Appendix I: Niton XRF Chemistry

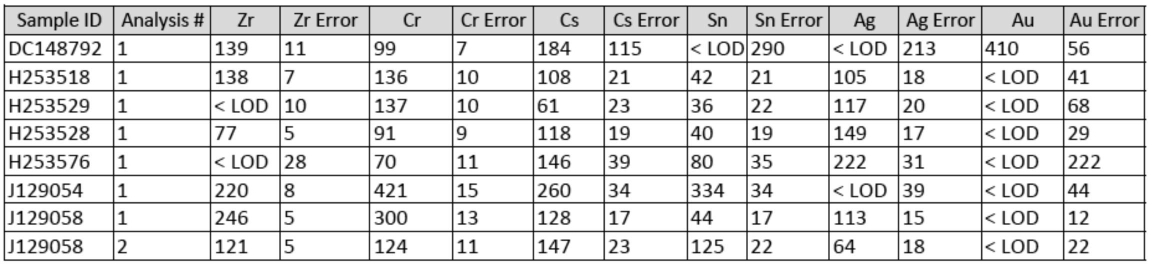

Sample ID	Analysis #	Zr	Zr Error	Cr	Cr Error	Cs	Cs Error	Sn	Sn Error	Ag	Ag Error	Au	Au Error
DC148792	1	139	11	99	7	184	115	< LOD	290	< LOD	213	410	56
H253518	1	138	7	136	10	108	21	42	21	105	18	< LOD	41
H253529	1	< LOD	10	137	10	61	23	36	22	117	20	< LOD	68
H253528	1	77	5	91	9	118	19	40	19	149	17	< LOD	29
H253576	1	< LOD	28	70	11	146	39	80	35	222	31	< LOD	222
J129054	1	220	8	421	15	260	34	334	34	< LOD	39	< LOD	44
J129058	1	246	5	300	13	128	17	44	17	113	15	< LOD	12
J129058	2	121	5	124	11	147	23	125	22	64	18	< LOD	22

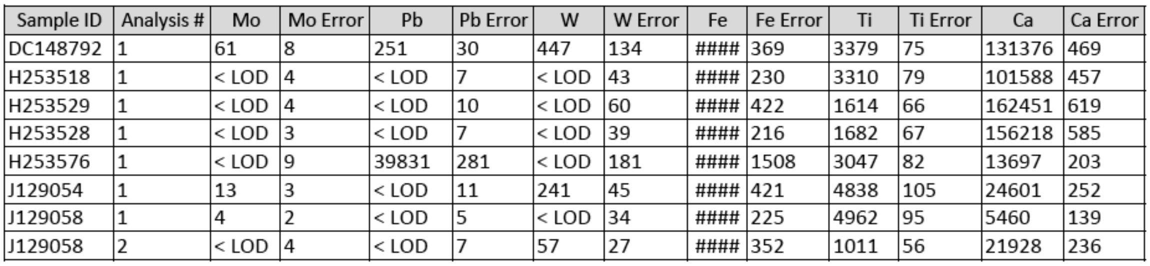

Sample ID	Analysis #	Mo	Mo Error	Pb	Pb Error	W	W Error	Fe	Fe Error	Ti	Ti Error	Ca	Ca Error
DC148792	1	61	8	251	30	447	134	####	369	3379	75	131376	469
H253518	1	< LOD	4	< LOD	7	< LOD	43	####	230	3310	79	101588	457
H253529	1	< LOD	4	< LOD	10	< LOD	60	####	422	1614	66	162451	619
H253528	1	< LOD	3	< LOD	7	< LOD	39	####	216	1682	67	156218	585
H253576	1	< LOD	9	39831	281	< LOD	181	####	1508	3047	82	13697	203
J129054	1	13	3	< LOD	11	241	45	####	421	4838	105	24601	252
J129058	1	4	2	< LOD	5	< LOD	34	####	225	4962	95	5460	139
J129058	2	< LOD	4	< LOD	7	57	27	####	352	1011	56	21928	236

Appendix J: R commands

```
Livengood <- read.table(file='LivengoodSusina.csv', header=TRUE,
row.names=1, sep=',')

LivengoodLog <- Livengood
LivengoodLog[ ,2:4] <- log10(Livengood[ ,2:4])
attach(LivengoodLog)


cor.test(Auppm,Asppm)

AsRegression<-lm(Auppm~Asppm)
summary(AsRegression)

plot(Auppm~Asppm, xlab='Log(Au(ppm))', ylab='Log(As(ppm))')
abline(a=-4.5415, b=1.2205)
text(x=4.1, y=-1.1, labels='Pearson Correlation Coefficient=0.71')


cor.test(Auppm,Sbppm)

SbRegression<-lm(Auppm~Sbppm)
summary(SbRegression)

plot(Auppm~Sbppm, xlab='Log(Au(ppm))', ylab='Log(Sb(ppm))')
abline(a=-0.55281, b=0.24596)
text(x=4.1, y=-1.1, labels='Pearson Correlation Coefficient=0.47')
```

Appendix K: Comma delineated data for R. Save as ‘LivengoodSusina.csv’ to use with the R code in Appendix J

```
DC128714,qtz-asp,0.74,3440,119
DC128724,qtz-asp,1.11,15400,77
DC128730,qtz-asp,1.92,13700,238
DC128732,qtz-asp,5.45,27300,265
DC128733,qtz-asp,2.20,16100,80
DC129044,qtz-asp,1.21,18500.00,66.20
DC129054,qtz-asp,1.95,31000.00,216.00
DC129057,qtz-asp,0.72,13200.00,57.10
DC129058,qtz-asp,0.61,7530.00,66.40
DC129059,qtz-asp,0.58,8940.00,47.60
DC140215,stib,13.75,21200,693
DC140217,stib,15.00,24700,2160
DC140218,stib,16.20,14800,57200
DC140219,stib,12.85,10700,81900
DC144215,stib,4.43,10600,134500
DC144216,stib,9.35,11100,20900
DC144217,stib,7.17,15100,4950
DC145738,qtz-stib,7.77,5250,25800
DC145786,qtz-asp,1.38,8370,62
DC145787,qtz-asp,0.64,3010,42
DC145790,qtz-asp,6.64,10000,98
DC145791,qtz-asp,1.51,3630,50
DC145795,qtz-asp,1.00,6360,62
DC145799,qtz-asp,0.75,9080,73
DC145800,qtz-asp,1.04,10000,83
DC146083,stib,11.30,10000,667
DC146084,stib,6.64,10000,1180
DC146085,stib,10.00,10000,5490
DC146086,stib,4.36,10000,2380
DC146087,stib,19.80,10000,10800
DC146089,stib,6.95,10000,8280
DC146092,stib,5.52,10000,3430
DC146093,stib,4.11,10000,29200
DC146094,stib,8.21,10000,33300
DC146095,stib,4.17,10000,4500
DC146096,stib,1.37,3610,2700
DC146097,stib,1.33,4360,2400
DC146250,stib,16.40,10000,9540
DC148143,qtz-asp,0.15,1545,41
DC148145,qtz-asp-stib,1.51,5900,11600
DC148789,qtz-asp,2.10,13300,99
DC148792,stib,6.06,18100,29500
DC148795,qtz-asp-stib,7.25,29700,14100
```

DC148796,stib,8.45,17200,11400
DC148799,qtz-asp,0.31,3400,526
DC148800,qtz-stib,4.47,14200,71700
DC149939,qtz-stib,0.28,2660,965
DC149942,qtz-stib,0.58,4180,4620
DC149944,qtz-stib,2.19,6370,14400
DC149946,qtz-stib,0.57,3410,776
DC149948,qtz-stib,0.62,4780,16400
DC149956,qtz-asp,1.50,13500,2200
DC149957,qtz-asp,1.88,12000,389
DC149958,qtz-asp,1.44,13900,5610
DC149959,qtz-asp,1.28,14500,5630
DC149962,qtz-stib,0.65,5290,4780
DC149964,qtz-stib,0.25,4470,54
DC149965,qtz-stib,1.25,10400,1125
DC149970,qtz-stib,0.74,5350,12800
DC149976,qtz-stib,1.63,12200,143
DC149980,qtz-asp,0.33,4100,729
DC149982,qtz-stib,0.05,796,73
H253518,qtz-stib,7.61,33500,61200
H253528,qtz-asp-stib,0.10,4820,841
H253529,qtz-asp-stib,0.17,7160,743
H253542,qtz-stib,0.78,2460,86000
H253576,qtz-asp-stib,1.48,35400,2870
H253859,stib,6.80,9790,8910
H253860,stib,3.45,5070,5900
H253861,stib,3.20,10100,1630
H253862,qtz-stib,5.43,13100,8050
H253863,qtz-stib,0.65,5010,1510
H253865,stib,1.15,7790,26400
H253866,stib,6.18,14650,3330
H253868,qtz-stib,4.69,13900,26200
H253869,stib,3.03,10650,7620
H253870,stib,6.20,16450,50200
H253871,stib,4.45,7580,804
H253872,stib,4.53,10250,21200
H253873,stib,4.73,8350,6400
H253875,stib,2.60,5770,18200
H253876,stib,5.72,7730,8350
H253877,stib,7.74,13650,6670
H253880,stib,2.04,6870,12400
H253881,stib,9.42,17000,32200
H253882,qtz-asp-stib,0.78,8700,512
H253885,stib,0.68,7570,97
H253887,qtz-asp,11.35,30900,76
H253890,qtz-asp,1.05,7020,1850

```
H253898,qtz-asp,1.32,9020,46
H253899,qtz-asp,1.05,5240,35
H253903,qtz-asp,0.53,8200,37
H253906,qtz-asp-stib,0.73,9250,51
H253908,qtz-asp,2.53,9200,47
H253909,qtz-asp,3.41,8440,59
H253910,qtz-asp,2.99,10850,57
J180561,stib,2.39,30800,1105
J180565,qtz-asp-stib,3.60,22700,101500
J180566,qtz-asp,7.04,32500,67700
J180568,qtz-asp,0.90,3500,849
J180569,qtz-stib,1.34,7640,6920
J180570,qtz-asp,1.03,3800,236
J180571,qtz-asp,0.64,3700,271
J180572,qtz-asp,0.25,2670,25
J180574,qtz-asp,0.07,1170,20
J180576,qtz-stib,5.70,27200,4130
J180577,qtz-stib,0.80,8050,9030
J180584,qtz-stib,1.26,9930,3540
J180585,qtz-stib,2.20,9730,350
J180586,qtz-asp,3.39,6650,678
J180597,qtz-asp-stib,1.41,18400,9670
J180599,qtz-stib,0.64,5900,8430
J180600,qtz-stib,0.31,2840,91
J180602,qtz-stib,0.75,6470,5420
J180604,qtz-stib,1.03,6950,24600
J180607,qtz-stib,0.90,7820,14400
J180612,qtz-stib,0.28,4040,3450
J180616,qtz-asp-stib,0.53,5910,296
J180617,qtz-stib,0.29,4160,11900
J180618,qtz-stib,0.32,3820,2980
J180619,qtz-stib,2.30,13000,9470
J180620,qtz-stib,0.28,2030,92
J180621,qtz-stib,0.53,3270,9790
J180622,qtz-stib,0.74,1470,66
J180624,qtz-stib,0.26,1525,54
J180625,qtz-stib,0.52,5430,8440
```